Reconstitution of Partially Recombinant 26S Proteasome Reveals Functional Asymmetries in its Heterohexameric AAA+ Unfoldase

By

Robyn Jeanne Beckwith

A dissertation submitted in partial satisfaction of the

requirements for the degree of

Doctor of Philosophy

in

Molecular and Cell Biology

in the

Graduate Division

of the

University of California, Berkeley

Committee in charge:

Professor Andreas Martin, Chair
Professor John Kuriyan
Professor David Wemmer
Professor James Berger

Spring 2014

Reconstitution of Partially Recombinant 26S Proteasome Reveals Functional Asymmetries in its Heterohexameric AAA+ Unfoldase

Abstract

Reconstitution of Partially Recombinant 26S Proteasome Reveals Functional Asymmetries in its Heterohexameric AAA+ Unfoldase

by

Robyn Jeanne Beckwith

Doctor of Philosophy in Molecular and Cell Biology

University of California, Berkeley

Professor Andreas Martin, Chair

The 26S proteasome is the major eukaryotic ATP-dependent protease, yet the detailed mechanisms utilized by the proteasomal heterohexameric AAA+ unfoldase to drive substrate degradation remain poorly understood. To perform systematic mutational analyses of individual ATPase subunits, I heterologously expressed the unfoldase, also known as the base subcomplex, from *Saccharomyces cerevisiae* in *Escherichia coli* and reconstituted partially recombinant 26S proteasomes *in vitro*.

My studies demonstrate that the six ATPases play distinct roles in degradation, corresponding to their positions in spiral staircases adopted by the AAA+ domains in the absence and presence of substrate. ATP hydrolysis in subunits at the top of the staircases is critical for substrate engagement and translocation. While the unfoldase relies on this vertical asymmetry for substrate processing, interaction of the base with the core peptidase exhibits three-fold symmetry with contributions from every other subunit. Preliminary data on establishing a bulk kinetic assay utilizing substrates of varying lengths to experimentally deconvolute the processes of substrate engagement and translocation is presented.

The diverse structural and functional asymmetries explored in this body of work demonstrate how the mechanisms of substrate engagement and processing may differ between the eukaryotic 26S proteasome and other simpler, homomeric AAA+ proteases. My findings provide an initial framework for elucidating the mechanochemical operating principles of the heterohexameric proteasomal motor. Future studies will be required to determine whether emerging mechanistic models of ATP-dependent substrate translocation established for homomeric AAA+ proteases can be generalized to the 26S proteasome.

This work is dedicated to everyone who has looked outside of themselves and wondered at the intricate workings of the world.

Contents

List of Figures

List of Tables

Acknowledgments

I would like to thank Andreas Martin for his scientific mentorship and intellectual guidance. I am incredibly grateful for your brilliance and innovative approaches in biochemistry, protein engineering, and enzyme kinetics. I will always utilize the skills I learned in the Martin Lab, and already I find myself wondering what questions you would ask and what experiments you would dream up!

I am very proud to have been a part of the Martin Lab from its inception - it was an honor and adventure to see it grow into a community of such dedicated and fun-loving scientists. We may joke around, but we were always there for each other. Thanks to Mary Matyskiela, who from the beginning helped shape our lab culture, provided mentorship and friendship when I needed it, and made sure that our Flag columns were treated like royalty. Eric Estrin and Charlene Bashore, you were the next ones to take the leap and I'm so glad you did - lab would never have been the same without SSLYBY, kitten calendars, and so many other things. Thanks to Evan Worden, the best bay-mate ever and fellow gummy-conoisseur, and Kris Nyquist, who brought invaluable perspective and endless optimism to the lab. To Ellen Goodall, who took me rock-climbing for the first time and shared my rocky relationship with the base. And to Brooke Gardner, who brought fun and organization to a lab that could always use more of both. Thanks to Chris Padovani for always being a good sport and having great lab hands, even though he never tolerated the Kanye that Mary and I played over the lab speakers. And to those who are carrying on the fine Martin Lab traditions, Jared Bard and Michal Olszewski - please figure out how these motors work so I can read about it in your future papers!

I would also like to thank my thesis committee members, James Berger, Dave Wemmer and John Kuriyan, as well as my past scientific mentors: Mari Golub, Zhihao Yu, Andrew Fisher, Kurt Giles, Melissa Mott and Christine Gee. Spanning my time at three University of California institutions (Davis, UCSF and Berkeley), you inspired me and helped me fulfill

my potential as a scientist. Thank you for the chance to learn the skills I needed and teaching me to start by asking the right questions. I always think about how much your mentorship meant to me and I try to pay it forward to others at every opportunity.

Special thanks to my friends and colleagues, especially Nicole Fay, Ellie Smith, Hanadie Yousef, Mark Herzik, Elsa Tretter, and Nate Krefman. I would not have made it through without having you as partners in crime for commiseration and escaping from the rigors of graduate school. And thank you to Andrey Shmakov for helping me learn LaTeX, explore the outdoors and never refusing to make a batch of caramel popcorn.

Finally, I am so thankful for my parents and my sister-in-practice, Lauren. You were always there with love and encouragement - thank you for believing in me. You shaped the person I am today and I hope that I will always make you proud.

CHAPTER 1

Introduction

1.1 Shaping the proteome by selective degradation

Proteins are complex and versatile macromolecules that are integral components of all cells. Among other things, proteins are responsible for structural organization, signaling and nearly every chemical reaction that occurs in order to sustain life. The lifetime of a given protein is crucial to its function and the proteome is thus constantly being adjusted in response to environmental and temporal cues through regulated protein expression and degradation. In all organisms, selective protein degradation is a tightly controlled process mediated by energy-dependent proteases. The precisely-timed degradation of specific proteins drives key cellular processes including cell division and differentiation, signal transduction, transcriptional gene regulation, stress responses and protein quality control (Gottesman, 1996; Pickart, 1997; Hanson and Whiteheart, 2005; Finley, 2009; Jung et al., 2009). A thorough understanding of the molecular principles that determine the timing and selectivity of protein degradation by cellular proteases has the potential to advance many areas of research, from the basic mechanism of mechanical force generation by molecular motors to the development of therapeutics for the multitude of human diseases that stem from protein dysregulation.

1.2 Architecture of energy-dependent proteases

Protein degradation by all energy-dependent proteases follows a similar trajectory (Figure 1.1), with selective degradation achieved through the common architecture of a barrel-shaped peptidase capped by an unfoldase ring. The peptidase, comprised of stacked oligomeric rings, forms an internal cavity with sequestered proteolytic sites and narrow axial pores. Compartmentalization of proteolytic activity inside the peptidase mandates that native protein substrates are physically relocated into the chamber for degradation. Substrate entry is mediated by a hexameric unfoldase ring of AAA+ (***A***TPases ***A***ssociated with various cellular ***A***ctivities) protein subunits that docks atop one or both ends of the peptidase. This interaction aligns the central pore of the unfoldase with the gated entrance of the peptidase, inducing the pore into the degradation chamber to widen (Rabl et al., 2008; Finley, 2009; Jung et al., 2009; Sauer and Baker, 2011). Coordinated cycles of ATP hydrolysis in the unfoldase subsequently threads the substrate through both pores, mechanically unfolding structured domains and translocating the denatured polypeptide into the peptidase for degradation (Maillard et al., 2011; Aubin-Tam et al., 2011; Sauer and Baker, 2011; Baker and Sauer, 2012; Nyquist and Martin, 2014).

While energy-dependent proteases in all organisms share core features, there is significant divergence in the number and complexity of these enzymes across all domains of life (Figure 1.2). Energy-dependent degradation in prokaryotes is accomplished by five classes of proteases with varying and sometimes redundant substrate specificity: ClpAP, ClpXP, Lon, FtSH and HslUV (Gottesman, 1996; Sauer and Baker, 2011). Archaea utilize Lon in addition to the archaebacterial proteasome, consisting of PAN (*p*roteasome-*a*ctivating

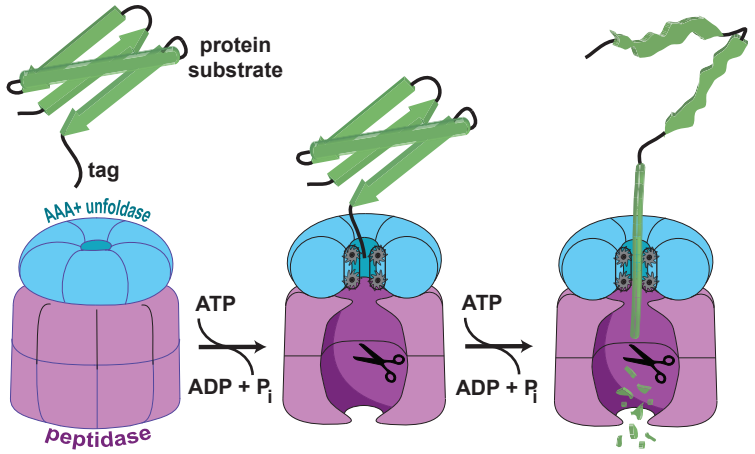

Figure 1.1: Common design of energy-dependent proteases.
AAA+ proteases are key components of all cells, degrading protein substrates to drive crucial cellular processes and maintain protein quality. Selective degradation is achieved through the highly conserved architecture of a barrel-shaped compartmental peptidase containing sequestered proteolytic active sites that is apically bound by an AAA+ unfoldase ring. Adapted from Nyquist and Martin (2014).

*n*ucleotidase) or putatively Cdc48 in complex with an archaeal homolog of the proteasomal peptidase (Fukui et al., 2002; Maupin-Furlow et al., 2005; Barthelme and Sauer, 2012). In stark contrast, eukaryotes rely on a single cytosolic protease, the 26S proteasome, to perform analogous functions and degrade an astonishingly diverse range of protein substrates (Voges et al., 1999; Matyskiela and Martin, 2013).

The structural complexity of these proteases ranges from a single polypeptide chain that encodes both proteolytic and ATPase domains (Lon and FtSH) to one or multiple subunits each containing distinct catalytic functions (HslUV, ClpXP, ClpAP) to the elaborate heteromeric architecture of the 26S proteasome, which is comprised of more than 32 distinct protein subunits (Schmidt et al., 1999; Gottesman, 2003; Cha et al., 2010). For the vast majority of these ATP-dependent proteases, the stacked hexameric or heptameric rings that form the unfoldase or peptidase consist of six or seven identical subunits (Figure 1.2). However, there are a few notable exceptions to this homomeric ring architecture. FtsH in plant chloroplasts is encoded by multiple genes and can form heteromeric complexes comprised of two different subunit types (Langer, 2000; Adam et al., 2006; Moldavski et al., 2012), and the *m*-AAA protease, a FtsH homolog in mitochondria, is similarly a hexamer formed from two subunits, Yta10 and Yta12 (Langer, 2000; Koppen and Langer, 2007; Lee et al., 2011). Even looking to more distantly-related AAA families, there are only a few additional examples of heteromeric rings: the Pex1/Pex6 heterohexamer involved in yeast peroxisome biogenesis (Grimm et al., 2012), the eukaryotic origin recognition complex, Orc1-6 (Bell

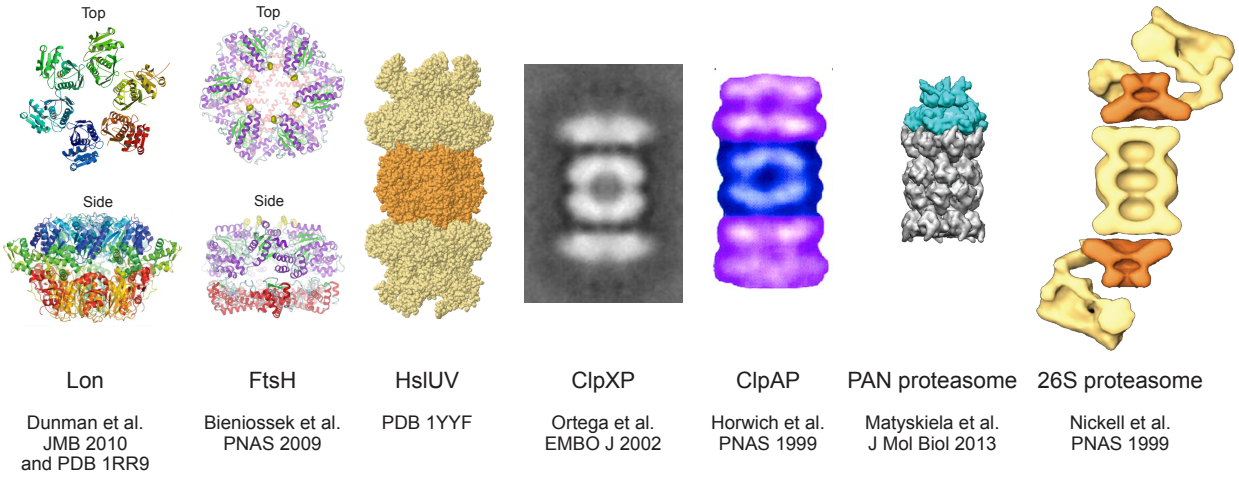

Figure 1.2: Divergence in energy-dependent protease structures.
Prokaryotes utilize multiple classes of energy-dependent proteases with varying structural complexities. In Lon (Dunman and Lowe, 2010) and FtsH (Bieniossek et al., 2009), the ATPase and proteolytic domains are fused into a single subunit that assembles into hexamers. HslUV is comprised of two stacked six-membered peptidase rings bound to a homohexameric unfoldase. The ClpP peptidase is formed from two stacked heptameric rings of identical proteolytic subunits that can be capped by hexameric unfoldases with either one (ClpX, Ortega et al. 2002) or two (ClpA, Horwich et al. 1999) ATPase domain rings. Archaea utilize Lon-type proteases as well as a homologous proteasomal peptidase of four stacked heptameric rings capped by the homohexameric PAN unfoldase (Matyskiela et al., 2013). The eukaryotic 26S proteasome (Nickell et al., 2009) has a peptidase with four stacked α-β-β-α rings, each comprised of 7 distinct α or β subunits, topped by an unfoldase formed by six distinct ATPase subunits arranged with a defined geometry.

and Stillman, 1992), and the cognate replicative helicase, Mcm2-7 (Bochman and Schwacha, 2009). As discussed in later detail (see Section 1.4), the 26S proteasome is unique among energy-dependent proteases due to the fully heteromeric architecture of both the peptidase and the unfoldase, in addition to the structural complexity required for proteasomal substrate recognition. The heterohexameric nature of the 26S proteasome unfoldase ring in particular raises questions as to whether the six distinct ATPase subunits contribute equally to substrate processing or if they may have specialized structural or mechanistic roles.

1.3 Substrate selection

Among the myriad of proteins present in a cell, proteins fated for destruction are targeted to ATP-dependent proteases by short amino acid sequences termed degrons (Inobe and Matouschek, 2008; Sauer and Baker, 2011). Degrons are recognized by either binding directly

to the pore of the AAA+ unfoldase ring, binding to an auxiliary site elsewhere on the protease, binding to an adapter protein that associates with the protease, or mediating covalent modification of the substrate with additional recognition factors (Sauer and Baker, 2011).

In general, prokaryotes use intrinsic degron tags encoded in the primary sequence of substrates that either have inherent affinity for the unfoldase or are recruited to the protease by adapters. This combinatorial approach provides additional levels of control by targeting substrate pools to various proteases that recognize either distinct or redundant degron signals. In the context of protein quality control, the 11-amino acid "ssrA" tag, which is appended to the C-terminus of nascent protein chains if ribosomes stall during protein translation (Giudice and Gillet, 2013), is recognized by both ClpXP and ClpAP (Gottesman et al., 1998; Gottesman, 2003; Sauer and Baker, 2011). The affinity of ClpXP for ssrA-tagged substrates can be enhanced through binding of the adapter protein SspB (Flynn et al., 2001; Baker and Sauer, 2012), while other competitive adapters for ClpX control degradation of the bacterial transcription factor σ_S according to environmental cues (Zhou et al., 2001; Bougdour et al., 2006, 2008; Baker and Sauer, 2012). ClpAP is also capable of associating with an adapter protein, ClpS, which globally reprograms the specificity of ClpAP from ssrA-tagged proteins to substrates with N-end rule degrons (Dougan et al., 2002; Schmidt et al., 2009; Román-Hernández et al., 2011). Lon also contributes to protein quality control by recognizing internal degrons, characterized by clusters of aromatic amino acids, that are normally buried in the native conformation of a substrate but become exposed when proteins misfold during stress or heat shock (Gottesman, 1996; Gur and Sauer, 2008; Sauer and Baker, 2011). Thus prokaryotes evolved multiple pathways for energy-dependent protein degradation that work independently and in parallel to finely tune the proteome in response to cellular conditions.

Rather than relying a variety of degrons that are recognized by different proteases, eukaryotes direct nearly all substrates targeted for degradation to a single enzyme, the 26S proteasome. Substrates are targeted for proteasomal degradation by post-translational modification with a polymeric chain of a small protein, ubiquitin. Ubiquitin contains seven lysine residues (K6, K11, K27, K29, K33, K48, and K63) which can be covalently linked to the terminal carboxyl group of another ubiquitin moiety via a three-tiered enzymatic cascade (Komander and Rape, 2012; Matyskiela and Martin, 2013). The length, linkage type, branching and placement of a polyubiquitin chain on a substrate are all factors that may affect proteasomal degradation. Ubiquitin chains containing at least four K48-linked moieties are well known to target substrates to the proteasome (Pickart, 1997; Thrower et al., 2000; Komander, 2009), yet it remains unclear how some substrates are completely degraded while others are only partially processed or selectively extracted from multi-protein complexes. The intrinsic characteristics of the substrates themselves, such as the thermodynamic stability of folded domains or slippery amino acid sequences, have been postulated to affect the efficiency of substrate unfolding and translocation by the proteasomal AAA+ unfoldase, and consequently degradation (Kenniston et al., 2005; Tian and Matouschek, 2006; Koodathingal et al., 2009; Kraut, 2013). Additionally, other chain linkage types have been demonstrated to also bind intrinsic proteasomal ubiquitin receptors or auxiliary shuttle factors to promote

selective degradation (Elsasser et al., 2004; Elsasser and Finley, 2005; Raasi et al., 2005; Komander, 2009).

Although we have yet to fully comprehend the ubiquitin code, the complexity of this system provides the precise signaling information required to carefully time the degradation of specific substrates in eukaryotes. An important ramification of using ubiquitin as a degradation signal results from its high thermodynamically stability and polymeric nature. Ubiquitin chains are not co-degraded with substrates but rather removed by the proteasome to facilitate degradation and replenish the cellular pool of available ubiquitin (Verma et al., 2002; Yao and Cohen, 2002; Matyskiela and Martin, 2013). This requirement of the ubiquitin-proteasome system may partially explain the enhanced structural complexity of the eukaryotic 26S proteasome.

1.4 Structure of the 26S proteasome

The 26S proteasome exhibits an unparalleled level of architectural complexity, with differentiated subunits arranged asymmetrically to facilitate the auxiliary structural modules required for ubiquitin-mediated substrate recognition (Table 1.1). The proteasomal core peptidase is comprised of four stacked heptameric α and β rings, each containing seven different subunits, arranged α_7-β_7-β_7-α_7 (Baumeister et al., 1998; Pickart and Cohen, 2004). Three β subunits contain proteolytic active sites, while the N-terminal domains of the α subunits form the gate of the axial peptidase pore (Lowe et al., 1995; Groll et al., 1997, 2000). The peptidase is apically capped on one or both ends by the regulatory particle, which is formed through the stable association of two sub-complexes, the base and the lid (Figure 1.3). The base constitutes the AAA+ unfoldase of the proteasome and contains six distinct ATPase subunits (Rpt1-Rpt6), two large scaffolding subunits (Rpn1, Rpn2) and an integral ubiquitin receptor (Rpn13). The base also contains binding sites for three non-integral proteasomal shuttle receptors (Rad23, Ddi1, Dsk2). The lid sub-complex is laterally bound to the base and makes additional contacts with the α-ring of the core peptidase (Lander et al., 2012; Beck et al., 2012). The lid contains nine subunits, including six PCI (*p*roteasome/*C*SN/e*I*F3)-domain subunits (Rpn3, Rpn5, Rpn6, Rpn7, Rpn9, Rpn12), two Jab1/MPN-domain containing proteins (Rpn8 and the essential deubiquitinating enzyme, Rpn11) and a second intrinsic ubiquitin receptor (Rpn10).

1.5 The base sub-complex

Like all energy-dependent proteases, the 26S proteasome contains a hexameric AAA+ unfoldase that couples ATP hydrolysis with mechanical substrate unfolding and translocation into the compartmental peptidase. Yet unlike its archaeal and prokaryotic counterparts, the proteasomal AAA+ ring is comprised of six distinct ATPase subunits arranged in a defined order (Tomko et al., 2010; Tomko and Hochstrasser, 2011). As this distinct heterohexameric

unfoldase arrangement is conserved in all eukaryotes, it has been postulated that this architecture may have evolved in conjunction with ubiquitin signaling and the enhanced structural complexity of additional proteasomal regulatory components (Volker and Lupas, 2002). The conserved heterohexameric composition of the eukaryotic proteasomal unfoldase has posed longstanding questions in the proteasome field about what consequences this architecture has for proteasome assembly, sub-complex interactions, ATP-hydrolysis within the AAA+ unfoldase and substrate processing.

Table 1.1: Subunit composition of 26S proteasome sub-complexes.

Subunits	Structure and function
	Lid sub-complex
Rpn3	PCI domain subunit
Rpn5	PCI domain subunit
Rpn6	PCI domain subunit
Rpn7	PCI domain subunit
Rpn9	PCI domain subunit
Rpn12	PCI domain subunit
Rpn8	Inactive Jab1/MPN domain
Rpn11	Jab1/MPN domain, JAMM motif deubiquitination active site
Rpn10	Ubiquitin binding by UIM, lid binding by VWA domain
	Base sub-complex
Rpt1	AAA + domain subunit
Rpt2	AAA + domain subunit
Rpt3	AAA + domain subunit
Rpt4	AAA + domain subunit
Rpt5	AAA + domain subunit
Rpt6	AAA + domain subunit
Rpn1	PC-repeat solenoid, binds Ubp6 and shuttle factors
Rpn2	PC-repeat solenoid, binds Rpn13
Rpn13	Ubiquitin binding via Pru domain
	Core peptidase sub-complex
α1-α7	Gating subunits
β1-β7	β1, β2, β5 contain proteolytic active sites

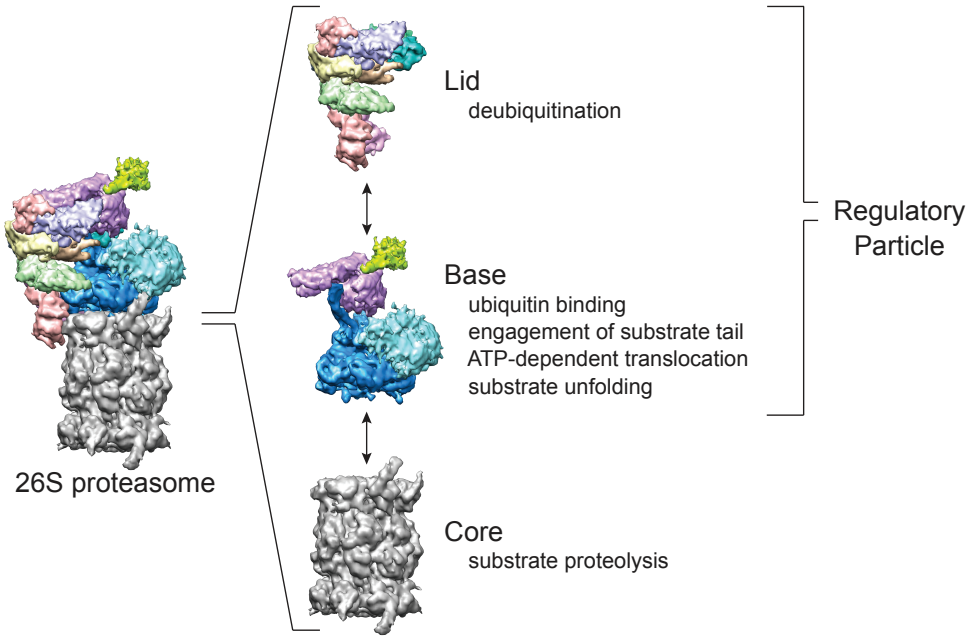

Figure 1.3: Structure of the 26S proteasome and its constituent sub-complexes.
The 26S proteasome can be dissociated into three stable sub-complexes: lid, base and core peptidase. The base, which comprises the ATP-dependent motor within the proteasome holoenzyme, docks atop the core and regulates substrate entry through the gated axial pores of the peptidase. The lid binds laterally in the holoenzyme and makes direct contacts with both the base and core peptidase. Together, the lid and base constitute the regulatory particle, which apically caps the core peptidase on one or both ends.

1.5.1 Structure

The eukaryotic base unfoldase shares basic structural homology with its simpler, homomeric relatives, PAN from archaea and ARC (*A*TPase forming *R*ing-shaped *C*omplexes) from actinobacteria (Zhang et al., 2009; Djuranovic et al., 2009). The domain architecture within the ATPase subunits includes a N-terminal domain, containing a coiled-coil helical region (CC) followed by an oligonucleotide/oligosaccharide-binding (OB) domain, and a C-terminal AAA+ ATPase domain (Figure 1.4) with short extensions, or tails. Insight into the structural organization of these domains came from crystal structures of the PAN homomeric unfoldase (Zhang et al., 2009), which demonstrated that the OB-folds of the six ATPases form a hexamer (N-ring) while the N-terminal helical regions pair between adjacent subunits to form three coiled coils. In PAN, a conserved proline residue between the N-terminal helical region and the OB-fold adopts *cis* and *trans* conformations in alternating subunits around the ring, producing a sharp kink that drives formation of the coiled coils between neighboring subunits (Zhang et al., 2009; Djuranovic et al., 2009; Tomko et al., 2010). In the proteasomal ATPase subunits, only Rpt2, Rpt3 and Rpt5 have a proline residue in this

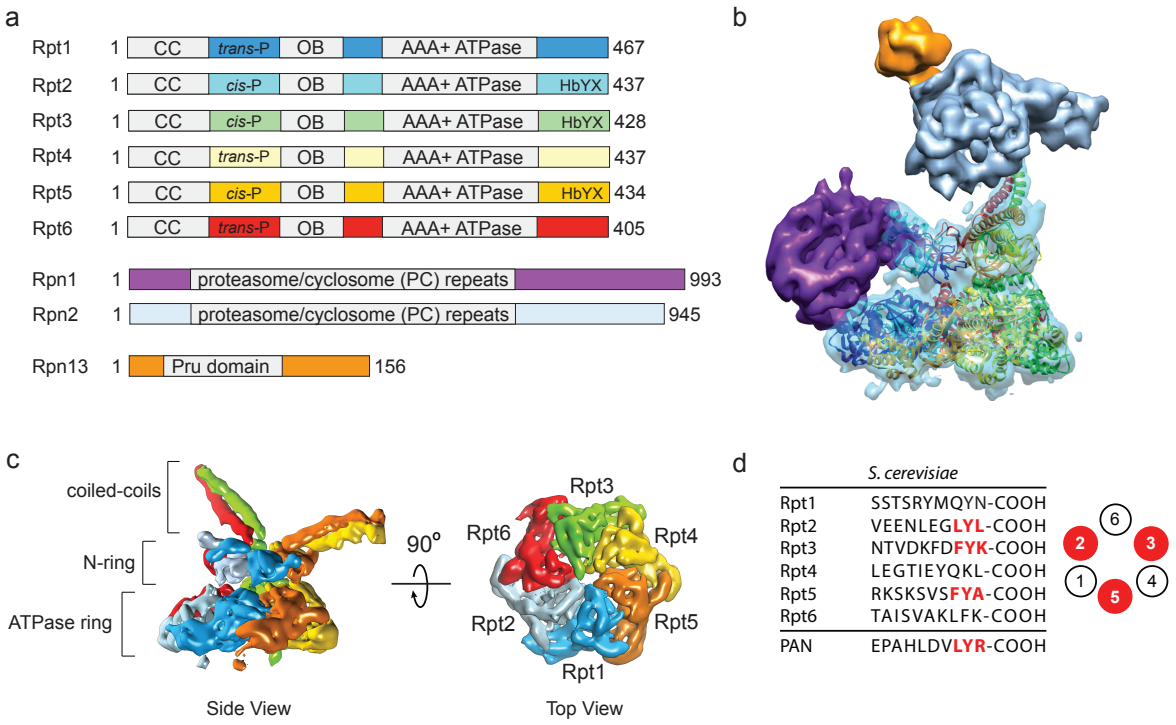

Figure 1.4: Architecture of the base.
(a) Domain structure of subunits in the base sub-complex. The base is comprised of nine different proteins, including six distinct AAA+ ATPases (Rpt1-Rpt6), two scaffolding subunits (Rpn1, Rpn2) and the ubiquitin receptor Rpn13. **(b)** EM density for the base sub-complex of the yeast proteasome in the absence of substrate (Lander et al., 2012; Matyskiela et al., 2013). A molecular model generated from the PAN crystal structure (Zhang et al., 2009) was docked into ATPase subunit density in the base heterohexamer. The N-termini of Rpt1 (dark blue) and Rpt2 (light blue) form the smallest coiled coil, which mediates peripheral docking of Rpn1 (purple) onto the base. Rpt6 (red) and Rpt3 (green) form the longest coiled coil that binds Rpn2 (light blue), which in turn binds to Rpn13 (orange), positioning them directly above the pore of the unfoldase. The coiled coil formed by the N-termini of Rpt4 (yellow) and Rpt5 (orange) does not appear to contact other proteasome subunits but may bind the UIM of Rpn10. Figure adapted from Matyskiela and Martin (2013). **(c)** Side view of the heterohexameric base unfoldase of the 26S proteasome and cutaway top view of the ATPase domain ring. Individual ATPase subunits are colored the same as in (a, b). Rpt subunits are arranged in the order 1-2-6-3-4-5. Visible in the side view are the N-terminal coiled coils, the N-ring formed from the OB domains, the ATPase ring and the C-terminal tails of Rpt2, Rp3 and Rpt5. EM density for the tails of Rpt1, Rpt4 and Rpt6 was not resolved (Lander et al., 2012). **(d)**. Sequence alignment of the C-terminal tail sequences of the proteasomal ATPases. Only Rpt2, Rpt3 and Rpt5 contain a C-terminal HbYX motif.

position (see Appendix B). Recent disulfide-engineered cross linking demonstrated that the ATPases within the proteasomal unfoldase are ordered Rpt1-Rpt2-Rpt6-Rpt3-Rpt4-Rpt5 (Tomko et al., 2010), suggesting that prolines in alternating subunits within the ring may similarly drive pairing of the N-terminal helical regions of adjacent subunits to ensure the appropriate Rpt arrangement within the ring. Interestingly, the proteasomal Rpt subunits are most divergent in their N-terminal helical domains (Appendix B), and EM structures of the proteasome show three coiled-coils of differing lengths formed by Rpt1/Rpt2, Rpt6/Rpt3 and Rpt4/Rpt5 (Beck et al., 2012; Lander et al., 2012). This asymmetry facilitates contacts with the laterally-bound lid subcomplex as well as other regulatory base subunits and base-specific assembly factors.

The large scaffolding subunits of the base, Rpn1 and Rpn2, bind to the Rpt1/Rpt2 and Rpt6/Rpt3 coiled coils, respectively. Rpn1 and Rpn2 contain a series of PC (*p*roteasome/*c*yclosome) repeats that form large α-solenoids with extended N-termini (Kajava, 2002; Effantin et al., 2009; He et al., 2012). Rpn1, positioned at the periphery of the Rpt1 and Rpt2 ATPase domains, provides binding sites for the non-essential proteasome deubiquitinating enzyme Ubp6, as well as the substrate shuttle receptors Rad23, Dd1 and Dsk2 (Gomez et al., 2011; Rosenzweig et al., 2012; Sakata et al., 2012). Rpn2, positioned above the pore of the base by strong contacts with both the base and lid, mediates binding of the integral ubiquitin receptor Rpn13 (Chen et al., 2010; Beck et al., 2012; Lander et al., 2012; Rosenzweig et al., 2012; Sakata et al., 2012). The Pru domain of Rpn13 binds polyubiquitin chains and tethers substrates to the proteasome for degradation (Husnjak et al., 2008; Schreiner et al., 2008). A second intrinsic ubiquitin receptor, Rpn10, was previously identified as component of the base but has now been shown to primarily bind to the lid subunits Rpn9 and Rpn11 via its VWA (von Willebrand A) domain (Riedinger et al., 2010; Lander et al., 2012; Matyskiela and Martin, 2013). The UIM (ubiquitin-interacting motif) domain of Rpn10 is still postulated to make additional contacts with the Rpt4/Rpt5 coiled-coil of the base (Sakata et al., 2012; Matyskiela and Martin, 2013).

1.5.2 Interaction with the core peptidase

The regulatory particle docks onto the core peptidase in an ATP-dependent manner through the C-terminal tails of the proteasomal ATPases (Figure 1.4), which bind to pockets formed by neighboring peptidase α subunits (Smith et al., 2005, 2007; Yu et al., 2010). The ATPase tails induce large structural rearrangements in the N-termini of the α subunits that gate the peptidase pore, facilitating substrate entry into the proteolytic chamber (Rabl et al., 2008). A consequence of the heteromeric architecture of the 26S proteasome and the asymmetric attachment of the lid is that the base must dock onto the core peptidase with a defined orientation. It has been suggested that assembly of the base sub-complex may in fact be templated by the core peptidase (Park et al., 2009). Recent data demonstrate that Rpt6 may function to ensure the correct register as its C-terminus is the only tail that binds one specific α pocket (Tian et al., 2011; Park et al., 2013). The inherent symmetry mismatch of the hexameric ATPase ring and the heptameric α ring of the peptidase has

motivated numerous structural and functional studies of the base-core tail interaction for both PAN and the 26S proteasome (Gillette et al., 2008; Tian et al., 2011). The ATPase tail of PAN subunits contains a conserved HbYX (hydrophobic/tyrosine/unspecified) motif that has been demonstrated to be involved in opening the gated peptidase pore (Smith et al., 2007). In the 26S proteasome base, the tails of only three ATPase subunits, Rpt2, Rpt3 and Rpt5, contain the HbYX motif (Figure 1.4, Appendix B). Analysis using short peptides corresponding to the sequences of the Rpt tails have suggested that Rpt2 and Rpt5 contribute to peptidase gate opening to varying extents (Smith et al., 2007). EM reconstructions in the absence and presence of substrate show density for only the HbYX-containing tails (Lander et al., 2012; Matyskiela et al., 2013), which are arranged in alternating positions within the ring (Figure 1.4), implying that the interaction of the remaining non-HbYX tails with the α pockets may be too dynamic to resolve.

It remains unclear precisely how the heterohexameric arrangement of the proteasomal ATPase ring may dictate specialized roles for the C-terminal tails in binding the core peptidase and inducing opening of the gated pore. Prior studies utilizing PAN and peptides corresponding to the proteasomal Rpt C-terminal tails have suggested that HbYX-containing Rpt tails may induce gate-opening whereas the non-HbYX tails could mediate peptidase binding (Gillette et al., 2008; Smith et al., 2011; Tian et al., 2011). The 3-fold symmetry of the Rpt tail arrangement, in conjunction with the ATP-dependence of the base-core interaction, have led to models in which the nucleotide state of individual subunits during the ATP hydrolysis cycle may dictate different tail conformations and thus modulate communication between the base and core peptidase (Nickell et al., 2009; Smith et al., 2011; Bar-Nun and Glickman, 2012). However, a unified mechanism for the roles of individual ATPase tails in binding and stimulating gate opening in the core peptidase of the 26S proteasome has yet to be established.

1.5.3 Assembly

Assembly of the base sub-complex is mediated by four designated chaperones: Nas2, Nas6, Hsm3 and Rpn14 (Funakoshi et al., 2009; Kaneko et al., 2009; Roelofs et al., 2009; Saeki et al., 2009; Tomko and Hochstrasser, 2013). These proteins facilitate the formation of Rpt pairs, which form N-terminal coiled-coils (Rpt1/Rpt2, Rpt6/Rpt3, Rpt4/Rpt5) to ensure the proper order of subunits in the heterohexameric ATPase ring of the base (Figure 1.5). Interaction of the Rpt N-terminal domains is strictly required for proper subunit pairing, as removal of the N-terminal helical and OB domains completely abrogates base assembly even in the presence of the chaperones (unpublished data, R.B. and A.M.). Although the four base chaperones do not share significant sequence homology, they all contain putative protein-protein binding domains that adopt uniformly crescent-shaped structures. Hsm3 contains Arm/HEAT repeats, Rpn14 contains WD40 motifs, Nas6 contains ankyrin repeats and Nas2 has a PDZ domain. All of the chaperones exhibit similar modes of interaction with the Rpts, binding to the lower surface of the C-terminal ATPase domains that will eventually form the interface with the core peptidase. Hsm3 binds primarily to the ATPase domain of Rpt1

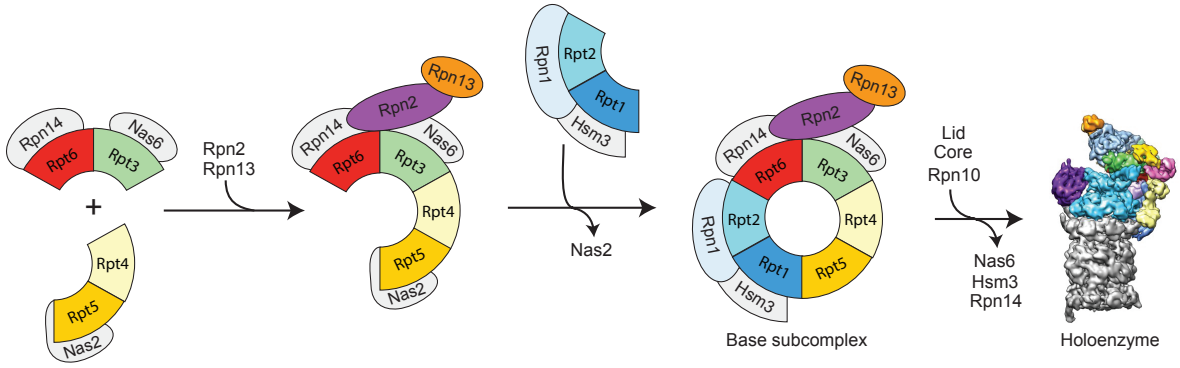

Figure 1.5: Chaperone-mediated assembly of the base.
Current model for assembly of the base sub-complex based on *in vivo*, *in vitro* and structural studies (Funakoshi et al., 2009; Kaneko et al., 2009; Roelofs et al., 2009; Saeki et al., 2009; Tomko and Hochstrasser, 2013). The formation of base precursors from pairs of ATPase subunits is mediated by four base-specific chaperones: Nas2, Nas6, Hsm3 and Rpn14. The Rpt3/Rpt6/Nas6/Rpn14 module assembles with Rpt4/Rpt5/Nas2, followed by association of Rpn2/Rpn13 to the Rpt3/Rpt6 coiled coil. The Rpt1/Rpt2/Rpn1/Hsm3 module binds and displaces Nas2, forming the complete base sub-complex with three remaining chaperones bound. Association of base and core peptidase displaces Nas6, Hsm3 and Rpn14. Incorporation of the lid before or after base-core complex formation completes assembly of proteasome holoenzyme.

but also makes direct contacts with Rpt2 and Rpn1 (Barrault et al., 2012; Takagi et al., 2012), thus acting to bridge the Rpt1-Rpt2 pair and stabilize the association of Rpn1 to their N-terminal coiled-coil. Nas6 binds to the lower face of the Rpt3 ATPase domain, while structural and biochemical data demonstrate that Rpn14 associates with the lower face of Rpt6 (Roelofs et al., 2009; Saeki et al., 2009). Nas2 binds to Rpt5 bivalently, interacting with both its C-terminal tail and the face of the ATPase domain that associates with Rpt1 (Satoh et al., 2014). Capping of the HbYX-containing tail of Rpt5 blocks nonspecific activation on the peptidase while masking the Rpt1-interacting surface acts as a quality control checkpoint during the assembly of the complete hexameric ATPase ring. The incorporation of the Rpt1/Rpt2/Rpn1/Hsm3 module to form the fully assembled base displaces Nas2 while the remaining three chaperones dissociate when the base docks onto the core peptidase (Park et al., 2009; Tomko et al., 2010; Satoh et al., 2014; Singh et al., 2014).

1.6 Conserved catalytic features of AAA+ protein unfoldases

The six distinct ATPases of the eukaryotic proteasome belong to the classical clade of the AAA+ superfamily of P-loop NTPases (Neuwald et al., 1999; Iyer et al., 2004; Erzberger and Berger, 2006). All AAA+ proteins form oligomeric assemblies of individual subunits comprised of a large and a small AAA+ domain. The interfaces of neighboring AAA+ subunits form bipartite active sites where ATP is bound and hydrolyzed by conserved catalytic residues (Figure 1.6). The Walker A (P-loop) motif, characterized by a GXXGXGK[S/T] sequence, is involved in binding the phosphate groups of ATP (Neuwald et al., 1999). The Walker B acidic motif, containing a hydrophobic stretch of amino acids directly followed by a DE sequence, uses a conserved glutamate to coordinate magnesium and activate a water molecule for nucleophilic attack on the scissile γ-phosphate bond (Erzberger et al., 2006). The Sensor-II arginine is postulated to contact the γ-phosphate of ATP and thus serve as a sensor for catalysis (Davey et al., 2002; Erzberger et al., 2006). However, members of the classical clade of AAA+ proteins, including the proteasomal ATPases, lack the Sensor-II motif (Iyer et al., 2004). The highly conserved arginine finger of the clockwise-next ATPase subunit reaches back, contacts the bound nucleotide and is critical for hydrolysis. The arginine finger has been demonstrated to be involved in subunit communication within the ATPase ring due to it's ability to "read out" the nucleotide state of its neighboring subunit (Hishida et al., 2004; Ogura et al., 2004; Augustin et al., 2009; Wendler et al., 2012).

Recent systematic bulk and single molecule studies of the ClpX unfoldase have led to an advanced mechanistic model for how this bacterial motor couples coordinated ATP hydrolysis with conformational changes in structural elements facing the central pore to drive substrate translocation (for a detailed review see Nyquist and Martin 2014). The large AAA+ domain of each ATPase subunit contains loops that project into the central pore of the AAA+ ring and transduce ATP-dependent conformational changes into directional pulling force applied to the substrate (Martin et al., 2005, 2007, 2008a; Glynn et al., 2009; Aubin-Tam et al., 2011; Maillard et al., 2011; Sen et al., 2013; Stinson et al., 2013). The pore-1 loop contains a conserved aromatic residue that has been demonstrated to directly contact the substrate by cross linking experiments with various bacterial unfoldases including ClpA (Hinnerwisch et al., 2005), ClpB (Schlieker et al., 2004) and ClpX (Martin et al., 2008b). Mutation of the pore-1 loop in ClpX altered the rate of ATP hydrolysis by the unfoldase and significantly affected substrate unfolding and degradation efficiency (Martin et al., 2008a). A second loop, termed the pore-2 loop, is located farther down in the central pore and has been shown to make contacts with both the substrate and the peptidase in the case of ClpX (Martin et al., 2008b) and Cdc48 (Barthelme and Sauer, 2013).

Crystal structures of the ClpX hexamer demonstrated that subunits within the ATPase ring adopt varying conformations when in different nucleotide states, and that these conformations correspond to differential positions of the pore loops (Glynn et al., 2009). This finding supports the model that pore loops contact the substrate and undergo power strokes

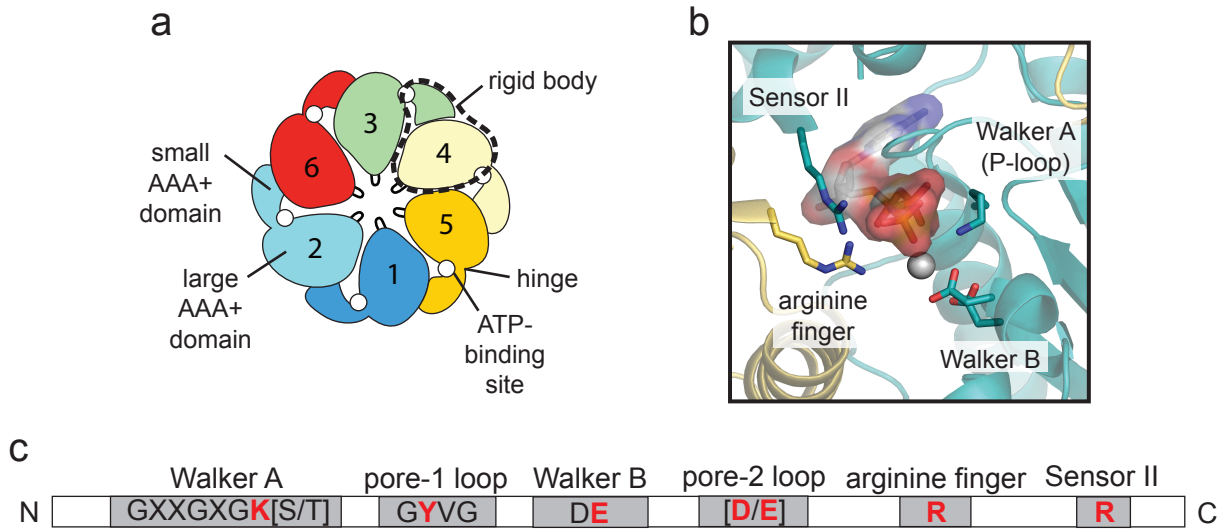

Figure 1.6: Overview of AAA+ unfoldases: conserved catalytic and structural features. **(a)** Schematic of the 26S proteasome heterohexameric ATPase ring. The order of the six distinct Rpt subunits is shown as well as the orientation of large and small AAA+ domains relative to ATP binding sites. Rigid bodies are formed by the small AAA+ domain of one subunit and the large AAA+ domain of its clockwise-next neighbor. These rigid bodies are thought to undergo ATP-dependent conformational changes that drive substrate translocation through direct contact of the central pore loops with the threaded substrate polypeptide chain. **(b)** Representative view of a single bipartite ATP-binding pocket formed by two neighboring AAA+ subunits (DnaA-AMPPCP, PDB 2HCB, Erzberger et al. 2006). The contributions of the two subunits is indicated by differential coloring (yellow or teal). The side chains of conserved catalytic residues that are important for nucleotide binding and catalysis are shown as sticks, as is the bound nucleotide with additional electrostatic surface representation. **(c)** N- to C-terminal arrangement of conserved catalytic and structural motifs in an AAA+ protein subunit.

in response to ATP hydrolysis to pull substrate through the central pore. Interestingly, the interfaces between the small AAA+ domain of a given subunit and the large AAA+ domain of its clockwise next neighbor were unchanged in all nucleotide states. These static units, or "rigid bodies," were proposed to rotate as a single unit around "hinges" in response to ATP hydrolysis and transmit these movements to the pore loops in order to drive substrate translocation (Glynn et al. 2012, Figure 1.6). Single molecule studies have provided evidence that translocation proceeds in a highly coordinated step-wise fashion such that the number of subunits productively hydrolyzing ATP within the hexamer corresponds to the number of steps taken in a given firing cycle (Sen et al., 2013).

It remains to be seen whether the mechanisms established for the homohexameric ClpX

motor can be generalized for all AAA+ enzymes. The 26S proteasomal base is clearly distinguished from other AAA+ protein unfoldases by its unique heterohexameric ATPase composition, the sequence heterogeneity in the N-terminal domains of the ATPases, and its association with additional regulatory modules required for ubiquitin-mediated substrate recruitment. A key aspect for further investigation stems from recent structural studies of the proteasome demonstrating that the large AAA+ domains, and consequently the pore-1 loops, of the six ATPase subunits adopt two different fixed spiral staircase arrangements in the absence and presence of substrate (Lander et al., 2012; Beck et al., 2012; Matyskiela et al., 2013). Only three other AAA translocases, E1 helicase (Enemark and Joshua-Tor, 2006), Rho (Thomsen and Berger, 2009) and DnaB (Itsathitphaisarn et al., 2012), have been structurally characterized in the presence of substrate and all three exhibit spiral staircase configurations of subunits within their ATPase rings. We do not yet understand whether the spiral staircase observed for the proteasomal unfoldase is the result of the heterohexameric ring architecture or if it is dictated by the auxiliary structural components of the proteasome. Furthermore, the potential consequences that this asymmetric configuration of the six distinct proteasomal ATPases may have for the mechanisms of coordinated ATP hydrolysis and substrate engagement, translocation and unfolding remain unknown.

1.7 Steps in proteasomal substrate processing

The ATP-dependent degradation of a vast array of ubiquitinated substrates by the 26S proteasome is enabled by the highly complex and asymmetrical architecture of the regulatory particle (Figure 1.7). Ubiquitinated substrates must bind to one of several intrinsic receptors in the base or lid, or alternately be delivered to the proteasome via shuttle adaptors that transiently bind to the base. Once tethered to the regulatory particle by one or potentially multiple ubiquitin receptors, the proteasomal AAA+ motor engages an unstructured portion of the substrate. This flexible degradation initiation region must of sufficient length to reach the pore of the ATPase ring (Prakash et al., 2004; Inobe et al., 2011), although the length requirement may vary depending on the ubiquitination and spatial positioning of the bound substrate (Inobe and Matouschek, 2008; Inobe et al., 2011). Pursuant to engagement, ATPase subunits within the AAA+ ring undergo conformational changes in response to coordinated ATP hydrolysis firing events that drive substrate unfolding and translocation into the proteolytic chamber of the peptidase for degradation.

In conjunction with substrate engagement, unfolding and translocation, the ubiquitin chain must be cleaved from the substrate through the coordinated action of the integral deubiquitinating enzymes Rpn11 and Ubp6 (Guterman and Glickman, 2004; Hanna et al., 2006). Rpn11 is positioned above the pore of the unfoldase and cleaves the isopeptide bond between the substrate and the proximal ubiquitin (Verma et al., 2002; Yao and Cohen, 2002; Lander et al., 2012; Matyskiela et al., 2013; Worden et al., 2014), whereas Ubp6 is bound to Rpn1 at the periphery of the base and trims ubiquitin moieties from the distal end of the chain (Lam et al., 1997; Matyskiela and Martin, 2013). Studies have shown that

deubiquitination is ATP-dependent, suggesting that translocation by the AAA+ motor may be required to properly position the substrate for ubiquitin chain cleavage by Rpn11 (Verma et al., 2002; Yao and Cohen, 2002; Matyskiela et al., 2013; Worden et al., 2014). The exact order and timing of deubiquitination relative to substrate engagement and unfolding remains unclear and is critical for our understanding of how proteins are processed for degradation by the proteasome.

The effect of ubiquitin chain linkage and length on substrate affinity and binding orientation is also unknown. The geometry of substrate presentation to the base unfoldase could significantly affect the amount of time spent on engagement and deubiquitination. The relative timing of these events may determine substrate escape from proteasomal degradation (Kraut et al., 2007), which would occur if the tethering ubiquitin chain is cleaved before engagement occurs. The thermodynamic stability of folded substrate domains is also likely to be an important determinant of substrate release versus degradation (Lee et al., 2001; Kenniston et al., 2005; Finley, 2009; Koodathingal et al., 2009; Sauer and Baker, 2011) as the intrinsic pulling force of the motor may not be sufficient to unfold extremely stable domains or may lose grip on "slippery" amino acid sequences (Kraut, 2013; Too et al., 2013). Ultimately we do not understand how the mechanism of substrate engagement, unfolding,

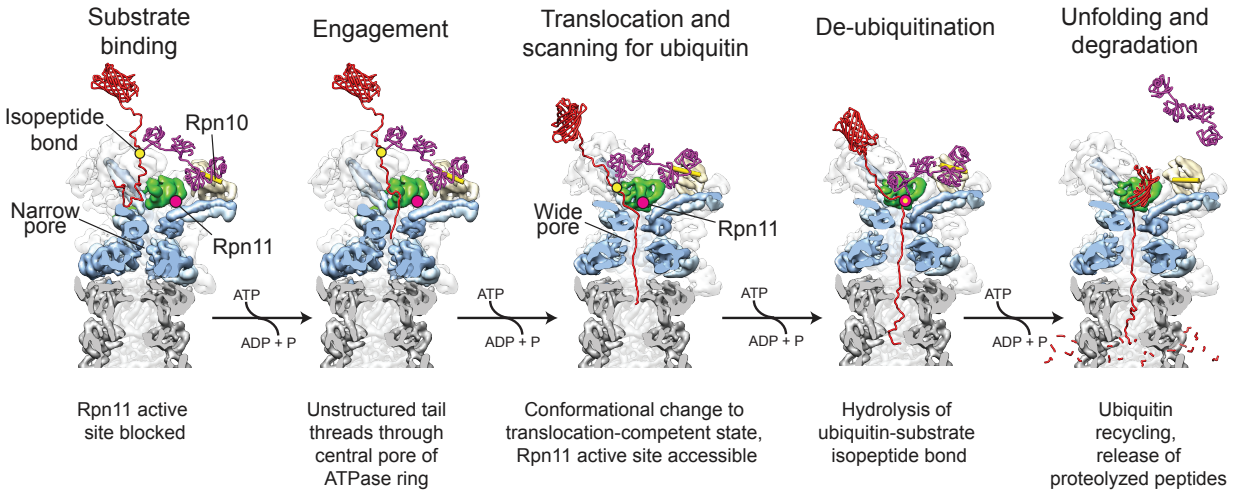

Figure 1.7: Sequence of events during substrate processing by the 26S proteasome. Degradation of a polyubiquitinated substrate by the 26S proteasome requires multiple enzymatic activities. Our current model for the reaction pathway for proteasomal substrate processing includes substrate binding to intrinsic proteasomal ubiquitin receptors, engagement of unstructured region of the substrate, translocation and unfolding, deubiquitination and ultimately proteolysis. Figure adapted from Matyskiela et al. (2013).

translocation and degradation depends on the heterohexameric architecture of the proteasomal AAA+ motor and whether individual ATPase subunits may have specialized roles in these processes. A further question relates to the mechanism of coordinated ATP hydrolysis by this uniquely complex motor and whether the proteasomal AAA+ ATPase ring might utilize mechanisms to generate mechanical force that deviate from those proposed for its simpler, homomeric counterparts.

1.8 Subunit specialization in the heterohexameric AAA+ unfoldase of the 26S proteasome

In this dissertation, I explore how the six distinct ATPase subunits of the proteasomal unfoldase (Rpt1-6) are involved in substrate processing, interaction with the core peptidase and coordinated ATP hydrolysis. To accomplish unprecedented systematic *in vitro* studies, I developed a heterologous expression system to produce the unfoldase sub-complex from *S. cerevisieae* in *E. coli* and established conditions to reconstitute partially recombinant 26S proteasomes (Chapter 2).

Detailed analyses of the individual roles of the six proteasomal ATPase subunits in substrate processing required the biochemical characterization of catalytic mutations in conserved AAA+ motifs (Chapter 3). A mutation in the canonical AAA+ Walker-B motif was used to trap single subunits in a static ATP-bound state in order to define the contributions of individual ATPases to substrate degradation. I demonstrate that the six ATPase subunits are functionally distinct and that ATP hydrolysis by Rpt3, Rpt4 and Rpt6 is crucial for successful substrate degradation. These subunits are located at the top of the spiral staircase configuration observed for the ATPase subunits of the base unfoldase in the absence of substrate, indicating that ATP hydrolysis in these subunits may be required for substrate engagement. I also examined the importance of individual ATPase subunits for base-core association and demonstrated that peptidase binding and gate opening do not depend on the nucleotide state of specific Rpt C-terminal tails.

Pursuant to these studies of substrate processing by the proteasome I developed a series of unfolded substrates of varying lengths to deconvolute the processes of substrate engagement verses translocation by the base unfoldase (Chapter 4). This tool will facilitate a more mechanistic understanding of how various mutants compromise substrate engagement or translocation by the proteasome as well as elucidate the timing of various events in substrate processing.

Prior to these studies an understanding of how the heterohexameric architecture of the base unfoldase affects proteasomal substrate processing was lacking. This dissertation provides systematic and quantitative insights into the specialization of ATPase subunits in various aspects of proteasome function and sub-complex interactions.

CHAPTER 2

Heterologous expression of the base unfoldase

A portion of the work presented in this chapter has been previously published as part of the following paper: Beckwith, R., Estrin, E., Worden, E., and Martin, A. Reconstitution of the 26S proteasome reveals functional asymmetries in its AAA+ unfoldase. Nat Struct Mol Biol, 20:1164-1172, 2013.

2.1 Introduction

Previous work investigating proteasome function has been complicated by the fact that cell viability is strictly dependent on proteasome function. The essential nature of the proteasome has limited mutational studies both *in vivo* and *in vitro*, severely hindering systematic analyses of the mechanisms of proteasomal protein degradation and subcomplex interactions. Furthermore, isolation of proteasome holoenzyme or subcomplexes from yeast has been limited by low sample yields and significant subunit heterogeneity in the resulting preparations. Heterologous expression of the base subcomplex circumvents these issues by generating high yields of base with defined subunit composition that can be mutated or altered without affecting bacterial cell viability. To facilitate detailed mechanistic studies of the proteasomal unfoldase we therefore designed a system for the expression of the base subcomplex from *Saccharomyces cerevisiae* in *Escherichia coli* and established conditions for the reconstitution of partially recombinant 26S holoenzyme.

2.2 Results

2.2.1 Cloning, expression and purification of recombinant base

The base subcomplex of the proteasome from *Saccharomyces cerevisiae* was produced in *Escherichia coli* by co-expression of thirteen yeast proteins, including nine integral base

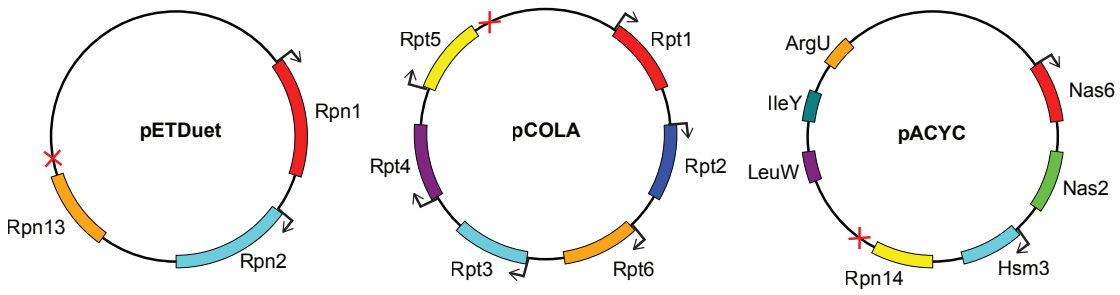

Figure 2.1: Plasmid maps for recombinant base expression.
The base subcomplex from *S. cerevisiae* was heterologously produced in *E. coli* by co-expression of thirteen proteins encoded on three plasmids with different antibiotic resistances. pETDuet (Amp^{res}) contained three non-ATPase subunits of the base, while the six distinct ATPases were encoded by pCOLA (Kan^{res}). Base production required co-expression of four base-specific proteasome chaperones that were included on pACYC (Chl^{res}), which also contained genes for rare tRNAs. T7 promoters are indicated as arrows whereas T7 terminators are marked with red crosses.

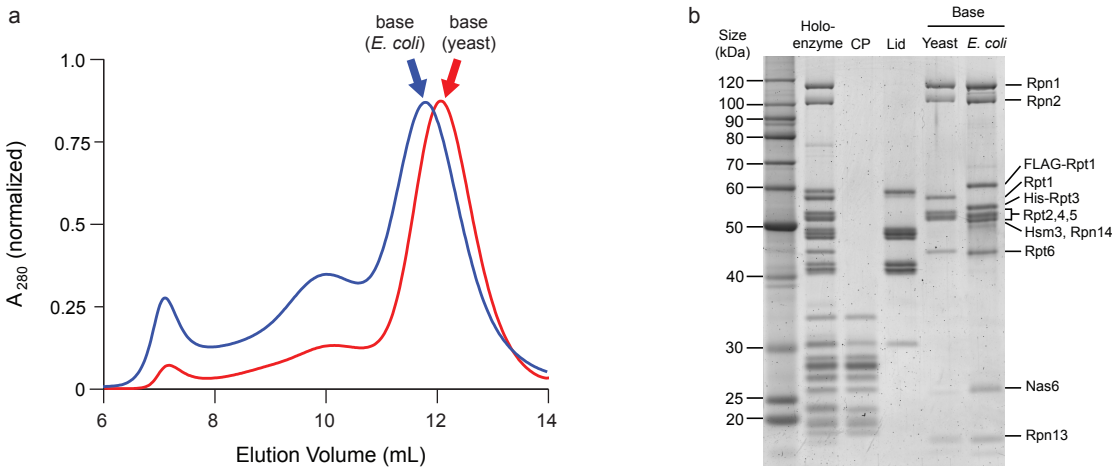

Figure 2.2: Purification of the recombinant base and yeast proteasome subcomplexes. **(a)** Endogenous (red) and *E. coli*-expressed, recombinant (blue) base subcomplexes show similar elution profiles from a Superose 6 size-exclusion column. The slightly smaller elution volume for recombinant base is attributed to the co-purification of proteasome-specific chaperones that stably associate with the complex when heterologously expressed in the absence of core particle in *E. coli*. The absorbance at 280 nm is normalized for comparison. For equal cell mass, recombinant base expression yields approximately 10-fold more protein than the purification of endogenous base from yeast. **(b)** Sypro-Ruby stained SDS-PAGE of the purified proteasomal subcomplexes used in this study. Endogenous complexes were isolated from yeast using FLAG tags on Rpn11 for holoenzyme and lid, on Pre1 for core particle (CP), and on Rpn2 for base preparations. Recombinant base expressed in *E. coli* was purified using a FLAG tag on Rpt1 and a His_6 tag on Rpt3. Proteasome chaperones Nas6, Hsm3 and Rpn14 only co-purify with the base subcomplex produced in *E. coli*.

subunits (Rpt1-6, Rpn1, Rpn2, Rpn13) and four proteasome assembly chaperones (Nas2, Nas6, Rpn14, Hsm3 (Funakoshi et al., 2009; Roelofs et al., 2009; Saeki et al., 2009; Kaneko et al., 2009)) as depicted in Figure 2.1. We isolated assembled base by tandem-affinity purification using tags on two different subunits, followed by gel-filtration chromatography (Figure 2.2a). The purified base exhibited appropriate stoichiometry and no subunit truncations, as revealed by SDS–PAGE (Figure 2.2b) and mass spectrometry (data not shown, R.B.). We observed Nas6, Hsm3, and Rpn14 stably associated with the recombinant base, whereas these chaperones were not present in the base purified from yeast, as indicated by SDS-PAGE, size-exclusion chromatography, and native PAGE (Figure 2.3).

This result is consistent with studies of *in-vivo* proteasome assembly indicating that Nas6, Hsm3, and Rpn14 are displaced upon base binding to the core particle and lid, whereas Nas2 dissociates at an earlier stage of base assembly (Funakoshi et al., 2009; Roelofs et al., 2009; Park et al., 2009, 2013). One model for *in-vivo* base assembly proposes that the core particle

might act as a template to facilitate the proper arrangement of Rpts in the hexameric ring (Park et al., 2009). However, our successful production of the base subcomplex in *E. coli* rules out a strict requirement for such templated assembly.

We compared the activities of the recombinant base to endogenous yeast base. Both base subcomplexes hydrolyzed approximately 51 ATP enz^{-1} min^{-1} in the absence of substrate (Table 2.1). The ability of the ATP-bound base to interact with core particle and induce gate opening was determined by monitoring the fluorescence increase upon peptidase cleavage of the fluorogenic peptide succinyl-Leu-Leu-Val-Tyr-(7-amino-4-methylcoumarin). In the presence of ATP, recombinant base stimulated core-particle activity approximately 20-fold, similar to endogenous yeast base. In agreement with previous reports, we measured about two-fold higher peptide hydrolysis with the non-hydrolysable analog ATPγS compared to ATP (Smith et al., 2005; Liu et al., 2006) which may be due to potential differences in the ATPase-ring conformation (Sledz et al., 2013) or the dynamics of base-core interactions.

2.2.2 Reconstitution of functional 26S proteasome

Importantly, we reconstituted 26S holoenzyme using either endogenous or recombinant base and the lid and core particle purified from yeast. Successful reconstitution was assessed by native PAGE (Figure 2.3) and *in-vitro* degradation of a polyubiquitinated model substrate, a green fluorescent protein (GFP)-titin^{V15P}-cyclin-PY fusion, whose degradation could be measured through the decrease of GFP fluorescence (Figure 2.4, Figure 2.5).

Proteasomes reconstituted with saturating recombinant or endogenous base degraded substrate at a maximal rate of 0.3 enz^{-1} min^{-1}, comparable to 0.32 enz^{-1} min^{-1} observed for holoenzyme purified from yeast (Table 2.1). Substrate degradation by reconstituted proteasomes strictly required addition of recombinant Rpn10, an intrinsic ubiquitin-receptor that does not co-purify with isolated lid or base subcomplexes. Consistent with previously described degradation defects in the absence of Rpn10 (Verma et al., 2004), we found that omitting Rpn10 or deleting its ubiquitin-interacting motif resulted in 40-fold slower degradation (Figure 2.4a, Figure 2.6), despite the presence of the second ubiquitin receptor, Rpn13. Since proteasome formation did not depend on Rpn10 (data not shown, R.B.) and degradation was not facilitated by Rpn10 lacking its ubiquitin-interacting motif (Figure 2.6), this

Table 2.1: Biochemical characterization of reconstituted 26 proteasome.

	basal ATPase rate		peptidase stimulation		degradation rate (k_{deg})	
	min^{-1}	% WT	fold increase	% WT	(enz^{-1} min^{-1})	% WT
Holoenzyme	107	–	–	–	0.32	–
WT (*E. coli*)	51	100	21	100	0.30	100
WT (yeast)	54	106	22	103	0.29	97

result suggests that Rpn10 is either the primary receptor for our model substrates or required in combination with Rpn13 for multivalent ubiquitin-chain binding.

2.3 Discussion

Heterologous expression of the yeast base subcomplex in *E. coli* provides an unprecedented tool for interrogating the mechanism of ATP-dependent substrate processing by the proteasomal AAA+ motor. Recombinant production of the proteasomal unfoldase enables previously intractable *in vitro* functional analyses of individual subunits, structural elements and catalytic motifs in the context of both the isolated base and the 26S proteasome holoenzyme. Futhermore, we now have the potential to address key mechanistic questions about the operating principles of this highly complex energy-dependent protease. Current models for how AAA+ protein unfoldases transduce chemical energy into mechanical force are largely based on bulk and single molecule studies of a homohexameric bacterial unfoldase, ClpX. Our system opens the door for similarly detailed mechanistic studies of the 26S proteasomal motor, which is distinguished from other AAA+ protein unfoldases by having six distinct ATPase subunits arranged in a defined order. The heterohexameric motor and added structural complexity conferred by the lid subcomplex poses the question of how the substrate processing mechanism of the 26S proteasome compares to that of simpler, homomeric energy-dependent proteases.

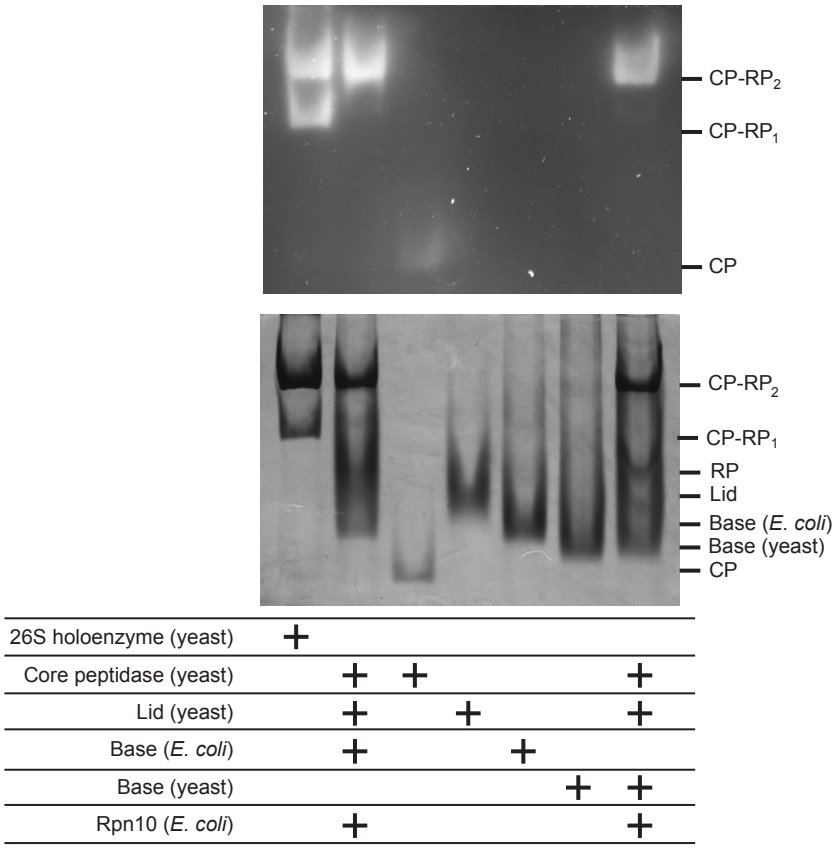

Figure 2.3: Native gel of purified subcomplexes and reconstituted 26S proteasomes. 26S holoenzyme reconstituted with CP, lid, Rpn10, and either endogenous or recombinant base was analyzed by native gel electrophoresis. Endogenous yeast 26S holoenzyme and individual CP, lid and base subcomplexes were also analyzed for comparison. Yeast holoenzyme migrated as two bands corresponding to proteasomes singly (CP-RP_1) and doubly (CP-RP_2) capped with regulatory particles (RP). Excess lid and base was used for reconstituted proteasome samples, which therefore migrated only as doubly capped holoenzyme.

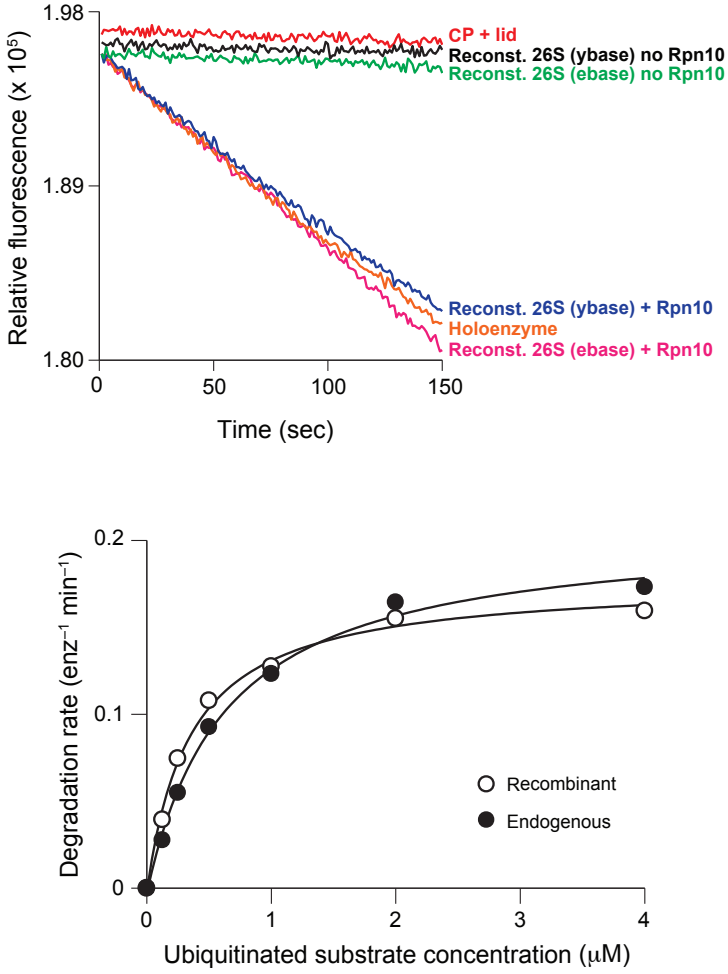

Figure 2.4: Degradation of a GFP-fusion substrate by reconstituted proteasomes. **(a)** Degradation of a polyubiquitinated GFP fusion substrate by endogenous yeast holoenzyme or 26S proteasomes reconstituted with saturating recombinant base (ebase) or endogenous yeast base (ybase). Substrate degradation was monitored by the loss of GFP fluorescence and strictly required the addition of Rpn10, despite the presence of Rpn13 (see Figure 2.2b). **(b)** Michaelis-Menten analyses of substrate degradation by proteasomes reconstituted with endogenous or recombinant base. Degradation reactions were performed using limiting base and excess core particle, lid and Rpn10 to ensure that reconstituted proteasome holoenzymes were singly capped. K_M and V_{max} values were 0.63 μM and 0.21 enz^{-1} min^{-1} for holoenzyme with endogenous base, and 0.35 μM and 0.18 enz^{-1} min^{-1} for holoenzyme with recombinant base.

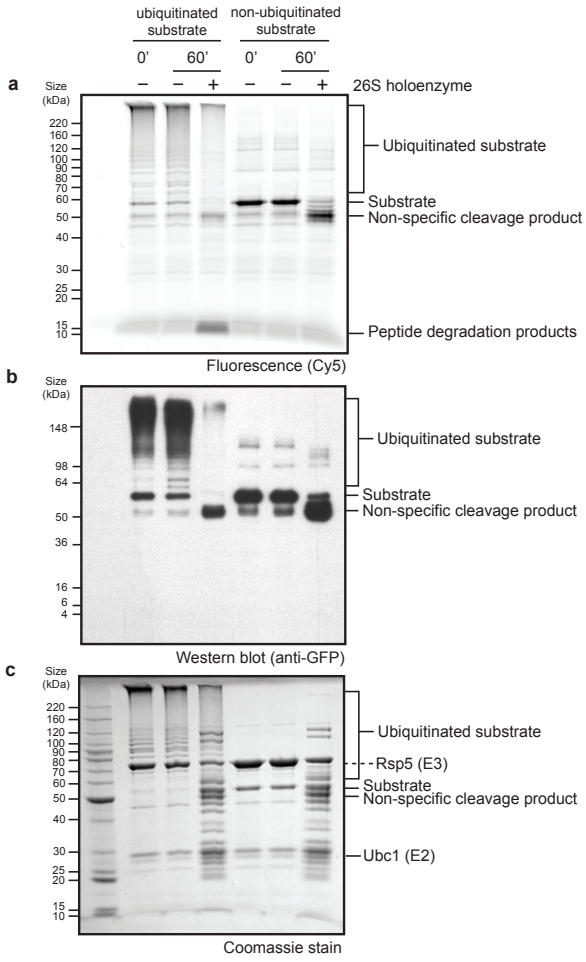

Figure 2.5: Gel-based assay for proteasomal degradation of GFP-fusion substrate.
To demonstrate degradation of the GFP-titin^{V15P}-cyclin-PY fusion substrate in a gel-based assay, ubiquitinated or non-ubiquinated substrates were incubated with or without 26S proteasome purified from yeast in the presence of ATP at 30 °C for one hour. Samples were then run on a SDS-PAGE gel followed by (a) fluorescence scanning to detect the Cy5-label, (b) western blotting using an anti-GFP antibody, or (c) Coomassie staining for total protein. The fluorescence scan clearly shows the accumulation of small peptide degradation products only for the ubiquitinated substrate in the presence of holoenzyme. Some level of ubiquitin-independent partial cleavage of an unstructured region of the GFP model substrate was detectable in all three assays. Additional ubiquitination of the substrate was visible in the absence of holoenzyme, which was not unexpected as the enzymes used for *in vitro* ubiquitination of the substrate were still present.

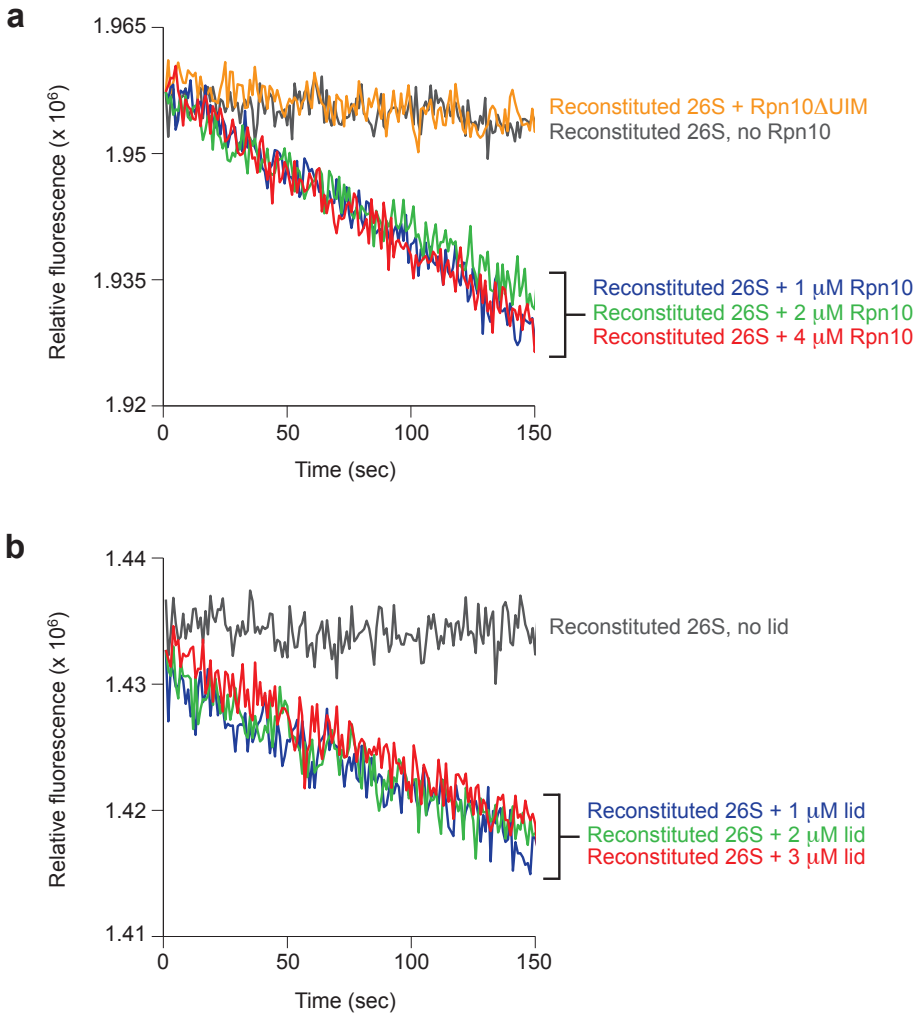

Figure 2.6: Excess lid or Rpn10 do not affect proteasomal degradation rates.
Proteasomal degradation was monitored by the decrease in fluorescence of a polyubiquitinated GFP-fusion substrate (excitation 467 nm, emission 511 nm) upon incubation with reconstituted 26S proteasome. Degradation reactions contained limiting amounts of core particle (yeast) and saturating concentrations of base (*E. coli*-expressed), lid (yeast), and 1 μM Rpn10 (*E. coli*-expressed). To establish that excess amounts of free lid and Rpn10 did not interact with our ubiquitinated substrate and adversely affect the measured degradation rates, we added increasing amounts of **(a)** Rpn10 or **(b)** lid and observed that the degradation rate remained constant.

2.4 Materials and Methods

2.4.1 Cloning, expression and purification of recombinant base

Thirteen subunits were cloned into three Novagen vectors including pCOLA-1 (FLAG-Rpt1, Rpt2, His_6-Rpt3, Rpt4, Rpt5, Rpt6), pETDuet-1 (Rpn1, Rpn2, Rpn13), and pACYC Duet-1 (Nas2, Nas6, Hsm3, Rpn14). Each subunit was preceded by a T7 promoter and all plasmids contained one T7 terminator at the end of the multiple cloning sites. Genes for rare tRNAs were also included in the pACYCDuet-1 plasmid to account for differences in codon usage between yeast and *E. coli*. Base expression strains were generated by co-transforming the pETDuet-1, pCOLA-1 and pACYCDuet-1 plasmids into *E. coli* BL21-star (DE3) cells. The base subcomplex was produced by growing the expression strain to OD_{600}=0.6-0.8 and inducing with 1 mM isopropyl-β-D-thiogalactopyranoside overnight at 18 °C. Cells were harvested by centrifugation at 5000 rpm for 15 minutes, resuspended in nickel buffer (25 mM HEPES pH 7.6, 100 mM NaCl, 100 mM KCl, 10% glycerol, 10 mM $MgCl_2$, 0.5 mM EDTA, 20 mM imidazole) supplemented with 2 mg ml^{-1} lysozyme, protease inhibitors and benzonase. Cells were lysed by freeze-thaw and sonication on ice for 1 minute 30 seconds in 15 second bursts. Lysate was clarified by centrifugation at 15,000 rpm at 4 °C for 30 minutes. A two-step affinity purification of the base subcomplex was performed using Ni-NTA agarose (Qiagen) to select for His_6-Rpt3 and anti-FLAG M2 resin (Sigma-Aldrich) selecting for FLAG-Rpt1. 0.5 mM ATP was present in all purification buffers. The Ni-NTA and anti-FLAG M2 columns were eluted with nickel buffer containing 250 mM imidazole or 0.15 mg ml^{-1} 3xFLAG peptide, respectively. The Flag column eluate was concentrated using a 30,000 MWCO concentrator (Amicon) and run on a Superose 6 gel filtration column (GE Healthcare) equilibrated with gel filtration buffer (60 mM HEPES pH 7.6, 50 mM NaCl, 50 mM KCl, 10% glycerol, 5 mM $MgCl_2$, 0.5 mM EDTA, 1 mM DTT, 0.5 mM ATP). See Appendix C for detailed protocol.

2.4.2 Purification of endogenous yeast complexes

Yeast holoenzyme, core particle, base and lid subcomplexes were purified from *S. cerevisiae* essentially as previously described (Leggett et al., 2005). Frozen yeast cells were lysed using a Spex SamplePrep 6870 Freezer/Mill. Holoenzyme was purified from a yeast strain containing FLAG-Rpn11. Lysed cells were resuspended in lysis buffer containing 60 mM HEPES pH 7.6, 100 mM NaCl, 100 mM KCl, 10% glycerol, 5 mM $MgCl_2$, 0.5 mM EDTA, 0.2% NP-40 and ATP regeneration mix (5 mM ATP, 0.03 mg ml^{-1} creatine kinase, 16 mM creatine phosphate). Holoenzyme was bound to anti-FLAG M2 resin and washed with wash buffer (60 mM HEPES pH 7.6, 100 mM NaCl, 100 mM KCl, 10% glycerol, 5 mM $MgCl_2$, 0.5 mM EDTA, 0.1% NP-40, 0.5 mM ATP). Holoenzyme was eluted with 0.15 mg ml^{-1} 3xFLAG peptide and further purified by gel filtration using a Superose 6 column with gel filtration buffer (see above). Lid and base subcomplexes were isolated from FLAG-Rpn11 or FLAG-Rpn2 yeast strains, respectively, and purified by exposure to a 1 M NaCl wash while

bound to anti-FLAG M2 resin. Base purification buffers included 0.5 mM ATP. Core particle was purified from a 3xFLAG-Pre1 yeast strain using a 500 mM salt wash. All subcomplexes underwent size exclusion chromatography using a Superose 6 column as described above.

2.4.3 Yeast strains

Yeast lid and holoenzyme were purified from strain YYS40 (genotype MATa ade2-1 his3-11,15 leu2-3,112 trp1-1 ura3-1 can1 Rpn11::Rpn11-3XFLAG(HIS3), source Y. Saeki). Core particle was prepared either from strain RJD1144 (genotype MATa his3-200 leu2-3,112 lys2-801 trp-63 ura3-52 PRE1-FLAG-6xHIS::Ylpac211(URA3) source R. Deschaies) or strain yAM14 (genotype MATa ade2-1 his3-11,15 leu2-3,112 trip1-1 ura3-1 can1-100 bar1 PRE1::PRE1-3XFLAG(KanMX), this work).

2.4.4 Native gel electrophoresis

Analysis of proteasome holoenzyme and subcomplexes by native gel was performed as described previously (Leggett et al., 2005). Assembly reactions were incubated for 15 minutes at 23 °C with 5 mM ATP, followed by electrophoresis on a 3.5% native polyacrylamide gel. Electrophoresis was conducted at 4 °C with stirring and running buffer containing 0.5 mM ATP. The gel was overlaid with developer solution (running buffer with 100 nM Suc-LLVY-AMC peptide (Boston Biochem) and 0.02% SDS) and incubated at 30 °C for 10 minutes prior to imaging. Fluorescence imaging was performed using a Typhoon scanner (GE Healthcare) and followed by Coomassie staining.

2.4.5 ATPase and peptidase stimulation assays

ATPase activity was quantified using an NADH-coupled ATPase assay. 500 nM base was incubated with 1x ATPase mix (3 U ml^{-1} pyruvate kinase, 3 U ml^{-1} lactate dehydrogenase, 1 mM NADH, 7.5 mM phosphoenol pyruvate) at 30 °C. Absorbance at 340 nm was monitored for 900 seconds at 10 second intervals using a UV-Vis Spectrophotometer (Agilent). Peptidase stimulation was monitored by following the increase in fluorescence resulting from cleavage of a fluorogenic peptide substrate (Glickman et al., 1998), Suc-LLVY-AMC (Boston Biochem), using a QuantaMaster spectrofluorimeter (PTI). 50 nM core particle was incubated with saturating base subcomplex in the presence of an ATP regeneration system (5 mM ATP, 16 mM creatine phosphate, 6 mg ml^{-1} creatine phosphokinase) and 50 μM Suc-LLVY-AMC.

2.4.6 Gel-based substrate degradation assay

The model substrate, green fluorescent protein (GFP)-titin^{V15P}-cyclin-PY, was labeled at the N-terminus with Cy5 dye and subsequently modified with a polyubiquitin chain in vitro using Uba1, Ubc1, Rsp5 and wild-type ubiquitin. The non-ubiquitinated substrate

was prepared similarly except ubiquitin was omitted from the reaction. Degradation was assessed by incubating substrates with 26S holoenzyme purified from yeast in the presence of an ATP regeneration system at 30 °C for one hour. Substrate degradation was then assessed by running samples on a SDS-PAGE gel followed by fluorescence scanning to detect the Cy5-labeled substrate (670 nm band-pass 30 filter), western blotting using an anti-GFP antibody, or Coomassie staining for total protein.

2.4.7 Fluorescent substrate degradation assay

Proteasome holoenzyme was reconstituted from core particle, lid, base and Rpn10. A GFP-titin^{V15P}-cyclin-PY fusion protein was modified *in vitro* with a polyubiquitin chain using Uba1, Ubc1, Rsp5 and wild-type ubiquitin. Degradation reactions were performed at 30 °C in gel filtration buffer (60 mM HEPES pH 7.6, 50 mM NaCl, 50 mM KCl, 10% glycerol, 5 mM $MgCl_2$, 0.5 mM EDTA, 1 mM DTT, 0.5 mM ATP) supplemented with an ATP regeneration system. Degradation activities were monitored by the loss of GFP fluorescence (excitation 467 nm; emission 511 nm) using a QuantaMaster spectrofluorimeter (PTI). Multiple turnover degradation experiments were performed with 50 nM reconstituted holoenzyme under V_{max} conditions (saturating base, lid and Rpn10) with 2 μM substrate. Excess base, lid, and Rpn10 did not affect the observed degradation rate (see Figure 2.6 for lid and Rpn10).

CHAPTER 3

Functional asymmetry of the proteasomal AAA+ unfoldase

A portion of the work presented in this chapter has been previously published as part of the following paper: Beckwith, R., Estrin, E., Worden, E., and Martin, A. Reconstitution of the 26S proteasome reveals functional asymmetries in its AAA+ unfoldase. Nat Struct Mol Biol, 20:1164-1172, 2013.

Robyn Beckwith performed mutagenesis, protein purification, biochemical characterization, enzyme kinetics, and wrote the manuscript with Dr. Andreas Martin. Eric Estrin contributed data for the pore-2 loop base mutants. Evan Worden contributed data for the C-terminal tail base mutants.

3.1 Introduction

The ubiquitin-proteasome system (UPS) is the major pathway for selective protein degradation in all eukaryotic cells, where it mediates protein quality control and the destruction of critical regulatory proteins (Hochstrasser, 1996; Finley, 2009). Protein substrates are covalently modified with a poly-ubiquitin chain and targeted to the 26S proteasome for ATP-dependent proteolysis. Despite this crucial role of the UPS for protein degradation, the mechanistic principles of the proteasome still remain largely elusive.

The eukaryotic 26S proteasome is a 2.5 MDa molecular machine formed from at least 33 different subunits. It consists of a barrel-shaped 20S core particle that is capped on one or both ends by the 19S regulatory particle. The core particle contains an internal chamber with sequestered proteolytic active sites and gated axial pores to restrict substrate entry (Groll et al., 2000). Access to this chamber is controlled by the regulatory particle, which is also responsible for recognition, deubiquitination, engagement, unfolding, and translocation of substrate (Glickman et al., 1998; Thrower et al., 2000; Liu et al., 2006; Smith et al., 2007). The regulatory particle includes 19 different subunits and can be divided into the base and lid subcomplexes. The base contains a ring of six distinct AAA+ ATPases in the order Rpt1-2-6-3-4-5 (Tomko et al., 2010; Tomko and Hochstrasser, 2011), which constitute the ATP-dependent motor of the proteasome and dock atop the core particle. Additional integral components of the base are the ubiquitin receptor Rpn13 as well as two large scaffolding subunits, Rpn1 and Rpn2 (Hamazaki et al., 2006; Beck et al., 2012; Lander et al., 2012). The nine-subunit lid, which includes the deubiquinating enzyme Rpn11 (Verma et al., 2002; Yao and Cohen, 2002), binds asymmetrically to the side of the base-core complex and positions the second ubiquitin receptor, Rpn10, close to the lid-base interface above the entrance of the processing pore (Beck et al., 2012; Lander et al., 2012; Sakata et al., 2012)

Once a substrate is tethered to a proteasomal ubiquitin receptor, a complex set of enzymatic activities defines the pathway to degradation. The substrate must be deubiquitinated by Rpn11, while the ATPase ring of the base engages an unstructured degradation-initiation region of the protein, mechanically disrupts globular structures, and translocates the unfolded polypeptide into the peptidase chamber. ATP hydrolysis by the Rpt subunits of the base is crucial for substrate degradation, yet it remains unclear how these six distinct subunits work together to drive ATP-dependent unfolding and translocation.

Previous studies of the related homohexameric unfoldase ClpX suggest that ATP hydrolysis occurs in one subunit at a time with a certain degree of coordination, such that subunits may contribute additively and equally to substrate processing (Martin et al., 2005). However, the homomeric nature of ClpX hinders assessment of whether all six subunits indeed sequentially progress through the different stages of the ATP-hydrolysis cycle. The unique heterohexameric architecture of the proteasomal ATPase ring has thus prompted the fundamental question whether the six Rpts are functionally equivalent or play distinct roles in ATP hydrolysis and substrate processing. While Rpt1-6 share highly homologous AAA+ ATPase domains, they differ substantially in their N-terminal coiled-coil domains, which interact with the laterally bound lid, and in their C-terminal unstructured tails, which

mediate interaction with the core particle and trigger gate opening to the proteolytic chamber (Smith et al., 2007; Gillette et al., 2008; Rabl et al., 2008; Kim and DeMartino, 2011). Furthermore, recent EM structures of the apo and substrate-bound 26S proteasome revealed distinct vertical asymmetries within the base ATPase ring (Beck et al., 2012; Lander et al., 2012; Matyskiela et al., 2013; Sledz et al., 2013). In the absence of substrate, the large AAA+ subdomains of Rpt1-6 adopt a pronounced spiral-staircase configuration, with Rpt3 at the top and Rpt2 at the bottom position. Strikingly, upon substrate engagement, the base switches to a more planar ring conformation that is characterized by a spiral staircase with Rpt1 at the top and Rpt4 at the bottom (Matyskiela et al., 2013). However, the functional significance of these staircase configurations, potentially manifested as differential subunit contributions to substrate degradation or subcomplex interactions within the holoenzyme, has yet to be determined.

Endogenous 26S proteasome has been used to investigate the role of individual Rpts, revealing functional differences in their contributions to base assembly, 26S holoenzyme formation, ATP hydrolysis, peptidase gate opening, and substrate degradation (Rubin et al., 1998; Kohler et al., 2001; Smith et al., 2007; Park et al., 2009; Thompson et al., 2009; Kumar et al., 2010; Erales et al., 2012; Kim et al., 2012; Lee et al., 2012). Despite these results, limitations in working with endogenous proteasome, in part due to *in-vivo* assembly problems or lethal degradation defects, have largely prevented extensive systematic studies and a quantitative mechanistic understanding of the individual processes involved in substrate degradation.

Here, we investigated the mechanisms underlying ATP-dependent substrate processing by the heterohexameric unfoldase of the 26S proteasome. To define the differential contributions of individual Rpts to ATP hydrolysis, substrate degradation, peptidase binding, and gate opening, we developed systems for the heterologous expression of the base subcomplex and the *in-vitro* reconstitution of partially recombinant proteasomes, and performed systematic mutational analyses of key catalytic and structural motifs.

3.2 Results

3.2.1 Individual ATPase subunits have distinct roles in substrate processing

To examine the roles of Rpt1-6 in nucleotide-dependent substrate processing, we individually abolished their ATP hydrolysis by systematically introducing a catalytic mutation in the recombinant base. In the homohexameric bacterial unfoldase ClpX, mutation of the conserved Walker-B glutamate prevents hydrolysis and induces a permanently ATP-bound state in the mutated subunit (Hersch et al., 2005), but other AAA+ unfoldases require distinct Walker-B mutations to eliminate ATP-hydrolysis activity (Gomez et al., 2002; Weibezahn et al., 2004). We therefore tested the effects of various substitutions of the conserved Walker-B aspartate and glutamate residues by simultaneously placing them in all six Rpts (see Sec-

tion 3.4.2). Ultimately, mutation of glutamate to glutamine (EQ) allowed proper assembly of base that exhibited wild-type levels of peptidase-binding and gate-opening activities despite being inactive in ATP hydrolysis (Table 3.1), indicating that this mutation in fact traps Rpt subunits in a permanently ATP-bound state. We next introduced a single EQ mutation per hexamer to fix individual Rpts in the ATP-bound state and test their contributions to ATP hydrolysis as well as core-gate opening. Depending on which subunit was mutated, we observed considerable differences in activities (Table 3.1), indicating that the Rpt subunits are functionally non-equivalent.

ATP hydrolysis by the isolated base decreased by more than 60% upon mutation of Rpt3, whereas inactivating other subunits had either minor effects (Rpt1, Rpt4, Rpt5) or notably increased the hydrolysis rate (Rpt2, Rpt6). Peptidase stimulation by these base mutants also varied: mutated Rpt5, Rpt2, and Rpt6 caused 20%, 30%, and 60% stronger gate opening compared to wild-type base, mutated Rpt4 did not lead to noticeable changes, while mutations in Rpt3 or Rpt1 decreased gate-opening activity by 20% or 30% despite proper complex formation with the core particle. It is important to consider that the measured ATPase and gate-opening activities reflect an average of the unmutated five Rpt subunits and are influenced by subunit communication. The increase in ATPase activity resulting from mutation of Rpt2 and Rpt6, for instance, is likely caused by the response of neighboring subunits to a permanently ATP-bound state. Some of these stimulated ATP-hydrolysis events may be non-productive and thus not result in increased substrate-degradation rates. This is supported by the fact that most base variants containing a mutant Rpt showed no stimulation or even slight repression in ATP-hydrolysis activity upon the addition of substrate, whereas the ATPase rate of wild-type base approximately doubled (Figure 3.1).

To explore the distinct roles of individual Rpt subunits in substrate processing, we reconstituted proteasomes with base variants containing single-subunit EQ mutations and compared their rates of ubiquitin-mediated substrate degradation under multiple-turnover conditions (Figure 3.2). An EQ mutation in either Rpt3 or Rpt4 completely eliminated substrate degradation, and a mutated Rpt6 resulted in a 90% decrease in degradation rate. Mutations in Rpt1 and Rpt5 lowered the degradation rate by 73% and 56%, respectively, whereas the Rpt2 mutant showed no defect. Importantly, the observed degradation defects were not simply the result of compromised proteasome assembly, as all mutants stimulated peptidase-gate opening (Table 3.1) and bound lid and core particle (Figure 3.3). Considering the order of ATPase subunits within the base (Rpt1-2-6-3-4-5), it is strikingly evident that mutants with severe degradation defects (Rpt6, Rpt3, and Rpt4) map to one half of the ring.

Next we investigated the mechanistic role of individual Rpts at different stages of substrate processing by performing single-turnover degradation experiments (Figure 3.2, Figure 3.4). In contrast to steady-state analyses, these measurements discriminate between potential defects in substrate engagement versus translocation and unfolding. The resulting data for GFP-substrate turnover were best fit by a double-exponential decay. Since GFP loses fluorescence in a single unfolding step, this double-exponential behavior was likely due to two types of substrates that probably varied in their ubiquitin tagging and were degraded at different rates. As expected, the two rates averaged to roughly match the multiple-turnover

rate, and the base mutants exhibited the same ranking of activities as in multiple-turnover degradation (Figure 3.2, Table 3.1). Even under these single-turnover conditions, Rpt3 or Rpt4 mutants did not show any measurable degradation, whereas the Rpt6 mutant degraded substrate at 5% of the wild-type rate. This Rpt6 mutant exhibited a short lag preceding the

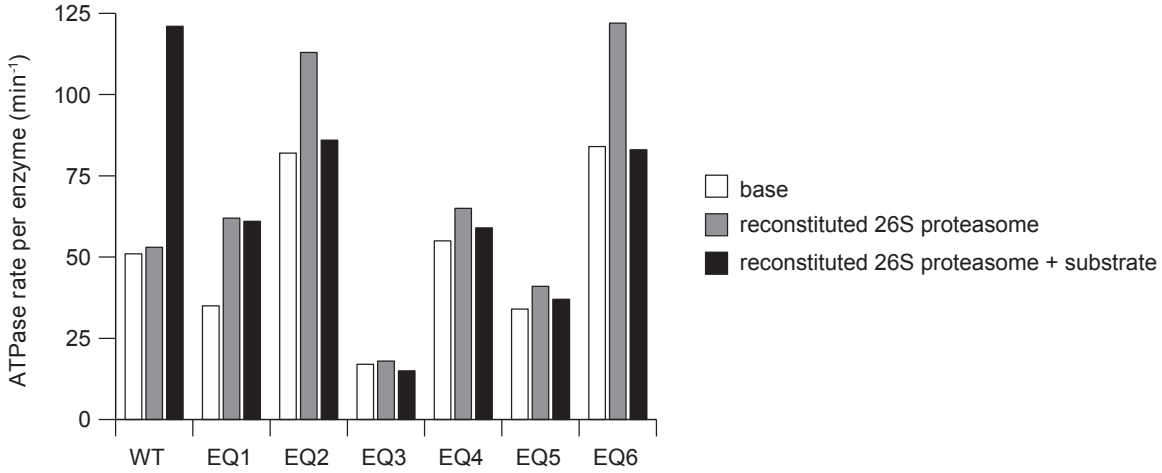

	basal ATPase rate (base)		basal ATPase rate (reconstituted 26S)		working ATPase rate (reconstituted 26S proteasome + ubiquitinated substrate)	
	min^{-1}	% WT	min^{-1}	% WT	min^{-1}	% WT
WT	51	100	53	103	121	237
EQ1	35	68	62	122	61	120
EQ2	82	161	113	221	86	169
EQ3	17	33	18	36	15	28
EQ4	55	108	65	127	59	116
EQ5	34	67	41	81	37	72
EQ6	83	164	122	240	83	162

Figure 3.1: ATP hydrolysis rates for Walker-B EQ mutant base subcomplexes are not stimulated by ubiquitinated substrate.
Stimulation of ATPase activity by the base in the presence of ubiquitinated substrate was determined using a NADH-coupled ATPase assay. **(a)** Basal rates of ATP hydrolysis per enzyme (base hexamer) were determined both for base subcomplexes alone (white) and reconstituted 26S proteasomes containing the base variants (gray). Working ATPase rates were measured by adding ubiquitinated substrate to reactions containing reconstituted 26S proteasomes (black). **(b)** Table expressing the data from (a) in terms of ATP hydrolyzed per enzyme per minute and as a percentage of the rate observed for wild-type (WT) base alone. Errors for the ATPase assay were estimated to be ±10% of the WT mean value.

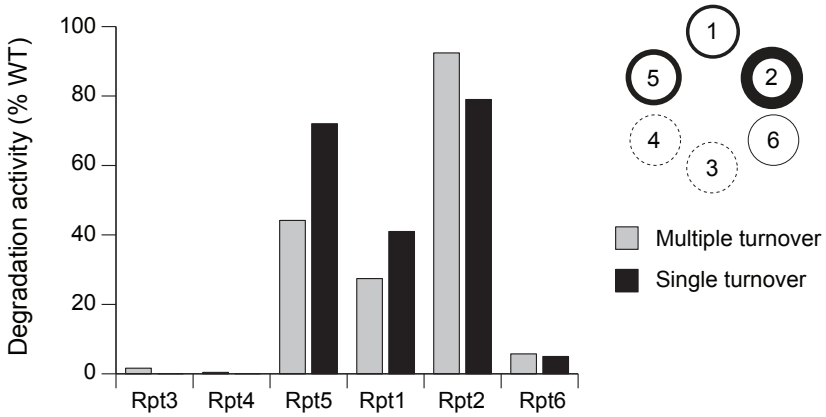

Figure 3.2: Single- and multiple-turnover degradation rates for proteasomes with EQ base mutants.
In vitro degradation rates for reconstituted proteasomes containing base variants with individual Rpt subunits fixed in a permanent ATP-bound state by the Walker-B E→Q mutation. Degradation under multiple-turnover (gray) and single-turnover (black) conditions was monitored by the loss of fluorescence during degradation of a polyubiquitinated GFP fusion substrate. Degradation activities were measured relative to that of the reconstituted proteasome containing wild-type (WT) recombinant base. Errors for multiple-turnover degradation rates were estimated to be ±10% (s.d.) of the mean WT value on the basis of repeat measurements. The circular diagram is an alternative representation of the multiple-turnover data, with each number referring to the respective Rpt subunit and the line thickness corresponding to the observed degradation activity for a mutation in that subunit.

exponential fluorescence decay (Figure 3.4), which may indicate delayed substrate translocation and unfolding due to defects in engagement. The 95% decrease in degradation rate may thus originate from slower engagement instead of or in addition to compromised unfolding and translocation. The complete lack of substrate degradation for ATPase-deficient Rpt3 or Rpt4 may similarly be a consequence of severe engagement defects.

3.2.2 Spiral staircase configuration of ATPase large AAA+ domains

EM reconstructions of the ATP-bound 26S proteasome in the absence of substrate revealed that the large AAA+ subdomains of the Rpts adopt a pronounced spiral-staircase configuration around the ring (Beck et al., 2012; Lander et al., 2012). Rpt3 occupies the highest and Rpt2 the lowest position relative to the core particle, with Rpt6 bridging the vertical gap between the two subunits (Figure 3.5). The degradation defects of EQ mutants and the inferred contributions of individual Rpts to substrate degradation largely correlate with the vertical positions of subunits in this pre-engaged staircase. Conformational changes

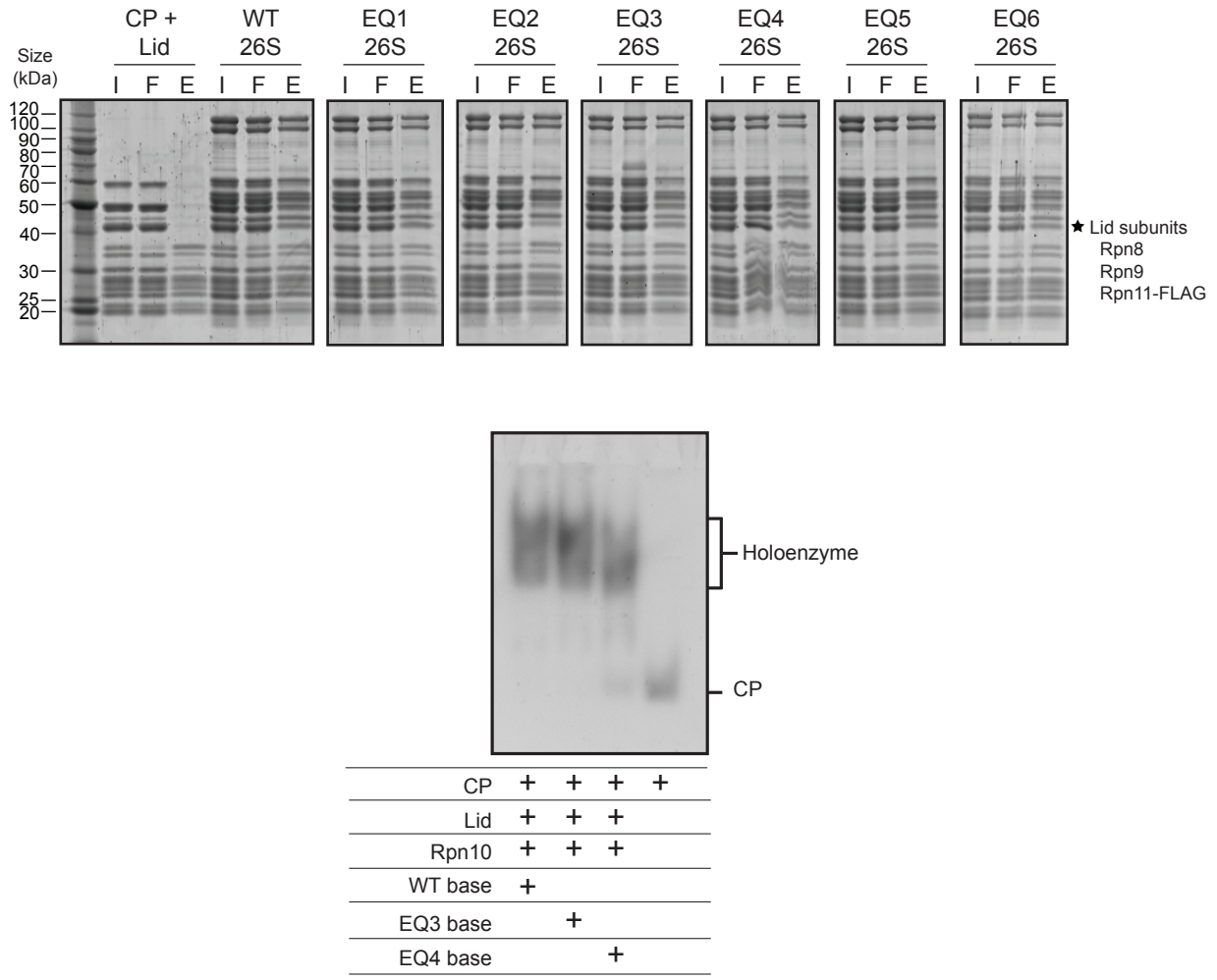

Figure 3.3: Base variants with single-subunit Walker-B EQ mutations assemble into 26S proteasome holoenzymes.
(a) Nickel affinity pulldown assay followed by SDS-PAGE analysis with Sypro Ruby staining to examine the assembly state of 26S proteasomes reconstituted with either wild-type (WT) or EQ base mutants. Untagged lid subcomplex was pulled down using His_6 tags on Rpt3 (base), Pre1 (core particle, CP) and Rpn10. Lanes for each sample are labeled I (input), F (flow through) and E (elution). Equivalent amounts of lid were observed for 26S proteasomes reconstituted with WT or EQ mutant base variants as indicated by a strong band containing the lid subunits Rpn8, Rpn9 and Rpn11-FLAG (black star). **(b)** Native gel analysis demonstrating that WT, EQ3 and EQ4 base variants are competent for assembly into 26S holoenzyme. Assembly of proteasomes was performed by incubating constituent subcomplexes with ATP, followed by native polyacrylamide gel electrophoresis as described in the methods.

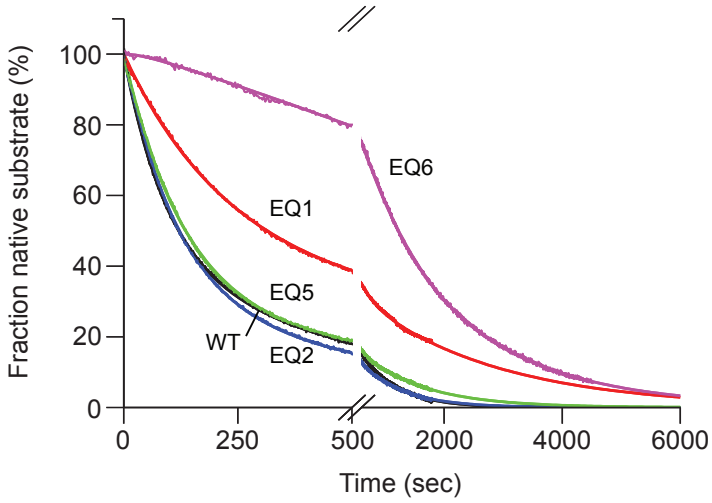

Figure 3.4: Single-turnover degradation traces for proteasomes with EQ base mutants. Degradation under single-turnover conditions was monitored by the decrease in fluorescence of 100 nM polyubiquitinated GFP-fusion substrate (excitation 467 nm, emission 511 nm) upon incubation with 2 μM 26S proteasome reconstituted with either WT base or EQ base variants. Proteasomes reconstituted with EQ3 or EQ4 base variants did not exhibit any measurable degradation even under single turnover conditions. Curves were best fit with a double exponential decay, likely reflecting degradation of two subpopulations of the substrate. These classes of substrate probably differ in the number or location of conjugated polyubiquitin chains but their affinity for the proteasome is expected to be similar.

in subunits at the top of the apo spiral (Rpt3, Rpt4 and Rpt6) thus appear to be critical to engage a substrate and initiate translocation, whereas subunits in lower positions are less important.

Our recent EM reconstruction of the translocating proteasome (Matyskiela et al., 2013) demonstrated that substrate engagement induces substantial conformational changes in the regulatory particle, leading to a more planar ATPase-ring with a rearranged staircase of pore loops, in which Rpt1 is at the top and Rpt4 at the bottom position (Figure 3.5). Based on the static appearance of the spiral, in combination with single-molecule data for the related protease ClpXP, we previously proposed that the substrate-engaged staircase represents a default dwell state that is adopted by the base before or after coordinated ATP-hydrolysis events progress around the ATPase ring (Matyskiela et al., 2013). Interestingly, in the present study we observed an approximately 70% reduction in degradation activity when ATP hydrolysis was eliminated in Rpt1, located at the top of the substrate-engaged staircase. Rpt1 may therefore play a special role in processive substrate translocation, possibly by triggering the coordinated ATP hydrolysis of subunits.

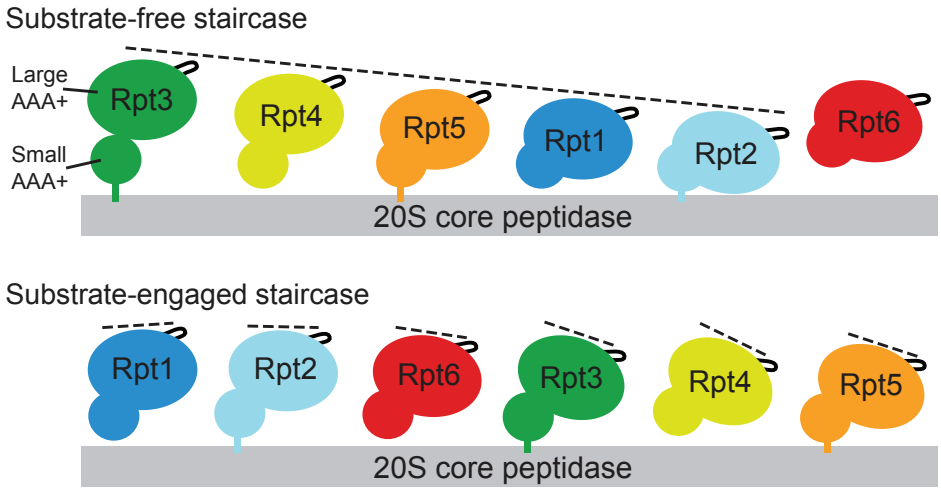

Figure 3.5: Spiral staircase configurations of proteasomal ATPases in the presence and absence of substrate.
The large AAA+ subdomains of Rpt1-Rpt6 adopt distinct spiral staircase arrangements in the absence or presence of substrate. Shown are cartoon representations of the pre-engaged (top) and substrate-engaged (bottom) staircases based on cryo-EM reconstructions (Lander et al., 2012; Matyskiela et al., 2013). In the pre-engaged spiral, the small AAA+ subdomains of Rpt1-Rpt6 are arranged in a relatively planar fashion, whereas the large AAA+ subdomains are differentially lifted out of the ring plane, resulting in a pronounced spiral staircase with Rpt3 in the highest position and Rpt2 in the lowest position. In the substrate-engaged spiral, the small and large AAA+ subdomains are mostly level, and the staircase orientation of the pore loops originates primarily from differential rotations of subdomains in the plane of the ring.

3.2.3 Contribution of individual pore loops to substrate processing

Previous work on various AAA+ unfoldases proposed that a conserved aromatic hydrophobic (Ar-ϕ) loop protrudes from every ATPase subunit into the central channel and undergoes nucleotide-dependent power strokes to drive substrate translocation (Wang et al., 2001; Yamada-Inagawa et al., 2003; Hinnerwisch et al., 2005; Park et al., 2005; Martin et al., 2008a,b; Aubin-Tam et al., 2011; Maillard et al., 2011; Erales et al., 2012). To study these loop functions in the proteasome, we constructed base variants with tyrosine-to-alanine mutations in the Ar-ϕ loop of individual Rpts (Table 3.1, Figure 3.6a). Loop mutations in Rpt3, Rpt4, or Rpt6 decreased the rate of ATP hydrolysis by 15-25%, whereas mutations in Rpt1, Rpt2, and Rpt5 stimulated ATPase activity by 30-75% compared to wild-type base. Ar-ϕ-loop mutations have been observed to stimulate ATP hydrolysis in some AAA+ unfoldases, including ClpX and the proteasome (Martin et al., 2008a; Erales et al., 2012), likely

due to reduced steric constraints on loop movements within the central pore. In addition, subunit communication may induce changes in neighboring, non-mutated subunits, making it infeasible to specify individual Rpt contributions to overall ATP-hydrolysis activity using only the Ar-ϕ-loop data.

All Ar-ϕ-loop mutants exhibited peptidase-gate opening activities at 65-85% of the wild-type level, with the exception of mutant Rpt2, which had 38% activity (Table 3.1). Rpt2 occupies the lowest position in the apo staircase of ATPases, and docking the PAN crystal structure into the Rpt2 EM density indicates that its Ar-ϕ loop is located close to the core-particle interface, where direct or indirect contacts with the N-termini of α-subunits may affect gating. However, despite this defect in gate-opening activity, the Ar-ϕ-loop mutation in Rpt2 did not lower the base affinity for the core particle (K_D = 138 nM versus K_D = 127 nM for wild-type base).

Proteasomes reconstituted with the Ar-ϕ mutant base variants degraded substrate at substantially different rates (Figure 3.6a). The biggest defects were observed for mutations in Rpt4 and Rpt2, which are localized clockwise-next to the top subunit in the substrate-free

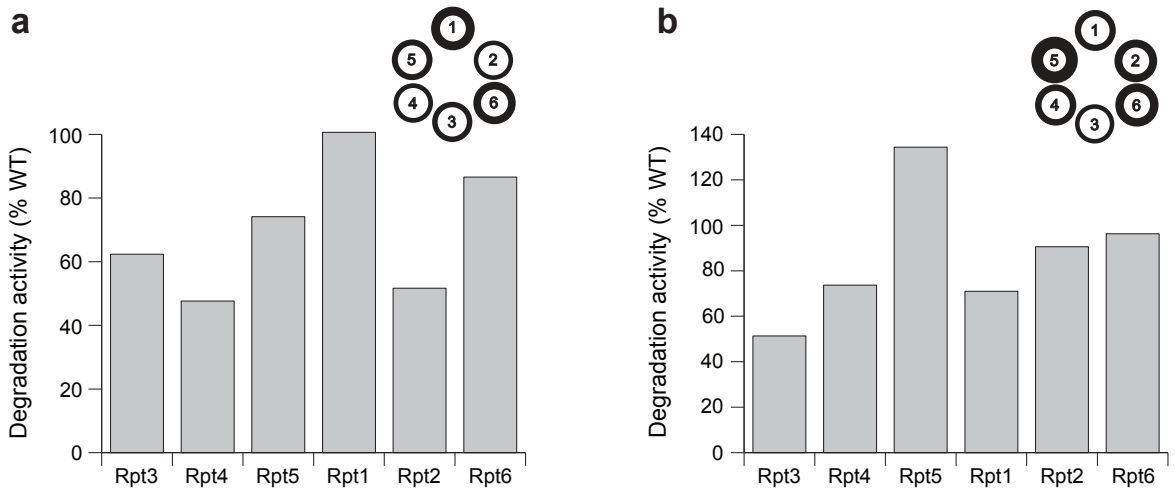

Figure 3.6: Degradation activities for base variants containing single-subunit pore-1 or pore-2 loop mutations.
Degradation of the polyubiquitinated GFP fusion substrate was monitored by the loss of fluorescence after addition of proteasomes reconstituted with base variants containing **(a)** Y→A mutations in the Ar-ϕ loops or **(b)** D→N mutations in the pore-2 loops of single Rpt subunits. Degradation activities under saturating conditions were measured relative to that of the reconstituted proteasome containing WT recombinant base. Errors were estimated to be ±10% (s.d.) of the mean WT value on the basis of repeat measurements (n = 3 technical replicates). The circular diagrams are alternative representations, with the line thickness corresponding to the observed degradation activities for a mutation in the respective subunit.

and substrate-engaged spiral staircase, respectively. That the ranking of defects for Ar-ϕ-loop mutations appears shifted clockwise by one subunit relative to the defects observed for Walker-B mutants likely results from the fact that loop mutations primarily act in cis on a subunit's ability to translocate, whereas eliminating ATP-hydrolysis may affect conformational changes in the clockwise-next subunits. This would be consistent with the rigid-body model recently proposed for ClpX (Glynn et al., 2009, 2012), in which the small AAA+ subdomain of one subunit and the large AAA+ subdomain of its clockwise-next neighbor move as one unit to propel substrate through the pore. ATP hydrolysis in a particular subunit might thus drive movements of the clockwise-next rigid body, which includes the substrate-interacting Ar-ϕ loop of the neighboring subunit. For the proteasome, only the rigid body between Rpt3 and Rpt4 at the top of the spiral staircase appears to be present in the absence of substrate (Lander et al., 2012), while the remaining rigid bodies form during substrate-induced conformational changes (Matyskiela et al., 2013). Those rigid bodies within the substrate-engaged ATPase ring could thus cause the ranking of Rpt contributions to appear shifted by one subunit when comparing Ar-ϕ-loop and Walker-B mutants.

Our data qualitatively coincide with results from a recent study using endogenous 26S proteasomes from yeast, demonstrating a comparable ranking of degradation defects for individual Ar-ϕ-loop mutations (Erales et al., 2012), with the exception of Rpt2. The fact that no single Ar-ϕ-loop mutation completely abrogated degradation may indicate that multiple Rpts simultaneously interact with substrate during engagement and translocation, as suggested for the bacterial unfoldase ClpX (Martin et al., 2008a). Furthermore, removal of the Ar-ϕ-loop tyrosine may not fully abolish pore-loop function and thus cause much weaker defects than a Walker-B mutation, which traps the entire subunit in a static ATP-bound state.

The pore-2 loop, located below the Ar-ϕ loop in the central channel and directly adjacent to the Walker-B motif, has been implicated in substrate binding and unfolding as well as peptidase interaction and the control of ATPase activity in ClpX (Martin et al., 2007, 2008b; Glynn et al., 2009). A recent study on the archaeal homohexameric unfoldases Cdc48 and PAN suggested that the pore-2 loop also interacts with the proteasomal core particle (Barthelme and Sauer, 2013). As the importance of the pore-2 loop for 26S-proteasome function is still unknown, we replaced the highly conserved aspartate with asparagine (DN) in the pore-2 loops of individual Rpts, with Rpt2 requiring a glutamate to asparagine mutation in this position. Base variants with a single pore-2-loop mutation hydrolyzed ATP up to three-fold faster than wild type, with the exception of Rpt1, which showed a 25% decrease (Table 3.1). The increased ATPase rates are reminiscent of previous observations for ClpX49 and may result from induced structural changes in the pore-2 loop that affect the adjacent Walker-B portion of the ATPase active site. Proteasomes reconstituted with pore-2-loop mutants exhibited a wide range of degradation rates (Figure 3.6b), with the most severe defect observed for Rpt3, located at the top of the substrate-free staircase. Changes in substrate degradation did not directly correlate with changes in ATP hydrolysis, indicating that, similar to our observations for the Ar-ϕ loop, pore-2-loop mutations may interfere with substrate interactions and thus result in futile ATP-hydrolysis events. The largest discrepancies

between ATPase and degradation activities were observed for pore-2-loop mutations in Rpt3 and Rpt4, corroborating that Rpt subunits at the top of the pre-engaged staircase are particularly important for substrate processing, presumably by enabling efficient engagement. The degradation defects do not appear to be a consequence of compromised gate opening, as all pore-2-loop mutants show robust peptidase-gate opening activity, ranging from 84% to 192% compared to wild-type base (Table 3.1). The substantial variations in gate opening indicate that pore-2 loops are involved in unfoldase-peptidase communication and the Rpt C-terminal tails are not the sole determinants of the interaction between these subcomplexes. Our results thus further emphasize the functional differences between individual Rpts.

3.2.4 HbYX-containing C-terminal ATPase tails mediate both peptidase binding and gate opening

In contrast to the half-ring asymmetry of individual Rpt contributions to substrate degradation, previous studies suggested a three-fold symmetry for the base-core interaction, in which the C-terminal tails of Rpt2, Rpt3, and Rpt5 dock into core-particle pockets (Beck et al., 2012; Lander et al., 2012). Only these subunits contain the conserved C-terminal HbYX (hydrophobic/tyrosine/unspecified) motif that is critical for inducing core-particle gate opening (Smith et al., 2007; Gillette et al., 2008; Kim and DeMartino, 2011). The three remaining tails have been postulated to stabilize the complex (Smith et al., 2007), but recent crosslinking, structural, and biochemical studies provided further conflicting results on which C-terminal tails mediate core-particle binding (Tian et al., 2011; Lander et al., 2012; Matyskiela et al., 2013; Park et al., 2013). Moreover, it has been suggested that the nucleotide state of a Rpt subunit affects the conformation of its C-terminal tail, thereby modulating peptidase interaction (Smith et al., 2011). Individual Rpt subunits are thus expected to contribute differently to base-core interactions, but a detailed model for the specialized roles of C-terminal tails in peptidase binding, gate opening, and substrate transfer is lacking.

Our recombinant expression and *in-vitro* reconstitution system allows truncation of the Rpt C-terminal tails to quantitatively characterize their contributions to stability and function of the base-core complex. Consistent with previous studies, we found that the HbYX-containing tails of Rpt2, Rpt3, and Rpt5 were crucial for gate opening of the core particle. These three tails were independently and nearly equally important, as their individual truncation reduced gate-opening activity of the base by 90-95% (Figure 3.7a, Table 3.1). Surprisingly, removing the tail from Rpt6, which lacks an HbYX motif, also decreased gate opening by 75%, whereas truncating Rpt1 and Rpt4 had little effect.

Titration experiments revealed that the C-terminal tails of Rpt1, Rpt4, and Rpt6 do not contribute to the stability of the base-core complex. The three individual tailless mutants and the triple mutant bound to core particle with K_D values similar to or even lower than the wild-type value (Figure 3.8), which may indicate that those tails cause steric clashes or compete with neighboring HbYX-containing tails for designated binding pockets. In contrast, truncating HbYX tails strongly affected peptidase binding. Tail truncations in Rpt2 and

Rpt5 lowered the affinity for peptidase approximately 1.3-fold and 5.6-fold, respectively. Base lacking all three HbYX tails did not bind the peptidase (Figure 3.9). Affinity measurements for the base with tailless Rpt3 were impeded by the lack of a quantitative readout, as this mutant neither triggered core-gate opening nor exhibited core-mediated repression of ATPase activity.

Proteasomes reconstituted with saturating amounts of base lacking a single tail from Rpt2, Rpt3, or Rpt5 showed decreased substrate degradation at 44%, 16%, or 47% of the wild-type rate (Figure 3.7b), which is likely a consequence of gate-opening defects. Base with tailless Rpt6 supported degradation at greater than 80% of the wild-type rate. Robust degradation despite compromised gate-opening activity, as observed for Rpt6, may occur because translocation by the base pushes substrate through a partially opened gate, whereas the gate-opening assay reports solely on peptide diffusion into the peptidase.

3.2.5 Individual ATPase tails modulate peptidase gate opening in a nucleotide-independent manner

Interaction of base and core particle to open the gate is known to be ATP-dependent and differentially stimulated by various ATP-analogs (Smith et al., 2005; Liu et al., 2006; Li and DeMartino, 2009). It has been postulated for some homohexameric unfoldases, including

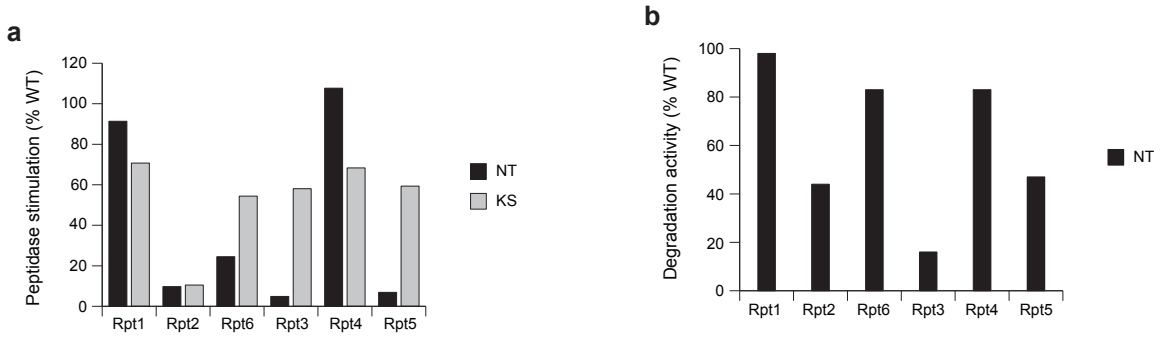

Figure 3.7: Rpt C-terminal tails contribute to gate opening differentially and in a nucleotide-independent manner.
(a) Base variants with either a C-terminal tail truncation (no tail, NT; black) or an empty-state Walker-A K→S mutation (KS, gray) in individual Rpt subunits were assessed for their ability to stimulate gate opening of the core particle relative to WT base. **(b)** Substrate degradation activities for proteasomes reconstituted with base subcomplexes containing C-terminal tail truncations of single Rpt subunits. Degradation of the polyubiquitinated GFP fusion substrate was monitored by the loss of fluorescence. Degradation rates under saturating conditions were measured relative to that of reconstituted proteasome containing WT recombinant base. Errors were estimated to be ±10% (s.d.) of the mean WT value on the basis of repeat measurements (n = 3 technical replicates).

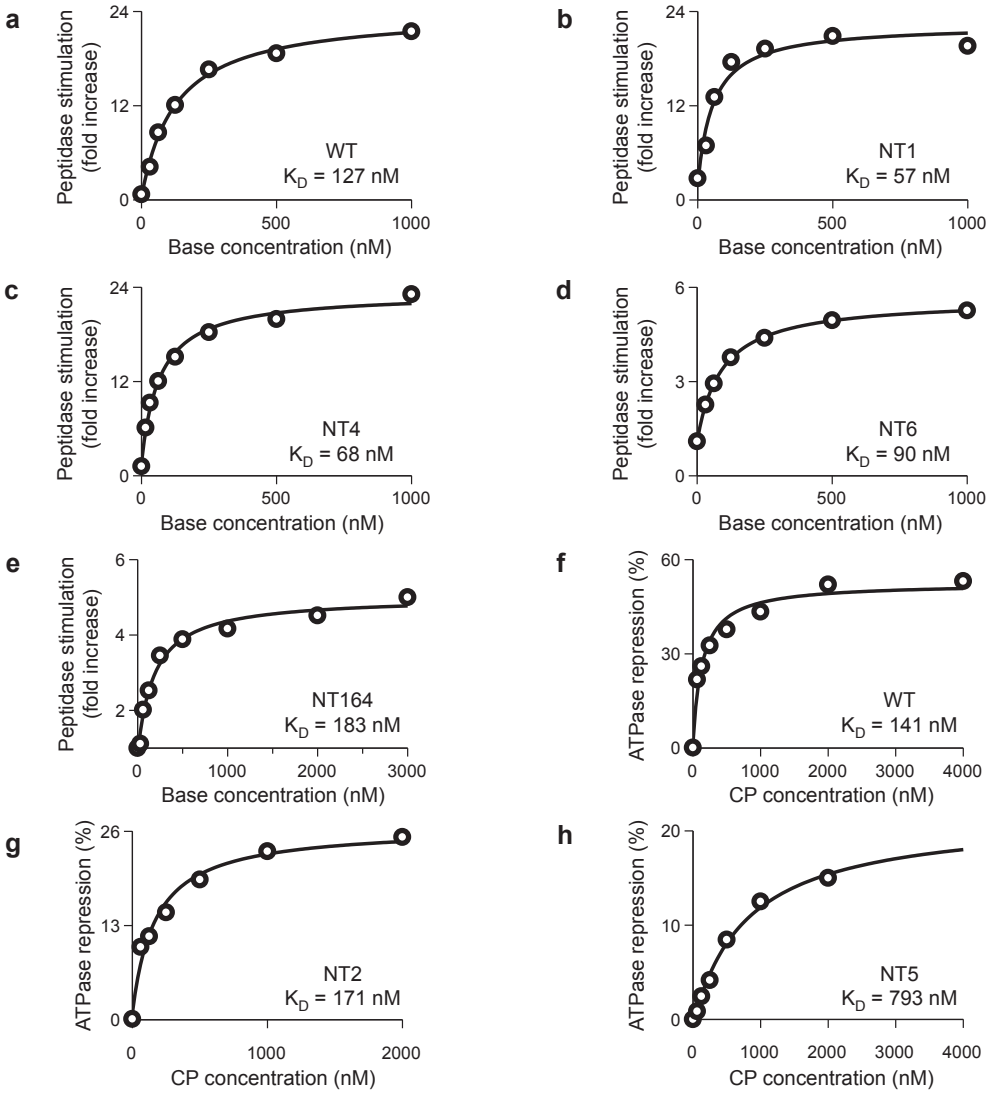

Figure 3.8: Affinities of core-peptidase binding for base variants lacking C-terminal tails. CP binding to base mutants with truncated C-terminal tails was quantified by titration measurements either in peptidase-stimulation or ATPase-repression assays. **(a-e)** Binding affinities of base variants competent to stimulate gate opening (NT1, NT4, NT6 and NT164) measured by titrating increasing amounts of base into a gate-opening assay containing 25 nM CP. **(f-h)** CP binding to base variants that did not exhibit substantial peptidase stimulation (NT2 and NT5) was assessed by titrating increasing amounts of CP into an NADH-coupled ATPase assay containing 100 nM base. CP-mediated repression of base ATPase activity yielded the bindings curves and K_D values.

PAN and HslU, that ATP hydrolysis may drive conformational changes in the C-terminal tails of individual subunits and thereby regulate nucleotide-dependent binding and gating interactions with the peptidase (Seong et al., 2002; Smith et al., 2005, 2007). Based on this model, an ATP-bound subunit would have an exposed C-terminal tail that interacts with the core particle, whereas an empty- or ADP-state subunit would have its tail buried in an occluded conformation. It was further proposed that at any given time the 26S proteasome has only two Rpt subunits, arranged in para position across the ring, in an ATP-bound state with C-terminal tails exposed for peptidase interaction (Smith et al., 2011).

We tested whether peptidase interaction of an Rpt tail in fact depends on the nucleotide state of the particular subunit. According to this model, removing a given tail should resemble trapping that subunit in an empty-state conformation. We therefore prevented nucleotide binding to individual Rpts by mutating the conserved lysine to serine (KS) in their Walker-A motifs (see Section 3.4.2). We produced base variants with single-subunit KS mutations and found that only mutation of Rpt2 caused severe base-assembly defects. Characterization of the other KS mutants demonstrated that trapping a particular Rpt subunit in an empty state has much weaker effects on gate-opening activity than truncating

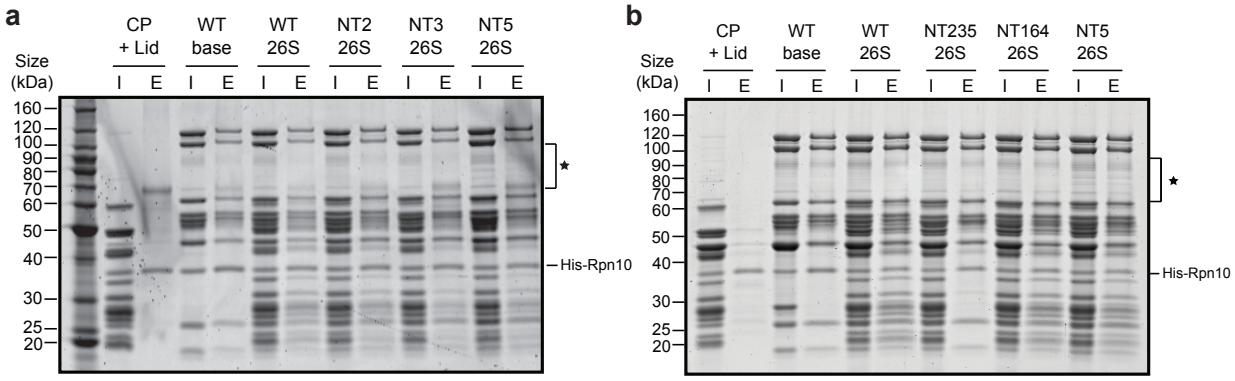

Figure 3.9: Pulldown assays examining CP binding to base variants lacking individual or multiple HbYX tails.
(a,b) Untagged lid and CP subcomplexes were pulled down using His_6 tags on Rpt3 (base) and Rpn10. Lanes are labeled I (input) and E (elution), and nonspecific contaminant bands are labeled with an asterisk. Removal of individual HbYX-containing tails (Rpt2, Rpt3 and Rpt5) did not abolish base binding to CP. The NT164 base variant exhibited CP binding comparable to that of WT base, whereas removal of the three HbYX-containing tails (NT235) abrogated CP binding. The NT235 base mutant also exhibited reduced lid binding, consistent with the fact that purified base and lid subcomplexes did not form stable regulatory particle when reconstituted in the absence of CP (R.B., unpublished data). This observation was made for WT base and lid subcomplexes independent of whether they were isolated from endogenous or recombinant sources.

its C-terminal tail (Figure 3.7a). Base containing a KS mutation in Rpt3 or Rpt5 retained 58% or 59% of wild-type gate-opening activity, whereas the corresponding tailless mutants showed only 5% or 7% activity. Trapping Rpt6 in an empty state preserved 54% of wild-type activity, whereas removing its tail reduced gate opening to 25%. Moreover, all base variants with single KS mutations exhibited some degree of misassembly, such that the measured gate-opening activities represent only lower bounds. Thus, contrary to previous models, the C-terminal tails are accessible for peptidase binding independent of the nucleotide state of individual Rpt subunits, even though the base-core interaction depends on a global ATP-bound conformation of the Rpt ring.

The Walker-A mutants were not suited to qualitatively analyze the contribution of individual Rpt subunits to substrate processing as they caused universally severe degradation defects (Table 3.1). In contrast to fixing subunits in an ATP-bound state with a Walker-B mutation, empty-state subunits potentially influence the hexamer conformation or compromise subunit communication required for processive ATP-hydrolysis in the ring.

Table 3.1: *see next page.*
Biochemical characterization of reconstituted 26S proteasome base mutants: summary of ATP hydrolysis rates (base), peptidase stimulation (CP and base) and degradation rates (reconstituted 26S proteasomes) for all base variants included in this study. Values for each assay are expressed in both absolute terms and as a normalized percentage of WT base activity (% WT). Base mutants are designated as EQ (E→Q, Walker-B), YA (Y→A, pore-1 loop), DN (D→N, pore-2 loop), EN (E→N, pore-2 loop), NT (C-terminal tail truncation) or KS (K→S, Walker-A) followed by a number indicating which Rpt subunit contained the mutation (1-6). Degradation activities for the E→Q mutants are included for both multiple-turnover and single-turnover conditions (shown as multiple-turnover rate/single-turnover rate). Errors were estimated to be ±10% (s.d.) on the basis of repeat measurements ($n \geq 3$ technical replicates). [a]ATPase and degradation activities for the K→S (Walker-A) mutants represent the lower bounds because of varying degrees of misassembly observed for these base mutants. ND, not determined.

Table 3.1: Biochemical characterization of reconstituted 26 proteasome base mutants.

	Mutated Residue	basal ATPase rate		peptidase stimulation		degradation rate (k_{deg})	
		min^{-1}	% WT	fold increase	% WT	(enz^{-1} min^{-1})	% WT
Holoenzyme	-	107	-	-	-	0.32	-
WT (*E. coli*)	-	51	100	21	100	0.30	100
WT (yeast)	-	54	106	22	103	0.29	97
E→Q hexamer	-	2	4	24	110	0.00	0.00
EQ1	310	35	68	15	68	0.08/0.12	27/40
EQ2	284	82	161	29	134	0.28/0.24	92/79
EQ3	273	17	33	19	89	0.005/0.00	2/0
EQ4	282	55	108	20	95	0.001/0.00	0.41/0
EQ5	282	34	67	25	118	0.13/0.21	44/72
EQ6	249	83	164	35	161	0.02/0.01	6/5
YA1	284	66	129	18	84	0.30	101
YA2	257	75	148	8	38	0.15	52
YA3	246	44	87	17	81	0.19	62
YA4	255	38	75	14	65	0.16	54
YA5	255	89	174	15	68	0.22	74
YA6	222	38	76	18	82	0.26	87
DN1	327	39	76	23	106	0.21	71
EN2	300	59	115	24	110	0.27	91
DN3	289	65	127	20	91	0.16	52
DN4	298	141	278	41	192	0.22	74
DN5	298	90	177	32	149	0.40	134
DN6	265	58	113	18	84	0.29	96
NT1	464-468	61	121	20	91	0.29	98
NT2	434-438	45	88	2	10	0.13	44
NT3	424-428	65	127	1	5	0.05	16
NT4	433-437	49	97	23	108	0.25	83
NT5	430-434	86	169	1	7	0.14	47
NT6	401-405	53	104	5	24	0.25	83
KS1	257	32^a	62^a	15	71	0.07^a	24^a
KS2	230	13^a	25^a	2	10	ND^a	ND^a
KS3	219	29^a	57^a	12	58	0.08^a	26^a
KS4	228	15^a	29^a	15	68	0.001^a	0.40^a
KS5	228	74^a	147^a	13	59	0.02^a	6^a
KS6	195	22^a	43^a	12	54	0.04^a	15^a

3.3 Discussion

Our mutational studies using heterologously expressed base subcomplex and *in-vitro* reconstituted 26S holoenzymes revealed that substrate degradation by the proteasome relies on distinct functional asymmetries with strongly non-equivalent contributions of individual Rpts. While a static three-fold symmetry determines the interactions between the base ATPase ring and the core particle, substrate degradation seems to depend on asymmetric spiral-staircase arrangements of the ATPases in which subunits close to the pore entrance play crucial roles in substrate engagement (Figure 3.10).

Our data demonstrate a clear three-fold symmetry at the base-core interface, in which the HbYX-containing C-terminal tails of the alternating subunits Rpt2, Rpt3, and Rpt5 are critical for both binding the core particle and triggering gate opening (Figure 3.10). The tails of the interjacent Rpt1, Rpt4, and Rpt6 are dispensable for the base-peptidase interaction, and Rpt1 and Rpt4 are largely irrelevant for gate opening. The apparent function of the Rpt6 tail in core-particle gating may result from Rpt6's role in ensuring the correct register of the heterohexameric base atop the α-ring of the core particle. Recent structural and functional data suggest that Rpt6 plays a role in base-core assembly and its C-terminus is the only non-HbYX tail that docks into just one specific α pocket (Tian et al., 2011; Park et al., 2013). It is thus possible that Rpt6's tail prevents the neighboring HbYX-containing tails from mispairing with this pocket.

Interactions of the three HbYX-containing tails with the peptidase seem static and independent of the nucleotide state of the particular Rpt subunits. This finding contradicts previous models proposing that the Rpt C-terminal tails change conformation during the ATP-hydrolysis cycle and thus lead to a "wobbling" of the base atop the peptidase (Smith et al., 2005, 2007, 2011). Earlier structural studies demonstrated that in the absence of ATP several AAA+ hexamers adopt a "lockwasher" conformation (Singleton et al., 2000; Guo et al., 2002; Kim and Kim, 2003) that likely prevents binding to the planar surface of a peptidase. The ATP-dependence of the base-core interaction thus seems to originate not from conformational changes of individual tails, but rather from the global geometry of the ATPase ring, which must be at least partially nucleotide-bound to facilitate peptidase docking.

Eliminating ATP hydrolysis or introducing Ar-ϕ-loop mutations in single Rpts revealed that the lid-facing half of the ATPase ring is particularly crucial for substrate degradation. These key Rpts occupy top positions in the spiral-staircase arrangement adopted by the large AAA+ subdomains in the absence of substrate (Figure 3.10), and they must undergo ATP-hydrolysis-induced conformational changes to engage an incoming substrate and initiate translocation. The Rpt hexamer then transitions to an alternative, more planar staircase arrangement, in which Rpt1 occupies the top position and rigid-body interfaces are formed between most subunits (Matyskiela et al., 2013). Our data suggest that ATP hydrolysis in Rpt1 is more important than in neighboring subunits to drive substrate translocation, possibly because Rpt1 triggers a burst of coordinated hydrolysis events around the ring. Nevertheless, individual Rpts may contribute more equally to translocation once substrate

is engaged.

Spiral-staircase arrangements have been previously observed in several homohexameric motors of the AAA+ and RecA families, and it has been suggested that individual ATPase subunits successively transition through the different vertical registers of the spiral to drive substrate translocation (Singleton et al., 2000; Enemark and Joshua-Tor, 2006; Glynn et al., 2009; Thomsen and Berger, 2009; Costa et al., 2011). However, the apparently rigid spiral-

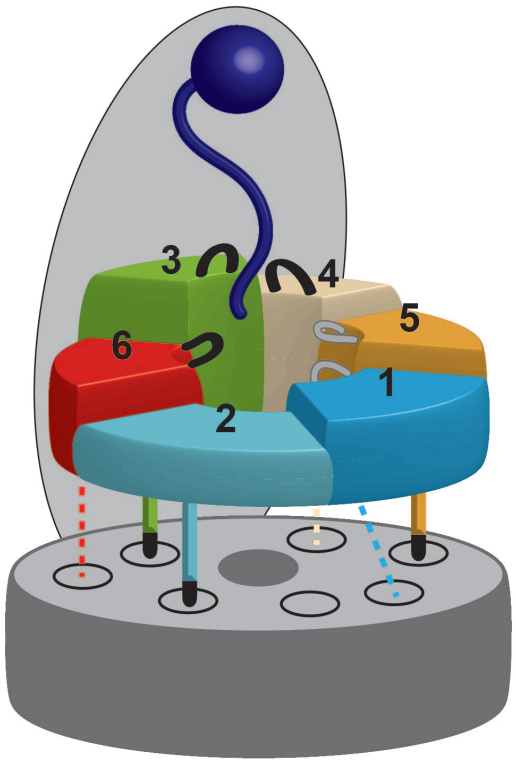

Figure 3.10: Model for the contribution of individual ATPase subunits to substrate processing and core particle interaction.
The substrate (dark blue) is bound to the proteasome lid and positioned for ATP-dependent processing by the heterohexameric ATPase ring of the base. Rpt6 (red), Rpt3 (green) and Rpt4 (beige), which are located at the top of the pre-engaged spiral staircase of ATPase subunits, have critical roles in substrate degradation. In contrast, Rpt5 (gold), Rpt1 (light blue) and Rpt2 (cyan) are less important. The C-terminal tails of the ATPases are docked into their cognate binding pockets in the core-particle α-ring (gray). Tails that are crucial for binding and gate opening (Rpt2, Rpt3 and Rpt5) are shown as solid lines with black termini, representing the HbYX motif. The remaining three tails that do not contribute to the stability of the base-core interaction (Rpt1, Rpt4 and Rpt6) are shown as dashed lines.

staircase configurations observed for the proteasomal ATPase ring in the absence and presence of substrate, together with the biochemical data presented here, contradict stepwise successive progression of individual Rpts through the different registers. Instead, the proteasome base relies on differential subunit contributions prescribed by the regulatory particle's asymmetric architecture. Conformational changes in the top subunits of a pre-engaged staircase thread an incoming substrate, before the ATPase ring switches to an engaged staircase arrangement, in which subunits contribute more equally to protein translocation.

Although all mutant base complexes in this study were characterized by *in-vitro* assays that may or may not wholly recapitulate the complexity of *in-vivo* conditions, our results agree with and substantially extend earlier findings, suggesting non-equivalent contributions of individual Rpt subunits to substrate processing by the 26S proteasome (Rubin et al., 1998; Erales et al., 2012; Kim et al., 2012). Protein degradation by the proteasome deviates from models previously proposed for other AAA+ unfoldases, pointing toward major differences between the operating principles of homo- and heterohexameric AAA+ motors. Future experiments will have to address to what extent these motor designs rely on different strategies for substrate engagement, generation of mechanical force for unfolding, and translocation of the polypeptide chain into a peptidase for degradation.

3.4 Materials and Methods

3.4.1 Base mutagenesis and purification of base variants

Point mutations in individual ATPase subunits were generated by PCR using pETDuet-1 plasmids containing individual Rpt subunits, which were then used for amplification and substitution into the wild type hexamer in pCOLADuet-1. Base expression strains were generated by co-transforming the pETDuet-1, pCOLA-1 and pACYC Duet-1 plasmids into *E. coli* BL21-star (DE3) cells. The base subcomplex was produced by growing the expression strain to OD_{600}=0.6-0.8 and inducing with 1 mM isopropyl-β-D-thiogalactopyranoside overnight at 18 °C. Cells were harvested by centrifugation at 5000 rpm for 15 minutes, resuspended in nickel buffer (25 mM HEPES pH 7.6, 100 mM NaCl, 100 mM KCl, 10 % glycerol, 10 mM $MgCl_2$, 0.5 mM EDTA, 20 mM imidazole) supplemented with 2 mg ml^{-1} lysozyme, protease inhibitors and benzonase. Cells were lysed by freeze-thaw and sonication on ice for 1 minute 30 seconds in 15 second bursts. Lysate was clarified by centrifugation at 15,000 rpm at 4 °C for 30 minutes. A two-step affinity purification of the base subcomplex was performed using Ni-NTA agarose (Qiagen) to select for His_6-Rpt3 and anti-FLAG M2 resin (Sigma-Aldrich) selecting for FLAG-Rpt1. 0.5 mM ATP was present in all purification buffers. The Ni-NTA and anti-FLAG M2 columns were eluted with nickel buffer containing 250 mM imidazole or 0.15 mg ml^{-1} 3xFLAG peptide, respectively. The Flag column eluate was concentrated using a 30,000 MWCO concentrator (Amicon) and run on a Superose 6 gel filtration column (GE Healthcare) equilibrated with gel filtration buffer (60 mM HEPES pH 7.6, 50 mM NaCl, 50 mM KCl, 10 % glycerol, 5 mM $MgCl_2$, 0.5 mM EDTA, 1 mM DTT,

0.5 mM ATP). See Appendix C for detailed protocol.

3.4.2 Mutation of conserved AAA+ motifs

See Appendix B for multiple sequence alignment of the six proteasomal AAA+ ATPase subunits (*S. cerevisiae*) and the single AAA+ ATPase subunit of ClpX (*E. coli*). Conserved catalytic and structural motifs have been annotated.

To fix subunits in a constitutively "ATP-bound" state (Hanson and Whiteheart, 2005), we examined mutations in the conserved Walker-B glutamate-aspartate motif by placing the same mutation in all six Rpt subunits simultaneously and characterizing the functional activities of the mutant base hexamers. We constructed a series of mutant hexamers containing single mutations of glutamate to glutamine (DN) or aspartate to asparagine (EQ) as well as the double DN EQ mutant. Rpt subunits carrying the DN mutation assembled properly into a hexamer that lacked ATPase activity. However, the DN mutation also had undesired deleterious effects, as this base variant was deficient in peptidase gate opening, even though a permanently ATP-bound hexamer is expected to interact with and maximally stimulate the core particle. The DN EQ double mutation resulted in an even stronger defect and prevented assembly of the ATPase hexamer, as indicated by the lack of an appropriate elution peak in size exclusion chromatography (unpublished data, R.B.). The EQ mutation supported proper base assembly, eluted at the appropriate volume from a size exclusion column, and was deficient in ATPase activity yet exhibited wild-type levels of peptidase stimulation (Table 3.1). We deduced that the EQ mutation approximated an "ATP-bound" state and utilized this mutation for subsequent studies of the contribution of individual Rpt subunits to base activities (Figure 3.1, Figure 3.2, Figure 3.3, Figure 3.4, Table 3.1).

We required an appropriate mutation to induce a permanent empty state, either by preventing the conformational response of a subunit to ATP binding or by interfering with ATP binding itself. For some AAA+ enzymes, including ClpX from *E. coli*, mutation of the Sensor-II arginine has been shown to induce an empty-state conformation (Song et al., 2000; Joshi et al., 2004; Hanson and Whiteheart, 2005), yet the proteasomal clade of classic AAA+ enzymes lacks a conserved Sensor-II arginine. We therefore mutated the Walker A lysine to abrogate nucleotide binding altogether. First we mutated the lysine to either arginine (KR) or serine (KS) in all six Rpt subunits simultaneously to clearly establish the effects on base activity. The KR mutant hexamer exhibited activities in ATP hydrolysis and peptidase stimulation that were similar to wild-type base (unpublished data, R.B.), indicating that the KR mutation does not interfere with ATP binding of Rpt subunits. Conversely, the KS mutation resulted in severe assembly defects that prevented us from purifying the six-fold mutant base. This finding would be consistent with a completely empty-state hexamer and supports previous observations that assembly of the base is ATP dependent (Lee et al., 2012). Furthermore, KS mutations in some individual Rpt subunits have been shown to interfere with cellular assembly of the 26S proteasome, compromise substrate degradation (Kim et al., 2012), and cause severe growth defects *in vivo* (Rubin et al., 1998). Preventing ATP binding simultaneously in all six subunits is likely more

deleterious for ring assembly than placing the KS mutation in just a single Rpt at a time, as the assembly process may require only some subunits to fill with nucleotide. We therefore placed KS mutations in single Rpt subunits and characterized the functional activities of the resulting mutant base subcomplexes (Figure 3.7a, Table 3.1). Only a mutation in Rpt2 caused extreme defects in base assembly, although all base variants with single KS mutations did exhibit some degree of misassembly.

3.4.3 Purification of endogenous yeast complexes

Yeast holoenzyme, core particle, base and lid subcomplexes were purified from *S. cerevisiae* essentially as previously described (Leggett et al., 2005). Frozen yeast cells were lysed using a Spex SamplePrep 6870 Freezer/Mill. Holoenzyme was purified from a yeast strain containing FLAG-Rpn11. Lysed cells were resuspended in lysis buffer containing 60 mM HEPES pH 7.6, 100 mM NaCl, 100 mM KCl, 10% glycerol, 5 mM MgCl2, 0.5 mM EDTA, 0.2% NP-40 and ATP regeneration mix (5 mM ATP, 0.03 mg ml^{-1} creatine kinase, 16 mM creatine phosphate). Holoenzyme was bound to anti-FLAG M2 resin and washed with wash buffer (60 mM HEPES pH 7.6, 100 mM NaCl, 100 mM KCl, 10% glycerol, 5 mM $MgCl_2$, 0.5 mM EDTA, 0.1% NP-40, 0.5 mM ATP). Holoenzyme was eluted with 0.15 mg ml^{-1} 3xFLAG peptide and further purified by gel filtration using a Superose 6 column with gel filtration buffer (see above). Lid and base subcomplexes were isolated from FLAG-Rpn11 or FLAG-Rpn2 yeast strains, respectively, and purified by exposure to a 1 M NaCl wash while bound to anti-FLAG M2 resin. Base purification buffers included 0.5 mM ATP. Core particle was purified from a 3xFLAG-Pre1 yeast strain using a 500 mM salt wash. All subcomplexes underwent size exclusion chromatography using a Superose 6 column as described above.

3.4.4 Yeast strains

Yeast lid and holoenzyme were purified from strain YYS40 (genotype MATa ade2-1 his3-11,15 leu2-3,112 trp1-1 ura3-1 can1 Rpn11::Rpn11-3XFLAG(HIS3), source Y. Saeki). Core particle was prepared either from strain RJD1144 (genotype MATa his3-200 leu2-3,112 lys2-801 trp-63 ura3-52 PRE1-FLAG-6xHIS::Ylpac211(URA3) source R. Deschaies) or strain yAM14 (genotype MATa ade2-1 his3-11,15 leu2-3,112 trip1-1 ura3-1 can1-100 bar1 PRE1::PRE1-3XFLAG(KanMX), this work).

3.4.5 ATPase and peptidase stimulation assays

ATPase activity was quantified using an NADH-coupled ATPase assay. 500 nM base was incubated with 1x ATPase mix (3 U ml^{-1} pyruvate kinase, 3 U ml^{-1} lactate dehydrogenase, 1 mM NADH, 7.5 mM phosphoenol pyruvate) at 30 °C. Absorbance at 340 nm was monitored for 900 seconds at 10 second intervals using a UV-Vis Spectrophotometer (Agilent). Peptidase stimulation was monitored by following the increase in fluorescence resulting from cleavage of a fluorogenic peptide substrate (Glickman et al., 1998), Suc-LLVY-AMC

(Boston Biochem), using a QuantaMaster spectrofluorimeter (PTI). 50 nM core particle was incubated with saturating base subcomplex in the presence of an ATP regeneration system (5 mM ATP, 16 mM creatine phosphate, 6 mg ml^{-1} creatine phosphokinase) and 50 μM Suc-LLVY-AMC.

3.4.6 Affinity measurements for base-core interaction

Titration experiments were conducted using either 25 nM core particle and increasing amounts of base (peptidase stimulation) or 100 nM base and increasing amounts of core particle (ATPase activity). K_D values were extracted by fits to a simple binding curve using Grafit (Erithacus Software).

3.4.7 Fluorescent substrate degradation assay

Proteasome holoenzyme was reconstituted from core particle, lid, base and Rpn10. A GFP-titin^{V15P}-cyclin-PY fusion protein was modified *in vitro* with a polyubiquitin chain using Uba1, Ubc1, Rsp5 and wild-type ubiquitin. Degradation reactions were performed at 30 °C in gel filtration buffer (60 mM HEPES pH 7.6, 50 mM NaCl, 50 mM KCl, 10 % glycerol, 5 mM $MgCl_2$, 0.5 mM EDTA, 1 mM DTT, 0.5 mM ATP) supplemented with an ATP regeneration system. Single and multiple turnover degradation activities were monitored by the loss of GFP fluorescence (excitation 467 nm; emission 511 nm) using a QuantaMaster spectrofluorimeter (PTI). Multiple turnover degradation experiments were performed with 50 nM reconstituted holoenzyme under V_{max} conditions (saturating base, lid and Rpn10) with 2 μM substrate. Excess base, lid, and Rpn10 did not affect the observed degradation rate (see Figure 2.6). For single turnover degradation, 2 μM holoenzyme was reconstituted from equimolar concentrations of subcomplexes and mixed with 100 nM substrate. Single turnover degradation traces were best fit with double exponential decay curves using Grafit (Erithacus Software).

3.4.8 Native gel electrophoresis

Analysis of proteasome holoenzyme and subcomplexes by native gel was performed as described previously (Leggett et al., 2005). Assembly reactions were incubated for 15 minutes at 23 °C with 5 mM ATP, followed by electrophoresis on a 3.5 % native polyacrylamide gel. Electrophoresis was conducted at 4 °C with stirring and running buffer containing 0.5 mM ATP. The gel was overlaid with developer solution (running buffer with 100 nM Suc-LLVY--AMC peptide and 0.02 % SDS) and incubated at 30 °C for 10 minutes prior to imaging. Fluorescence imaging was performed using a Typhoon scanner (GE Healthcare) and followed by Coomassie staining.

3.4.9 Affinity pulldown assay

Base subcomplexes were mixed with core particle, lid and Rpn10 in nickel buffer with 1x ATP regeneration system at 23 °C for 15 minutes. All components were present at a concentration of 900 nM in the reaction, which was then incubated with 5 μl of magnetic Dynabeads (Invitrogen) at 23 °C for 15 minutes. The beads were washed three times with nickel buffer supplemented with 0.05 % NP-40 and 0.5 mM ATP. Bound proteins were eluted with nickel buffer containing 500 mM imidazole. Pulldown samples were run on a 10 % SDS-PAGE gel, stained with Sypro Ruby and imaged using a Typhoon scanner (GE Healthcare).

CHAPTER 4

Deconvoluting substrate engagement and translocation

4.1 Introduction

The data in Chapter 3 defined the contributions of individual proteasomal ATPase subunits to substrate processing but major questions remain regarding the exact order and timing of substrate engagement, translocation, unfolding and deubiquitination by the 26S proteasome. Previous studies of partitioning between substrate unfolding and release by the bacterial unfoldase ClpX utilized unfolded titin concatamers of varying length to examine the length dependence of substrate degradation rates (Kenniston et al., 2005). This method can be used to quantify the translocation rate and the timing of non-translocation steps, which in the case of the proteasome includes substrate engagement and deubiquitination. In this chapter, I present the development of a fluorescence-based titin concatamer degradation assay and preliminary data quantifying the rates of substrate engagement and non-translocation-dependent processes for the 26S proteasome. This assay is a powerful tool for future studies of 26S proteasome function because mutants can be quantitatively characterized in terms of their effects on substrate engagement, substrate translocation, or both processes concurrently.

4.2 Results

4.2.1 Design and preparation of titin concatamer substrates

In order to establish a fluorescence-based assay to analyze the length-dependence of degradation by the 26S proteasome, I constructed a set of four proteasomal substrates with one, three, five or ten repeats of the I27 domain of titin containing the destabilizing V15P

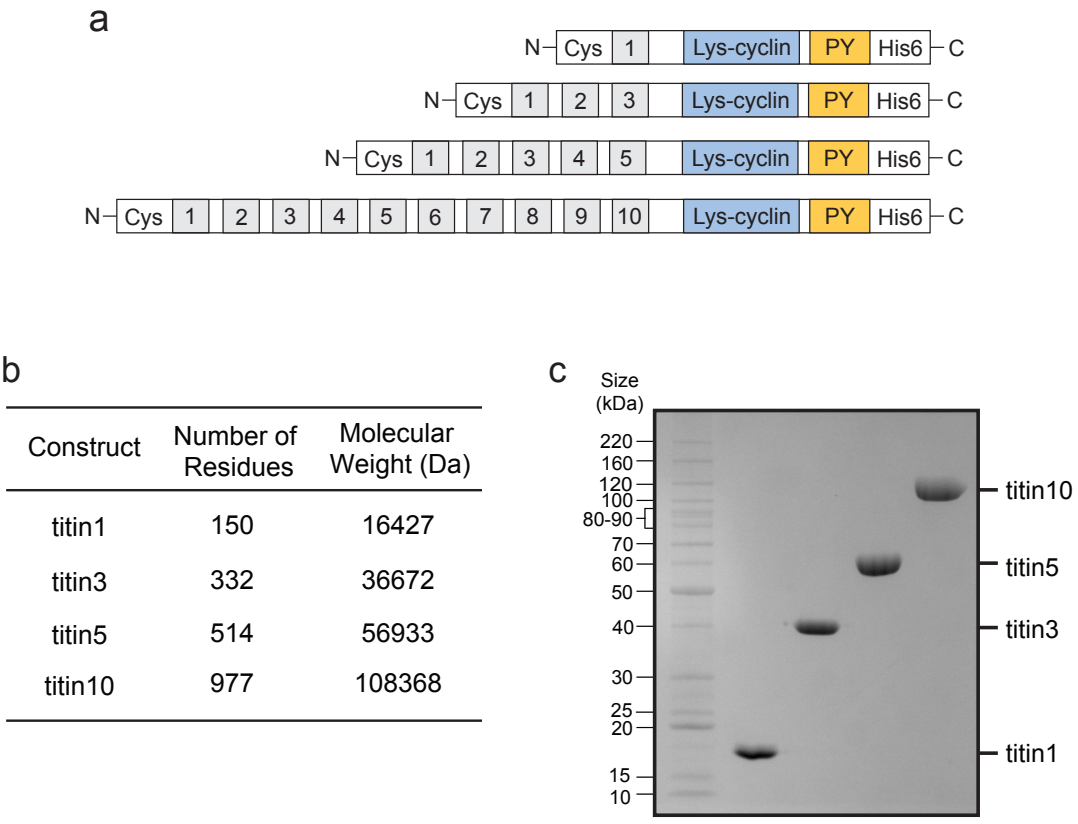

Figure 4.1: Design and expression of titin concatamers.
(a) Construct design for concatamer substrates. **(b)** Table of titin concatamer constructs with corresponding amino acid lengths and molecular weights. **(c)** Coomassie-stained SDS-PAGE gel of purified concatamer substrates containing 1, 3, 5 or 10 titin repeats.

mutation (Figure 4.1). Titin has been demonstrated to be completely unfolded upon alkylation of two internal cysteine residues (Kenniston et al., 2003), making this an ideal substrate for monitoring degradation rates without any contribution from domain unfolding. Eight intrinsic lysine residues were mutated to arginine to prevent the attachment of multiple ubiquitin chains to the substrate. An unstructured fragment of cyclin was appended to the C-terminus of the titin repeats to provide an engagement site for proteasomal degradation as well as a single lysine residue and PY motif for *in vitro* ubiquitination and a hexahistidine tag for affinity purification. A single solvent-exposed cysteine residue was engineered at the far N-terminus of the substrates in order to facilitate detection of when the proteasome reaches the end of the substrate. To obtain a fluorescent read-out for substrate degradation, I introduced a single lysine residue into the fluorogenic succinyl-LLVY-AMC peptide used in peptidase stimulation assays. This reporter peptide was chemically conjugated to the cysteine residue of the titin substrates using a heterobifunctional amine-to-sulfhydryl crosslinker

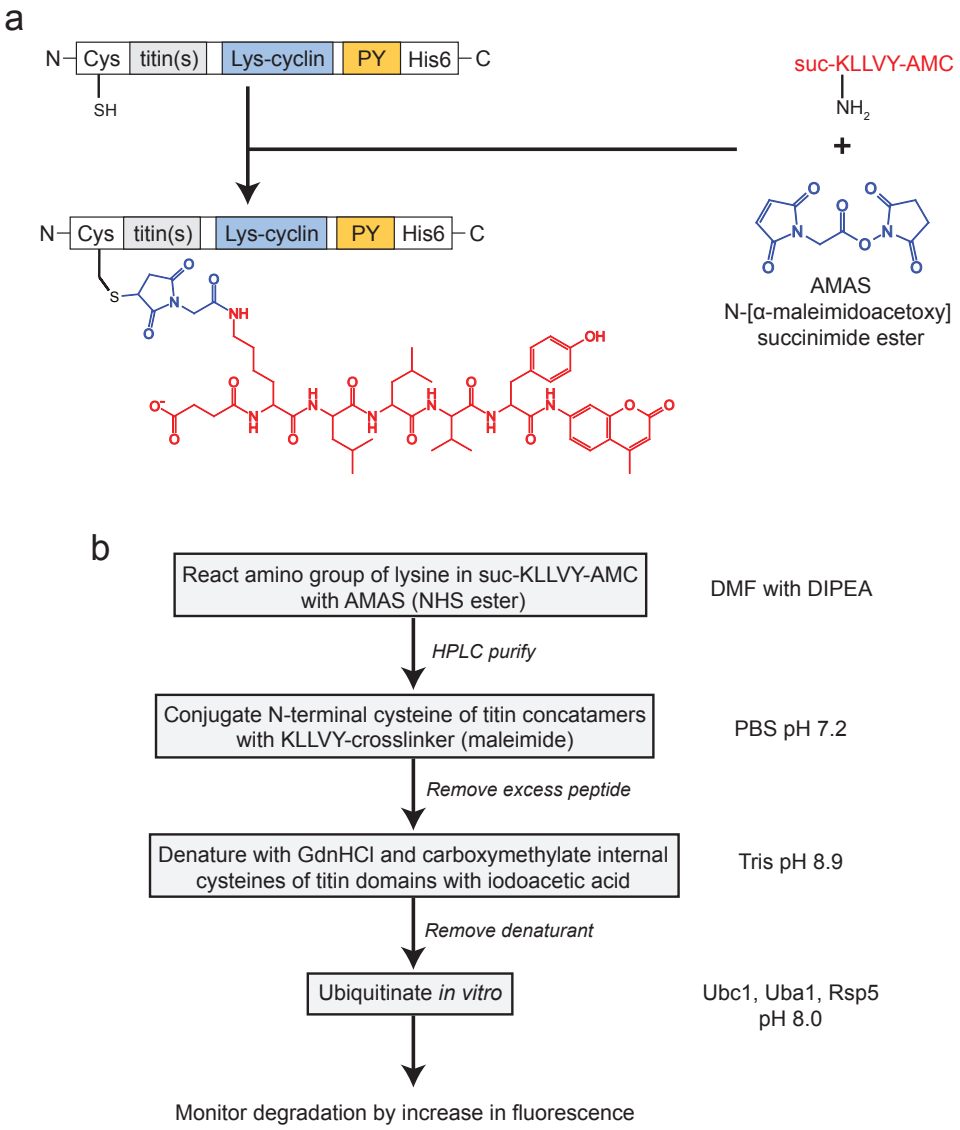

Figure 4.2: Reaction scheme for labeling titin concatamer substrates with reporter peptide. **(a)** Chemical structure of the peptide-crosslinker-titin conjugate. **(b)** Reaction schematic for preparation of titin concatamer substrates for fluorescence-based degradation experiments with the 26S proteasome. The amine group of the lysine residue in the succinyl-KLLVY-AMC peptide is reacted with the heterobifunctional crosslinker AMAS via NHS-ester chemistry in organic solvent, followed by HPLC purification. The peptide-crosslinker conjugate is then reacted with the single solvent exposed cysteine at the N-terminus of the titin substrate under aqueous conditions. The internal cysteines of the titin domains are alkylated under denaturing conditions to permanently unfold the titin domains, followed by ubiquitination of the single lysine residue in the C-terminal cyclin sequence.

(AMAS) composed of NHS-ester and maleimide reactive groups at the ends of a short 4-atom (4.4 Å) aliphatic spacer (Figure 4.2). The crosslinker was selected to closely resemble the polypeptide chain in order to minimize interference with proteasomal substrate processing. The peptide-crosslinker conjugate was purified by HPLC (Figure 4.3) and confirmed by mass spectrometry (Figures 4.4 to 4.7). Titin substrates with the chemically-linked reporter peptide were subsequently alkylated under denaturing conditions to permanently unfold the titin domains (Figure 4.8) and then ubiquitinated *in vitro* at normalized concentrations. For a full schematic of substrate preparation steps and conditions, see Figure 4.2b.

4.2.2 Quantifying steps in substrate processing by the 26S proteasome

Preliminary analyses of the relationship between proteasomal degradation rate and substrate length were performed by degrading the titin concatamer substrates under single turnover conditions. Degradation was monitored by the increase in fluorescence upon cleavage of the fluoregenic reporter peptide at the N-terminus of the substrates. All single-turnover degradation traces were best fit by a double exponential (Figure 4.9). The fast rate may result from substrate engagement at regions other than the C-terminal tail, leading to an artificially rapid increase in signal because the proteasome does not translocate the entire length of the substrate before cleaving the fluorogenic probe at the N-terminus. I therefore restricted the current analysis to the slow rates observed for single-turnover degradation of the titin concatamers, which demonstrated a clear linear dependence between substrate length and the time required for degradation by the 26S proteasome (Figure 4.10). The slope of the linear fit corresponds to the translocation rate, which was approximately 0.7 amino acids per second. The y-intercept provided a quantitative measurement of the time required for non-translocation-dependent processes, which was approximately 138 seconds. For the 26S proteasome, non-translocation processes include both substrate engagement and deubiquitination. In the context of previous work from our lab showing that substrate deubiquitination by the proteasome occurs on the order of 1 minute (Worden et al., 2014), my data suggest that the process of substrate engagement requires approximately 78 seconds.

4.3 Discussion

My preliminary data demonstrate that the fluorescence-based degradation assay using titin concatamers can be used to separately quantitate the rates of substrate engagement and translocation. This method represents an exciting approach for quantitatively assessing how proteasome mutants affect substrate processing. Future experiments utilizing this assay in conjunction with the catalytic and pore-loop base variants presented in Chapter 3 will be able to demonstrate whether these mutations affect substrate engagement (indicated by a shift in the y-intercept), substrate translocation (indicated by a change in slope), or both processes (shifted y-intercept and altered slope). Furthermore, the concatamer substrates could be used with natively folded titin domains in order to assess how unfolding contributes to

translocation rates. These analyses would provide initial insights into the mechanochemical operating principles of the base unfoldase and allow us to assess whether the 26S proteasome utilizes general mechanisms similar to those of simpler, homomeric unfoldases.

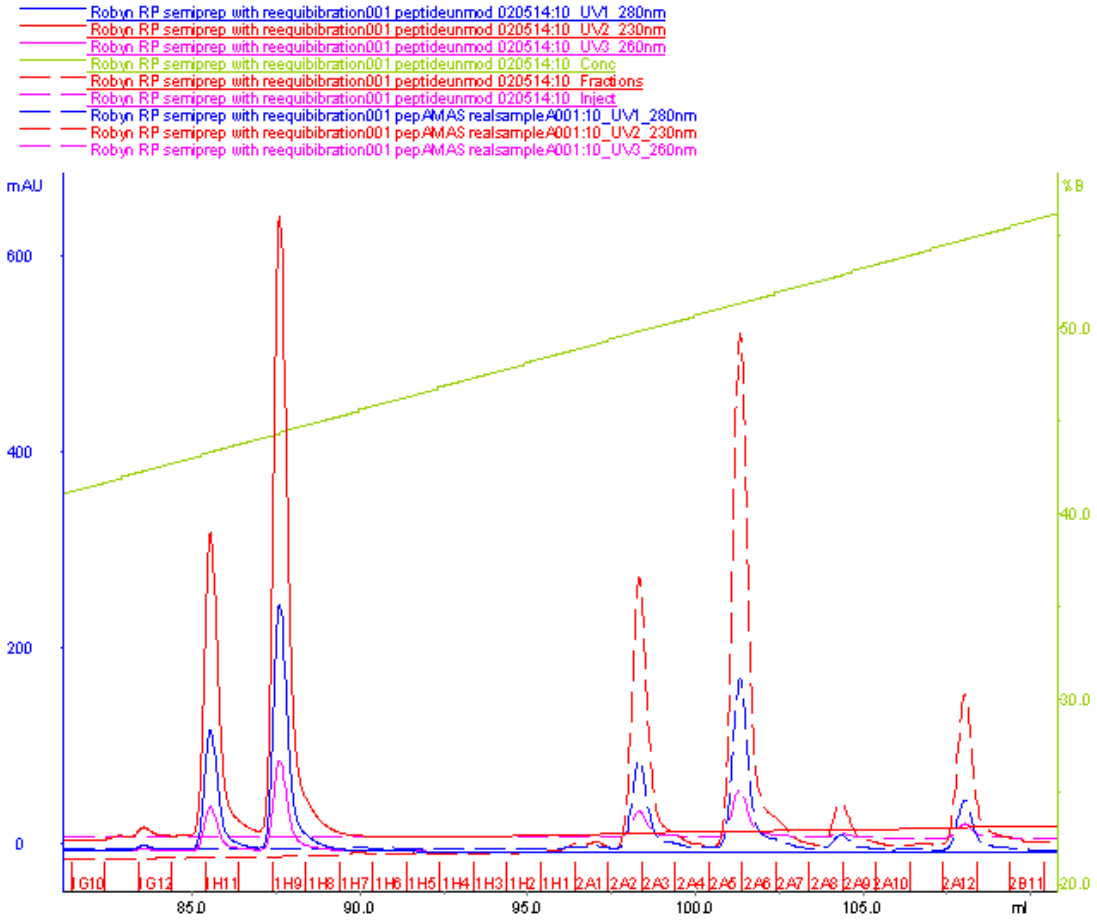

Figure 4.3: Reverse Phase HPLC of KLLVY peptide conjugated with AMAS crosslinker. Overlay of HPLC traces for unmodified and modified suc-KLLVY-AMC peptides run on a C18 reverse phase column with an acetonitrile gradient. Left-handed y-axis is absorbance at 280 nm (blue), right-handed y-axis is the percentage of acetonitrile (green). For the modified peptide sample, the amino group of the peptide's lysine residue was reacted by NHS-ester chemistry with the AMAS crosslinker. The two earliest eluting peaks (Peak A1: 85.5 mL; Peak A2: 87.5 mL) correspond to the unmodified peptide sample. The four later peaks (Peak B1: 99 mL; Peak B2: 102 mL, Peak B3: 104 mL, Peak B4: 109 mL) correspond to the conjugated KLLVY-AMAS sample. For mass spectrometry analysis of the main HPLC elution peaks, see Figures 4.4 and 4.5 (unmodified peptide) and Figures 4.6 and 4.7 (modified peptide).

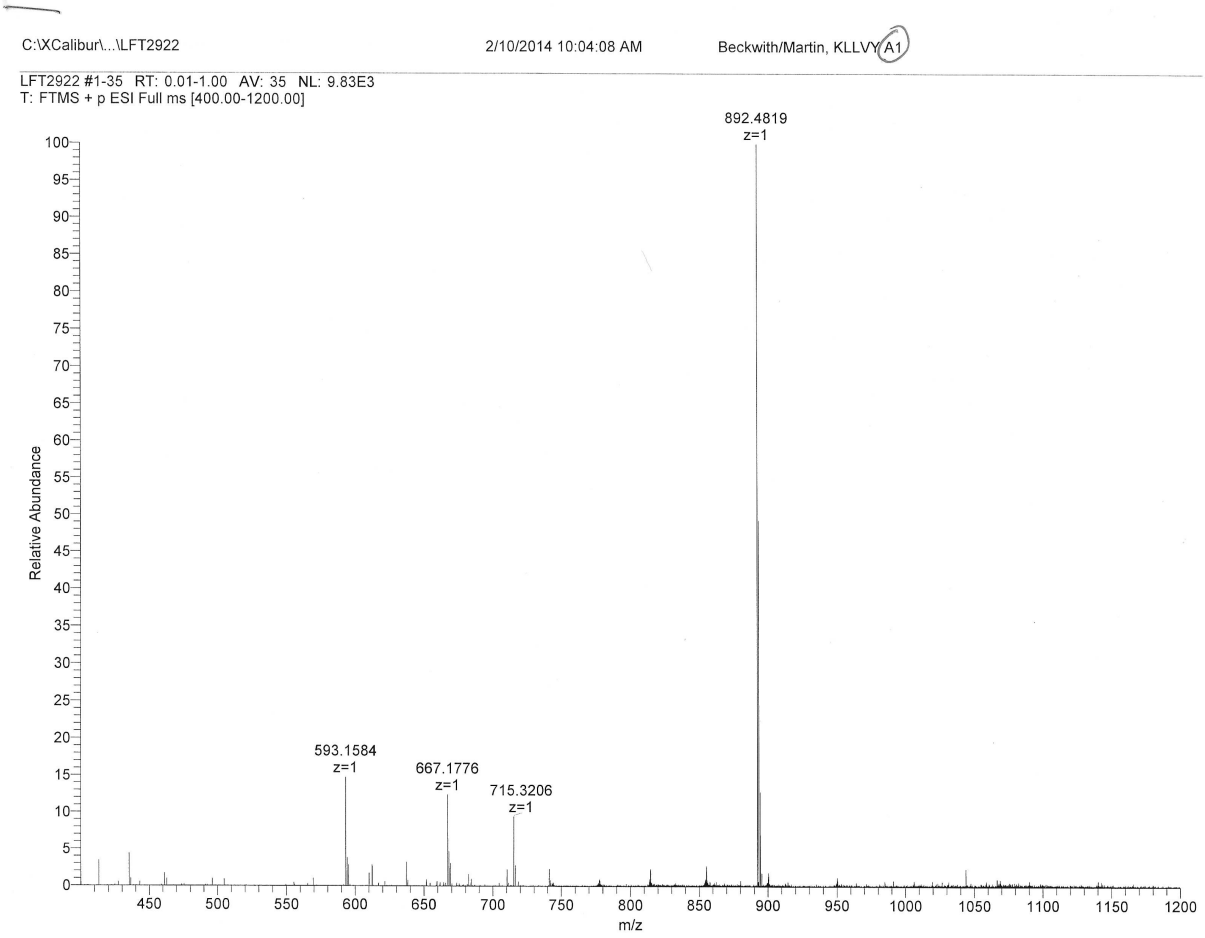

Figure 4.4: Mass Spectrometry of HPLC Peak A1.
Unmodified peptide sample. Major peak of HPLC elution, main species at appropriate mass (expected mass 892.05, actual mass 892.48) but lower mass contaminants detected ("messy" HPLC peak).

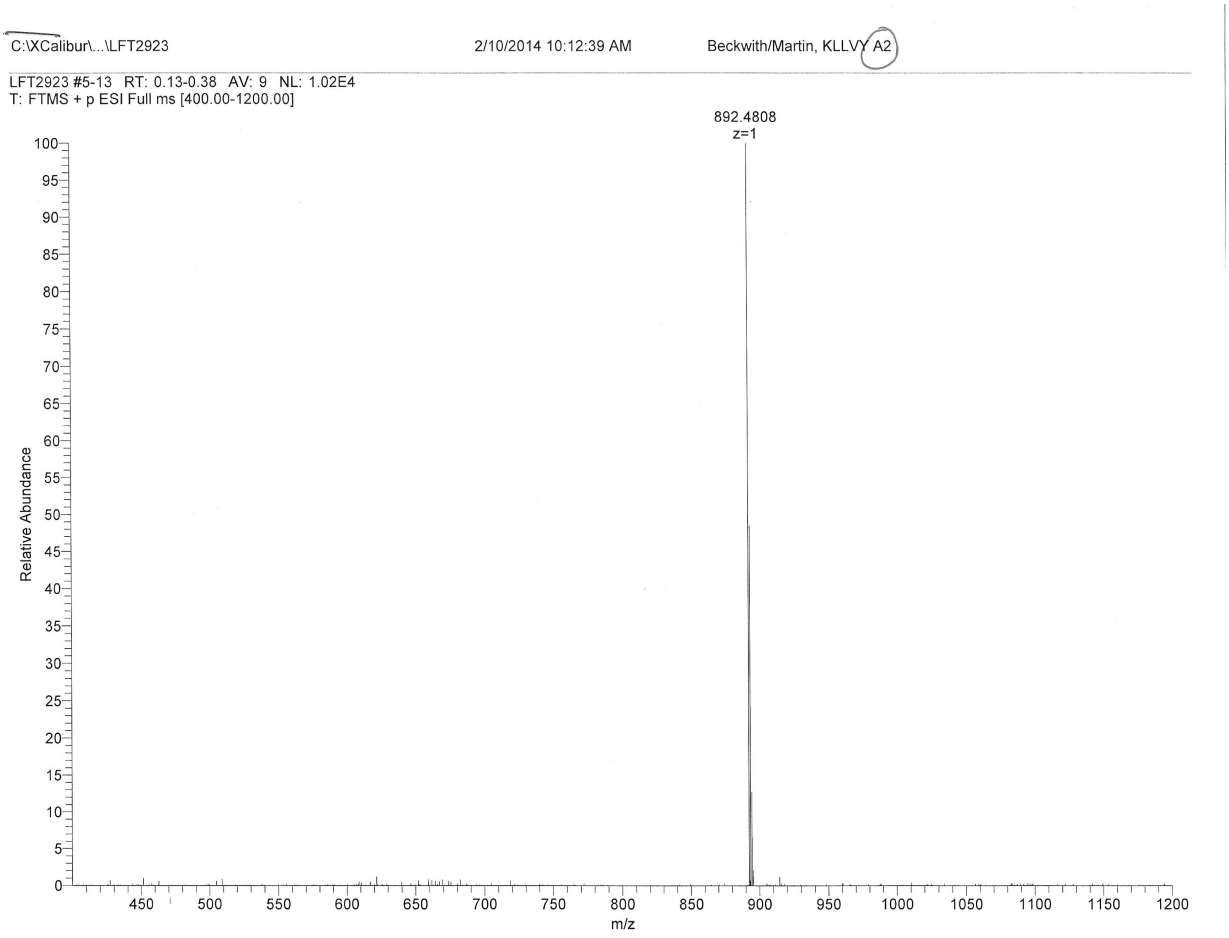

Figure 4.5: Mass Spectrometry of HPLC Peak A2.
Unmodified peptide sample. Major peak of HPLC elution, observed single species at appropriate mass: expected mass 892.05, actual mass 892.48 ("clean" HPLC peak).

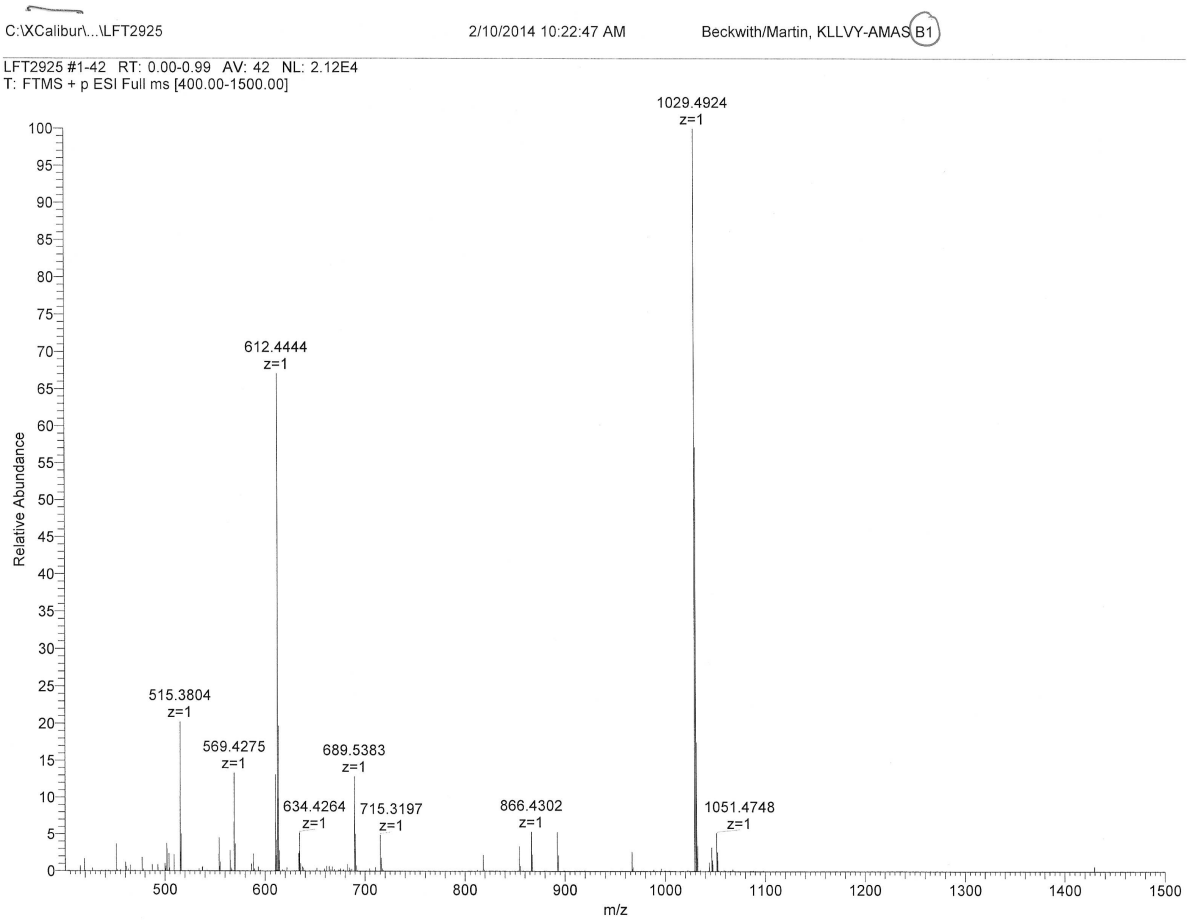

Figure 4.6: Mass Spectrometry of HPLC Peak B1.
Modified peptide sample. Major peak of HPLC elution, main species at appropriate mass (expected mass 1029.05, actual mass 1029.49) but lower mass contaminants detected ("messy" HPLC peak).

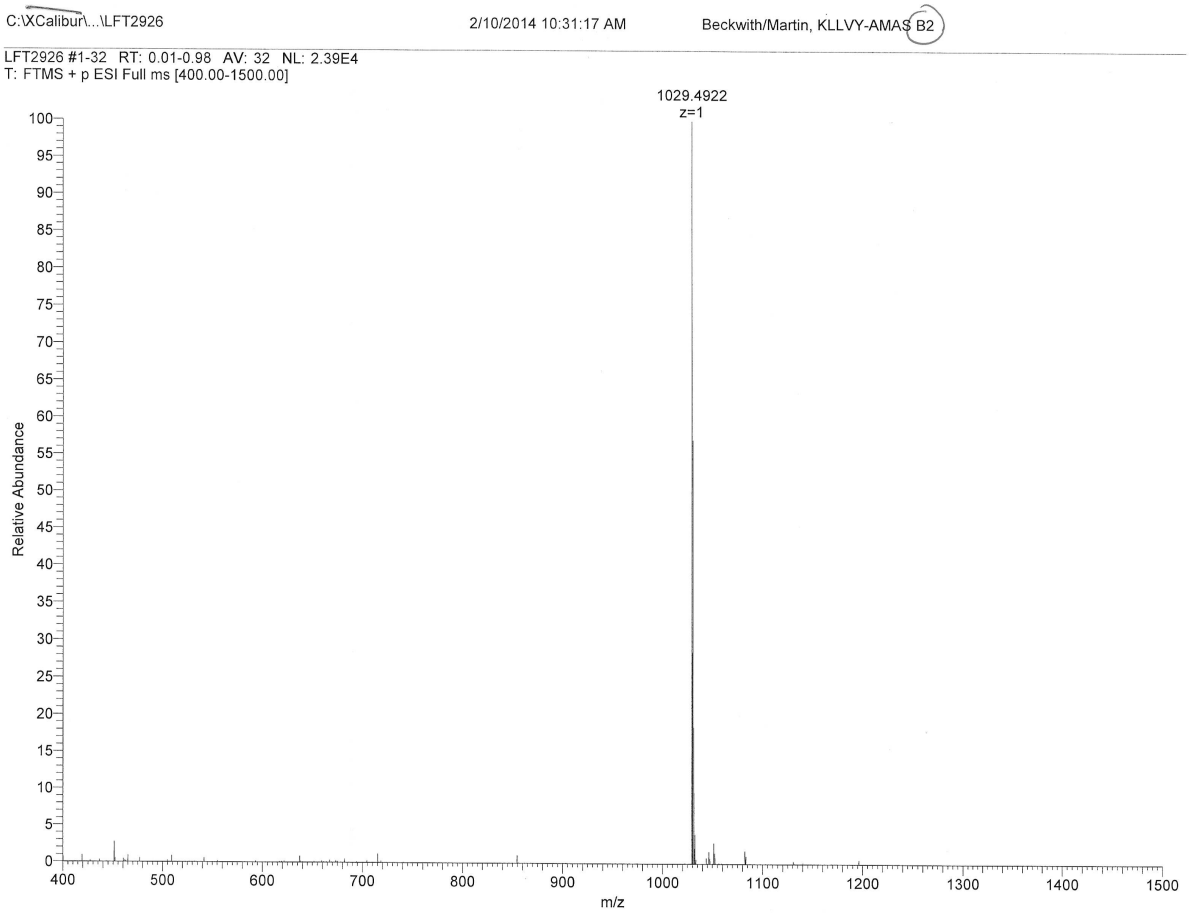

Figure 4.7: Mass Spectrometry of HPLC Peak B2.
Modified peptide sample. Major peak of HPLC elution, observed single species at appropriate mass for KLLVY-AMAS conjugate: expected mass 1029.05, actual mass 1029.49 ("clean" HPLC peak).

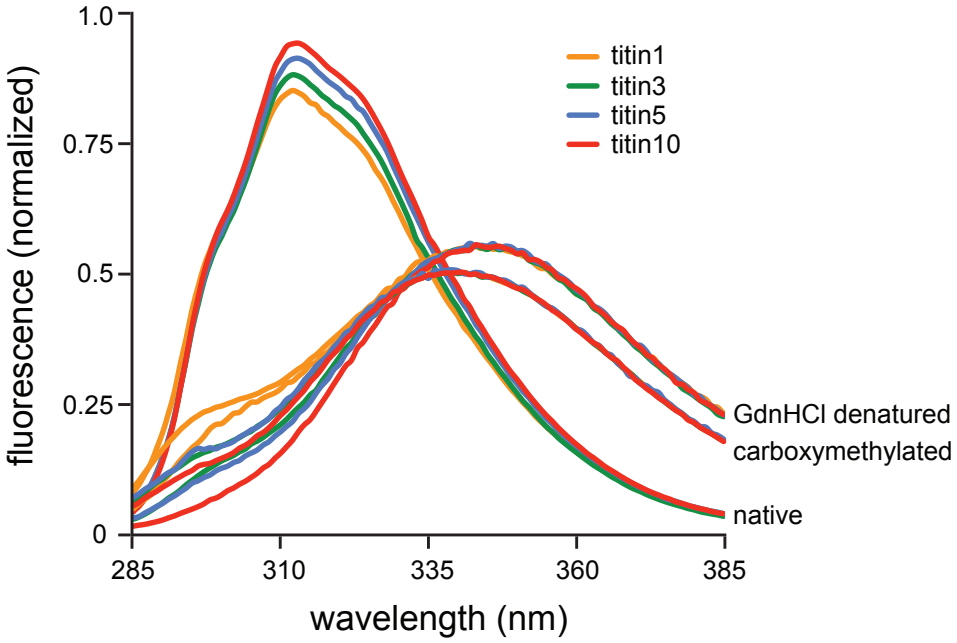

Figure 4.8: Carboxymethylation of titin concatamers.
Unfolded titin substrates were prepared essentially as previously described (Section 4.4.3, Kenniston et al. 2003). The fluorescence-emission spectra of the concatamer substrates denatured in 5 M GuHCl and carboxymethylated concatamers are red-shifted compared to the native protein, as expected for complete solvent exposure of the single tryptophan that is buried in the folded domain.

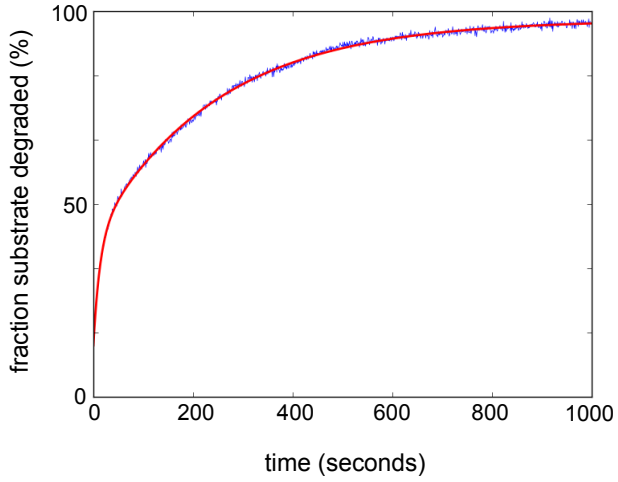

Figure 4.9: Representative single-turnover degradation trace and curve fit: titin1 substrate. Degradation was monitored by the increase in fluorescence upon cleavage of the AMC moiety from the substrate (excitation 350 nm, emission 440). The degradation curve for the titin1 substrate was similar to those obtained for the other concatamer substrates, all of which were best fit by a double exponential. The fast rate likely results from engagement of the substrate at locations other than the C-terminus, therefore we restricted preliminary analysis to the slow rate constant.

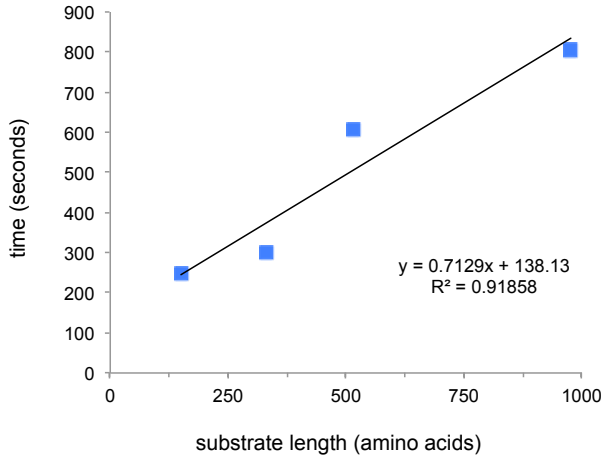

Figure 4.10: Effect of substrate length on degradation by the 26S proteasome.
Plotted times correspond to slow phase rates obtained from double-exponential fits of single-turnover degradation traces for the titin1, titin3, titin5 and titin10 concatamer substrates. The linear fit to these data points has a slope corresponding the translocation rate whereas the y-intercept represents the time required for non-translocation processes.

4.4 Materials and Methods

4.4.1 Cloning, expression and purification of titin concatamers

PCR was used to mutate eight lysine residues to arginine in the I27 domain of titin containing the V15P mutation. The titin1, titin3 and titin5 concatamers were cloned into pETDuet-1 between Nco and Xho via Golden Gate cloning. The titin10 concatamer was generated by cloning a derivative of the titin5 construct with no N-terminal cysteine and flanking Xho sites on the N- and C-terminal sides of the titin repeats that was consequently subcloned into the titin5 concatamer construct. A C-terminal unstructured tail containing a single lysine, the Rsp5 recognition motif and a His_6 purification tag was appended to the titin constructs via Xho/Pac (see Figure 4.1a). Vectors for the titin concatamer constructs were transformed into *E. coli* BLR (DE3) cells (*recA* knockout strain). Titin concatamer substrates were produced by growing expression strains at 37 °C to OD_{600}=0.6-0.8 and inducing with 1 mM isopropyl-β-D-thiogalactopyranoside for 5-6 hours at 30 °C. Cells were harvested by centrifugation at 5000 rpm for 15 minutes, resuspended in nickel buffer (25 mM HEPES pH 7.6, 100 mM NaCl, 100 mM KCl, 10% glycerol, 10 mM $MgCl_2$, 0.5 mM EDTA, 20 mM imidazole) supplemented with 2 mg ml^{-1} lysozyme, protease inhibitors, benzonase and 10 mM β-mercaptoethanol. Cells were lysed by freeze-thaw and sonication on ice for 1 minute 30 seconds in 15 second bursts. Lysate was clarified by centrifugation at 15,000 rpm at 4 °C for 30 minutes. The clarified lysate was incubated with Ni-NTA agarose (Qiagen) for 1 hour in batch. The nickel resin was then transferred to a gravity column and washed with nickel buffer containing 10 mM β-mercaptoethanol. Bound protein was eluted with nickel buffer containing 250 mM imidazole and 10 mM β-mercaptoethanol. The nickel eluate for each substrate was concentrated using appropriate MWCO concentrators (Amicon) and applied to a Superdex 200 (GE Healthcare) for gel filtration chromatography. Gel filtration buffer (60 mM HEPES pH 7.6, 50 mM NaCl, 50 mM KCl, 10% glycerol, 5 mM $MgCl_2$, 0.5 mM EDTA) was supplemented with 1mM DTT. Peak fractions were pooled, concentrated and flash frozen for storage at -80 °C.

4.4.2 Conjugation of reporter peptide to titin substrates

A synthesized peptide, succinyl-lysine-leucine-leucine-valine-tyrosine-(7-amino-4-methyl coumarin) (Genscript), was reacted with a heterobifunctional cross linker, AMAS (N-(α-Maleimidoacetoxy) succinimide ester, Pierce). The suc-KLLVY-AMC peptide was resuspended in dimethyl sulfoxide as a 50 mM stock. The peptide was reacted at a concentration of 1 mM with 3 mM AMAS and 3 mM Hünig's base (N,N-Diisopropylethylamine) in organic solvent (dimethylformamide) at 30 °C rotating overnight. The modified peptide was subjected to HPLC on a semi-preparative C18 reverse phase column using an acetonitrile gradient. The second peak to elute corresponded to the conjugated peptide (see Figure 4.3 and Figures 4.4 to 4.7). Fractions from this peak were pooled, aliquoted and lyophilized overnight, then stored at -20 °C. Aliquots of the titin concatamer substrates were thawed,

diluted to 1-2 mM with gel filtration buffer, reduced with 10 mM DTT for 30 minutes on ice and then desalted twice into conjugating buffer (PBS, pH 7.2) using Micro Bio-Spin 6 columns (Bio-Rad). The peptide-crosslinker conjugate was resuspended in a minimal volume of DMSO and the concentration was determined by absorbance at 280 nm (ε = 1280 cm^{-1} M^{-1}). The peptide was added to the conjugation reaction at the highest possible concentration while maintaining less than 10 % DMSO in the final reaction volume, and reacted for 2 hours at 23 °C. Generally a three fold molar excess of peptide to titin substrate was achieved.

4.4.3 Carboxymethylation and ubiquitination of titin substrates

Conjugation reactions were desalted twice into 100 mM Tris, pH 8.9 with Micro Bio-Spin 6 columns (Bio-Rad). Solid guanidine hydrochloride was pre-weighed in a microcentrifuge tube such that the final concentration of denaturant was 5.5-6 M (70-75 mg if adding 75 μl of protein sample). 300 mM iodoacetic acid was added to the solid GdnHCl before the protein sample was added (from a 2 M iodoacetic acid stock solution in Tris pH 8.9, pH adjusted with hydrochloric acid if necessary). The protein sample was added to the denaturant and iodoacetic acid and incubated at 23 °C for 2 hours. The extent of cysteine alkylation was assessed by comparing tryptophan fluorescence spectra for the native and carboxymethylated proteins to samples in 5 M GdnHCl using a QuantaMaster spectrofluorimeter (PTI). Carboxymethylated samples were desalted twice into ubiquitination buffer (25 mM Tris pH 8.0, 100 mM NaCl, 5 mM $MgCl_2$, 10 % glycerol) and ubiquitinated *in vitro* with Uba1, Ubc1, Rsp5 and wild-type ubiquitin such that the final substrate concentration was 2 μM (for single-turnover degradation experiments) or 20 μM (for multiple-turnover degradation experiments). Ubiquitination reactions were performed for 2 hours at 30 °C in the presence of an ATP regeneration system (5 mM ATP, 0.03 mg ml^{-1} creatine kinase, 16 mM creatine phosphate).

4.4.4 Cloning, expression and purification of recombinant base

Thirteen subunits were cloned into three Novagen vectors including pCOLA-1 (FLAG-Rpt1, Rpt2, His_6-Rpt3, Rpt4, Rpt5, Rpt6), pETDuet-1 (Rpn1, Rpn2, Rpn13), and pACYC Duet-1 (Nas2, Nas6, Hsm3, Rpn14). Each subunit was preceded by a T7 promoter and all plasmids contained one T7 terminator at the end of the multiple cloning sites. Genes for rare tRNAs were also included in the pACYCDuet-1 plasmid to account for differences in codon usage between yeast and *E. coli*. Base expression strains were generated by co-transforming the pETDuet-1, pCOLA-1 and pACYCDuet-1 plasmids into *E. coli* BL21-star (DE3) cells. The base subcomplex was produced by growing the expression strain to OD_{600}=0.6-0.8 and inducing with 1 mM isopropyl-β-D-thiogalactopyranoside overnight at 18 °C. Cells were harvested by centrifugation at 5000 rpm for 15 minutes, resuspended in nickel buffer (25 mM HEPES pH 7.6, 100 mM NaCl, 100 mM KCl, 10% glycerol, 10 mM $MgCl_2$, 0.5 mM EDTA, 20 mM imidazole) supplemented with 2 mg ml^{-1} lysozyme, protease

inhibitors and benzonase. Cells were lysed by freeze-thaw and sonication on ice for 1 minute 30 seconds in 15 second bursts. Lysate was clarified by centrifugation at 15,000 rpm at 4 °C for 30 minutes. A two-step affinity purification of the base subcomplex was performed using Ni-NTA agarose (Qiagen) to select for His_6-Rpt3 and anti-FLAG M2 resin (Sigma-Aldrich) selecting for FLAG-Rpt1. 0.5 mM ATP was present in all purification buffers. The Ni-NTA and anti-FLAG M2 columns were eluted with nickel buffer containing 250 mM imidazole or 0.15 mg ml^{-1} 3xFLAG peptide, respectively. The Flag column eluate was concentrated using a 30,000 MWCO concentrator (Amicon) and run on a Superose 6 gel filtration column (GE Healthcare) equilibrated with gel filtration buffer (60 mM HEPES pH 7.6, 50 mM NaCl, 50 mM KCl, 10% glycerol, 5 mM $MgCl_2$, 0.5 mM EDTA, 1 mM DTT, 0.5 mM ATP). See Appendix C for detailed protocol.

4.4.5 Purification of endogenous yeast complexes

Yeast holoenzyme, core particle, base and lid subcomplexes were purified from *S. cerevisiae* essentially as previously described (Leggett et al., 2005). Frozen yeast cells were lysed using a Spex SamplePrep 6870 Freezer/Mill. Holoenzyme was purified from a yeast strain containing FLAG-Rpn11. Lysed cells were resuspended in lysis buffer containing 60 mM HEPES pH 7.6, 100 mM NaCl, 100 mM KCl, 10% glycerol, 5 mM $MgCl_2$, 0.5 mM EDTA, 0.2% NP-40 and ATP regeneration mix (5 mM ATP, 0.03 mg ml^{-1} creatine kinase, 16 mM creatine phosphate). Holoenzyme was bound to anti-FLAG M2 resin and washed with wash buffer (60 mM HEPES pH 7.6, 100 mM NaCl, 100 mM KCl, 10% glycerol, 5 mM $MgCl_2$, 0.5 mM EDTA, 0.1% NP-40, 0.5 mM ATP). Holoenzyme was eluted with 0.15 mg ml^{-1} 3xFLAG peptide and further purified by gel filtration using a Superose 6 column with gel filtration buffer (see above). Lid and base subcomplexes were isolated from FLAG-Rpn11 or FLAG-Rpn2 yeast strains, respectively, and purified by exposure to a 1 M NaCl wash while bound to anti-FLAG M2 resin. Base purification buffers included 0.5 mM ATP. Core particle was purified from a 3xFLAG-Pre1 yeast strain using a 500 mM salt wash. All subcomplexes underwent size exclusion chromatography using a Superose 6 column as described above.

4.4.6 Yeast strains

Yeast lid and holoenzyme were purified from strain YYS40 (genotype MATa ade2-1 his3-11,15 leu2-3,112 trp1-1 ura3-1 can1 Rpn11::Rpn11-3XFLAG(HIS3), source Y. Saeki). Core particle was prepared either from strain RJD1144 (genotype MATa his3-200 leu2-3,112 lys2-801 trp-63 ura3-52 PRE1-FLAG-6xHIS::Ylpac211(URA3) source R. Deschaies) or strain yAM14 (genotype MATa ade2-1 his3-11,15 leu2-3,112 trip1-1 ura3-1 can1-100 bar1 PRE1::PRE1-3XFLAG(KanMX), this work).

4.4.7 Single and multiple turnover titin degradation assays

Proteasome holoenzyme was reconstituted from core particle, lid, base and Rpn10. Degradation reactions were performed at 30 °C in gel filtration buffer (60 mM HEPES pH 7.6, 50 mM NaCl, 50 mM KCl, 10% glycerol, 5 mM $MgCl_2$, 0.5 mM EDTA, 1 mM DTT, 0.5 mM ATP) supplemented with an ATP regeneration system. Degradation activities were monitored by the increase in fluorescence from cleavage of the 7-amino-4-methylcoumarin moiety (excitation 350 nm, emission 440 nm; optimal parameters were determined through excitation and emission scans) using a QuantaMaster spectrofluorimeter (PTI). Multiple turnover degradation experiments were performed with 100 nM reconstituted holoenzyme under V_{max} conditions (saturating base, lid and Rpn10) with 2 μM substrate. Single turnover degradation experiments were performed with 2 μM reconstituted proteasome holoenzyme and 100 nM substrate. Single turnover curves were best fit by a double exponential using MATLAB (MathWorks).

CHAPTER 5

Concluding Remarks and Future Directions

5.1 Concluding Remarks

The 26S proteasome is distinguished from all other energy-dependent proteases by its structural complexity and its unique substrate selection mechanism. Eukaryotes evolved to primarily rely on a single AAA+ protease to degrade a vast array of protein substrates that are selectively targeted through the ubiquitin-tagging system. The enhanced structural and functional asymmetry of the 26S proteasome may in fact result from the requirements for recognizing and binding specific ubiquitin chains, "non-specifically" engaging an unstructured initiation region of the substrate and concurrently removing the ubiquitin tag. Although the intricacies of this substrate delivery system may necessitate a more complex AAA+ protease, they potentially also facilitate some of the more specialized proteasomal substrate processing characteristics that have been observed. The 26S proteasome is known to drive some cellular processes by partially degrading certain protein substrates or selectively extracting and degrading subunits from multi-protein complexes (Baumeister et al., 1998; Tian and Matouschek, 2006; Finley, 2009), yet it is unclear exactly how the processing trajectories for these substrates differ from those that are completely degraded. Even for fully processed substrates, an intriguing question remains: how does the proteasome degrade such a wide variety of proteins with different thermodynamic stabilities and variations in ubiquitin chain length, linkage type and location within the substrate?

A detailed mechanistic model of the sequence and timing of events that occur once a substrate is tethered to the proteasome is key for advancing our understanding of when and how the proteasome selectively degrades proteins. A critical part of this model is understanding the role of the unique heterohexameric AAA+ unfoldase in the processes of substrate engagement, unfolding and translocation. Recent EM studies (Lander et al., 2012; Beck et al., 2012; Matyskiela et al., 2013) have demonstrated that major conformational changes

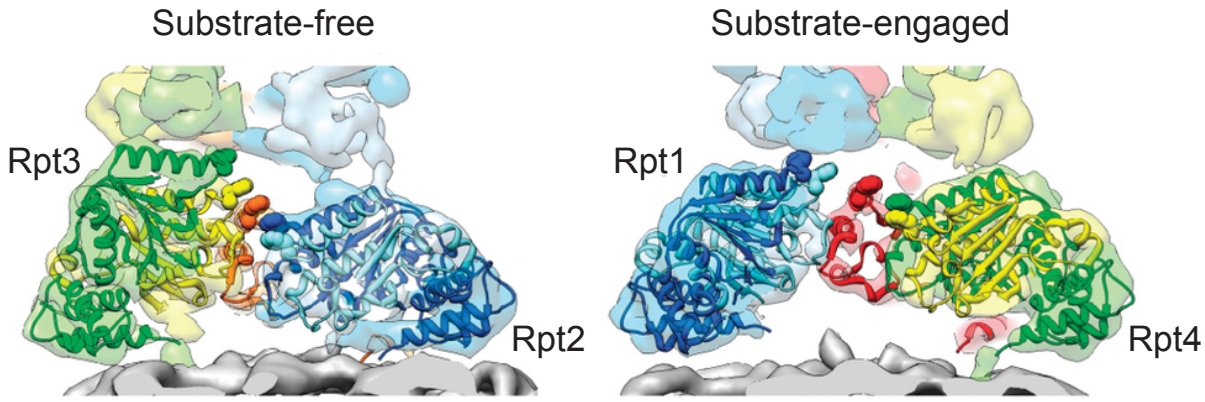

Figure 5.1: Staircase configurations of the proteasomal ATPases in the absence and presence of substrate.
Figure adapted from Matyskiela et al. 2013. The PAN crystal structure (PDB 3H4M, Zhang et al. 2009) was docked into ATPase subunit density in the base heterohexamer of EM reconstructions of the proteasome in the absence (Lander et al., 2012) or presence (Matyskiela et al., 2013) of substrate. The large AAA+ domains of the ATPase subunits adopt different spiral staircase configurations in the two states. In the substrate-free proteasome Rpt3 occupies the top position and Rpt2 the lowest, whereas in the translocating proteasome Rpt1 is in the highest position and Rpt4 the lowest. The bridging subunit between the highest and lowest positions in both staircases has been removed for clarity and to provide a view into the central pore (Rpt6 in the substrate-free staircase and Rpt5 in the substrate-engaged staircase). Residues in the substrate-interacting pore-1 loops are represented as spheres.

occur in the proteasome regulatory particle during substrate degradation and that subunits within the ATPase ring adopt alternate spiral staircase configurations in the absence and presence of substrate (Figure 5.1). Elucidating the importance of these conformational transitions and various structural arrangements for proteasomal substrate processing requires a fundamental understanding of how the base unfoldase operates and how individual ATPase subunits contribute to substrate engagement and translocation, coordinated ATP hydrolysis and inter-subcomplex communication with the lid and core peptidase.

Previous studies interrogating the function of the proteasomal unfoldase have been severely limited by low sample yields, heterogeneous subunit composition of complexes and mutant lethality. In Chapter 2, I presented a novel heterologous expression system to produce the base unfoldase subcomplex from *S. cerevisiae* in *E. coli*. The recombinant base subcomplex was then combined with lid and core peptidase subcomplexes isolated from yeast to yield reconstituted 26S holoenzyme that was fully functional in ATP hydrolysis, peptidase stimulation and substrate degradation.

In Chapter 3, I investigated the roles of individual ATPase subunits in proteasomal substrate degradation by systematic mutational analyses of conserved AAA+ motifs. Trapping

individual subunits in a permanently "ATP-bound" state with a Walker-B E→Q mutation revealed that Rpt3, Rpt4 and Rpt6 are crucial for substrate degradation. These subunits occupy positions at the top of the spiral staircase of ATPases observed in the apo proteasome structure (Lander et al., 2012; Beck et al., 2012) and may have specialized roles in engaging an unstructured initiation region of the substrate (Figure 5.2). I also measured degradation rates under single turnover conditions and identified a potential lag in the onset of degradation for the Rpt6 mutant, whereas the Rpt3 and Rpt4 mutants never degraded the substrate. Mutational analysis of the pore loops of individual ATPase subunits corroborated the importance of Rpt3 and Rpt4 in substrate degradation as pore-1 and pore-2 loop mutations in these subunits caused the most severe degradation defects. In order to separately monitor substrate engagement versus translocation, in Chapter 4 I presented an assay to measure the dependence of degradation rates on substrate length using substrates containing various numbers of unfolded titin domains. Preliminary data indicate that this method can be used to measure the rate of substrate translocation by the 26S proteasome and the time required for non-translocation processes, namely substrate engagement and deubiquitination.

I also examined the roles of the six proteasomal ATPases in the base-core interaction by making C-terminal tail truncations in individual Rpt subunits. Previous studies suggested that some of the C-terminal tails that contain a conserved HbYX motif (namely Rpt2 and Rpt5) may be specialized for opening the peptidase gate, whereas the remaining non-HbYX tails (Rpt1, Rpt4, and Rpt6) may bind to the pockets between adjacent core peptidase α subunits and mediate base-core association (Smith et al., 2007). To test this model, we assessed the effects of our C-terminal tail truncations on core peptidase gate opening and base-core binding. I found that all three HbYX-containing tails (Rpt2, Rpt3 and Rpt5) are required for stimulating gate opening. Furthermore, the HbYX tails also mediated core peptidase binding, whereas all three non-HbYX tails were dispensable for this interaction. Lastly, by comparing individual tail truncation mutants to fixing those subunits in an "empty" state with a Walker-A K→S mutation I demonstrated that the C-terminal tails contribute to gate opening in a nucleotide independent manner. These findings contradict a prior model postulating that the base dynamically "wobbles" relative to the core peptidase when the C-terminal tails undergo conformational changes in response to nucleotide hydrolysis (Smith et al., 2011).

5.2 Future Directions

The work presented in this dissertation explores how the individual ATPase subunits of the heterohexameric base unfoldase contribute to substrate processing by the 26S proteasome. These data provide a foundation for future studies of the mechanochemical basis for proteasomal substrate translocation. It remains to be seen whether the mechanistic model of ATP-dependent translocation that is emerging for simpler homomeric unfoldases will hold true for the AAA+ unfoldase of the proteasome. Compared to the bacterial unfoldase ClpX, the 26S proteasome exhibits significantly slower rates of ATP hydrolysis and substrate transloca-

tion. It has been proposed that the rapid ATP hydrolysis and substrate degradation rate of ClpX enables faster unfolding and degradation of less stable substrates but may also result in an increased frequency of substrate release for more stably folded proteins (Kenniston et al., 2005; Koodathingal et al., 2009). An integrated approach utilizing bulk biochemistry methods and single-molecule techniques to study the 26S proteasome could provide exciting insight into the mechanism of ATP-dependent substrate translocation by the heterohexameric proteasomal unfoldase. One possibility is that slower rates of ATP hydrolysis and substrate degradation could confer a greater unfolding ability to the 26S proteasome, which as the primary energy-dependent protease in eukaryotic cells must degrade a multitude of substrates that vary significantly in the stability of their folded domains.

Another fascinating question is posed by the spiral staircase configurations adopted by the proteasomal ATPase subunits and the conformational changes that occur within the regulatory particle during the transition between the substrate-free and substrate-translocating states (Figure 5.1). It is not clear why the ATPases adopt a fixed spiral staircase conformation in the absence of substrate. It is conceivable that the laterally-bound lid subcomplex induces the staircase conformation within the unfoldase to allow optimal engagement of incoming substrates by the subunits at the top of the staircase, Rpt3 and Rpt4 (Figure 5.2).

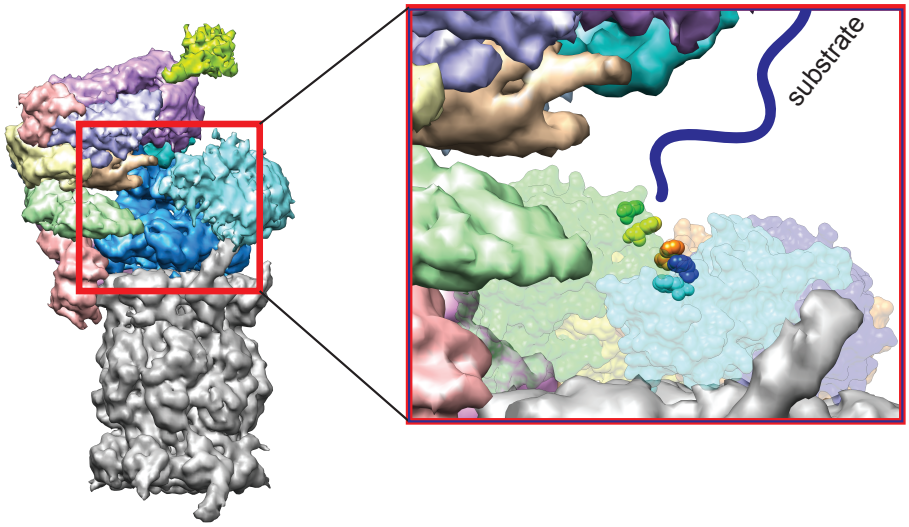

Figure 5.2: The spiral staircase of ATPases in the apo proteasome may be ideally positioned to engage incoming substrate.
The asymmetric spatial organization of DUBs and ubiquitin binding receptors within the regulatory particle may dictate that substrates approach the pore of the base unfoldase from preferred orientations. The upper-most ATPase subunits in the substrate-free spiral staircase may thus be critical for threading the incoming substrate through the unfoldase pore and initiating the structural transition to the translocation-competent state.

Further studies are required to understand how the length, linkage type and location of ubiquitin chains on a substrate, in addition to which proteasomal ubiquitin receptor interacts with the chain, affect the binding mode and thus the spatial geometry of how unstructured regions of the substrate enter the unfoldase pore. At some point during or after the incoming substrate has been engaged and threaded through the central pore, the proteasome regulatory particle undergoes a large-scale conformational change to the translocation-competent state. This transition is characterized by alignment of the unfoldase and peptidase pores, as well as a rearrangement of the spiral staircase of ATPases. Future work should focus on potential contacts between the lid, base and core peptidase that may be important for this structural transition. It will also be interesting to explore how contacts between the lid and the base are affected by conformational changes within the AAA+ unfoldase ring during cycles of ATP hydrolysis. Lastly, the alternative spiral staircase conformation of ATPases observed for the translocating proteasome raises the question of whether individual ATPase subunits within the heterohexameric proteasomal unfoldase contribute more equally to translocation once engagement has occurred.

References

Adam, Z., Rudella, A., and van Wijk, K. Recent advances in the study of Clp, FtsH and other proteases located in chloroplasts. *Curr Opin Plant Biol.*, 9(3):234–240, 2006.

Aubin-Tam, M. E., Olivares, A. O., Sauer, R. T., Baker, T. A., and Lang, M. J. Single-molecule protein unfolding and translocation by an ATP-fueled proteolytic machine. *Cell*, 145(2):257–67, 2011.

Augustin, S., Gerdes, F., Lee, S., Tsai, F. T., Langer, T., and Tatsuta, T. An Intersubunit Signaling Network Coordinates {ATP} Hydrolysis by m-AAA Proteases. *Molecular Cell*, 35(5):574–85, 2009.

Baker, T. and Sauer, R. ClpXP, an ATP-powered unfolding and protein-degradation machine. *Biochimica et Biophysica Acta (BBA) - Molecular Cell Research*, 1823(1):15–28, 2012.

Bar-Nun, S. and Glickman, M. H. Proteasomal AAA-ATPases: Structure and function. *Biochimica et Biophysica Acta (BBA) - Molecular Cell Research*, 1823(1):67–82, 2012.

Barrault, M., Richet, N., Godard, C., Murciano, B., Le Tallec, B., Rousseau, E., Legrand, P., Charbonnier, J.-B., Le Du, M.-H., Guérois, R., Ochsenbein, F., and Peyroche, A. Dual functions of the Hsm3 protein in chaperoning and scaffolding regulatory particle subunits during the proteasome assembly. *Proc Natl Acad Sci U S A*, 109(17):1001–1010, 2012.

Barthelme, D. and Sauer, R. Identification of the Cdc48-20S Proteasome as an Ancient AAA+ Proteolytic Machine. *Science*, 337(6096):843–846, 2012.

Barthelme, D. and Sauer, R. Bipartite determinants mediate an evolutionarily conserved interaction between Cdc48 and the 20S peptidase. *Proc Natl Acad Sci U S A*, 110:3327–32, 2013.

Baumeister, W., Walz, J., Zühl, F., and Seemüller, E. The Proteasome: Paradigm of a Self-Compartmentalizing Protease. *Cell*, 92(3):367–80, 1998.

Beck, F., Unverdorben, P., Bohn, S., Schweitzer, A., Pfeifer, G., Sakata, E., Nickell, S., Plitzko, J. M., Villa, E., Baumeister, W., and Forster, F. Near-atomic resolution structural model of the yeast 26S proteasome. *Proc Natl Acad Sci U S A*, 109(37):14870–5, 2012.

Beckwith, R., Estrin, E., Worden, E., and Martin, A. Reconstitution of the 26S proteasome reveals functional asymmetries in its AAA+ unfoldase. *Nat Struct Mol Biol*, 20:1164–1172, 2013.

Bell, S. P. and Stillman, B. ATP-dependent recognition of eukaryotic origins of DNA replication by a multiprotein complex. *Nature*, 357(6374):128–134, 1992.

Bieniossek, C., Niederhauser, B., and Baumann, U. The crystal structure of apo-FtsH reveals domain movements necessary for substrate unfolding and translocation. *Proc Natl Acad Sci USA.*, 106(51):21579–84, 2009.

Bochman, M. and Schwacha, A. The Mcm Complex: Unwinding the Mechanism of a Replicative Helicase. *Microbiol Mol Biol Rev*, 73(4):652–683, 2009.

Bougdour, A., Wickner, S., and Gottesman, S. Modulating RssB activity: IraP, a novel regulator of sigma(S) stability in Escherichia coli. *Genes Dev*, 20:884–97, 2006.

Bougdour, A., Cunning, C., Baptiste, P., Elliott, T., and Gottesman, S. Multiple pathways for regulation of sigmaS (RpoS) stability in Escherichia coli via the action of multiple antiadaptors. *Genes Dev*, 68:298–313, 2008.

Cha, S., An, Y., Lee, C., Lee, H., Kim, Y., Kim, S., Kwon, K., De Donatis, G., Lee, J., Maurizi, M., and Kangc, S. Crystal structure of Lon protease: molecular architecture of gated entry to a sequestered degradation chamber. *EMBO J.*, 29(20):3520–3530, 2010.

Chen, X., Lee, B. H., Finley, D., and Walters, K. J. Structure of Proteasome Ubiquitin Receptor hRpn13 and Its Activation by the Scaffolding Protein hRpn2. *Mol Cell*, 38(3): 404–15, 2010.

Costa, A., Ilves, I., Tamberg, N., Petojevic, T., Nogales, E., Botchan, M. R., and Berger, J. M. The structural basis for MCM2-7 helicase activation by GINS and Cdc45. *Nat Struct Mol Biol*, 18(4):471–7, 2011.

Davey, M., Jeruzalmi, D., Kuriyan, J., and O'Donnell, M. Motors and switches: AAA+ machines within the replisome. *Nat Rev Mol Cell Biol*, 3:826–835, 2002.

Djuranovic, S., Hartmann, M., Habeck, M., Ursinus, A., Zwickl, P., Martin, J., Lupas, A., and Zeth, K. Structure and activity of the N-terminal substrate recognition domains in proteasomal ATPases. *Mol Cell*, 34(5):580–90, 2009.

Dougan, D., Reid, B., Horwich, A., and Bukau, B. ClpS, a substrate modulator of the ClpAP machine. *Mol Cell*, 9:673–83, 2002.

Dunman, R. and Lowe, J. Crystal structures of Bacillus subtilis Lon protease. *J Mol Biol*, 401(4):653–70, 2010.

Effantin, G., Rosenzweig, R., Glickman, M. H., and Steven, A. C. Electron Microscopic Evidence in Support of α-Solenoid Models of Proteasomal Subunits Rpn1 and Rpn2. *J Mol Biol*, 386(5):1204–11, 2009.

Elsasser, S. and Finley, D. Delivery of ubiquitinated substrates to protein-unfolding machines. *Nat Cell Biol*, 7:742–49, 2005.

Elsasser, S., Chandler-Militello, D., Müller, B., Hanna, J., and Finley, D. Rad23 and Rpn10 Serve as Alternative Ubiquitin Receptors for the Proteasome. *J Biol Chem*, 279:26817–22, 2004.

Enemark, E. J. and Joshua-Tor, L. Mechanism of DNA translocation in a replicative hexameric helicase. *Nature*, 442(7100):270–5, 2006.

Erales, J., Hoyt, M. A., Troll, F., and Coffino, P. Functional asymmetries of proteasome translocase pore. *J Biol Chem*, 287(22):18535–43, 2012.

Erzberger, J. and Berger, J. Evolutionary Relationships and Structural Mechanisms of AAA+ Proteins. *Annu Rev Biophys Biomol Struct*, 35:93–114, 2006.

Erzberger, J., Mott, M., and Berger, J. Structural basis for ATP-dependent DnaA assembly and replication-origin remodeling. *Nat Struct Mol Biol*, 13:678–683, 2006.

Finley, D. Recognition and processing of ubiquitin-protein conjugates by the proteasome. *Annu Rev Biochem*, 78:477–513, 2009.

Flynn, J., Levchenko, I., Seidel, M., Wickner, S., Sauer, R., and Baker, T. Overlapping recognition determinants within the ssrA degradation tag allow modulation of proteolysis. *Proc Natl Acad Sci USA*, 98:10584–89, 2001.

Fukui, T., Eguchi, T., Atomi, H., and Imanaka, T. A Membrane-Bound Archaeal Lon Protease Displays ATP-Independent Proteolytic Activity towards Unfolded Proteins and ATP-Dependent Activity for Folded Proteins. *J. Bacteriol.*, 184(13):3689–98, 2002.

Funakoshi, M., Tomko, J. R. J., Kobayashi, H., and Hochstrasser, M. Multiple assembly chaperones govern biogenesis of the proteasome regulatory particle base. *Cell*, 137(5): 887–99, 2009.

Gillette, T. G., Kumar, B., Thompson, D., Slaughter, C. A., and DeMartino, G. N. Differential roles of the COOH termini of AAA subunits of PA700 (19 S regulator) in asymmetric assembly and activation of the 26 S proteasome. *J Biol Chem*, 283(46):31813–22, 2008.

Giudice, E. and Gillet, R. The task force that rescues stalled ribosomes in bacteria. *Trends Biochem. Sci*, 38:403–11, 2013.

Glickman, M. H., Rubin, D. M., Fried, V. A., and Finley, D. The regulatory particle of the Saccharomyces cerevisiae proteasome. *Mol Cell Biol*, 18(6):3149–62, 1998.

Glynn, S. E., Martin, A., Nager, A. R., Baker, T. A., and Sauer, R. T. Structures of asymmetric ClpX hexamers reveal nucleotide-dependent motions in a AAA+ protein-unfolding machine. *Cell*, 139(4):744–56, 2009.

Glynn, S. E., Nager, A. R., Baker, T. A., and Sauer, R. T. Dynamic and static components power unfolding in topologically closed rings of a AAA+ proteolytic machine. *Nat Struct Mol Biol*, 19(6):616–22, 2012.

Gomez, E. B., Catlett, M. G., and Forsburg, S. L. Different phenotypes in vivo are associated with ATPase motif mutations in Schizosaccharomyces pombe minichromosome maintenance proteins. *Genetics*, 160(4):1305–18, 2002.

Gomez, T., Kolawa, N., Gee, M., Sweredoski, M., and Deshaies, R. Identification of a functional docking site in the Rpn1 LRR domain for the UBA-UBL domain protein Ddi1. *BMC Biol*, 9(33), 2011.

Gottesman, S. Proteases and their target in *Escherichia Coli*. *Annu. Rev. Genet.*, 30: 465–506, 1996.

Gottesman, S. Proteolysis in bacterial regulatory circuits. *Annu. Rev. Cell Dev. Biol.*, 19: 565–87, 2003.

Gottesman, S., Roche, E., Zhou, Y., and Sauer, R. The ClpXP and ClpAP proteases degrade proteins with carboxy-terminal peptide tails added by the SsrA-tagging system. *Genes Dev*, 12(9):1338–47, 1998.

Grimm, I., Saffian, D., Platta, H., and Erdmann, R. The AAA-type ATPases Pex1p and Pex6p and their role in peroxisomal matrix protein import in Saccharomyces cerevisiae. *Biochimica et Biophysica Acta (BBA) - Molecular Cell Research*, 1823(1):150–58, 2012.

Groll, M., Bajorek, M., Kohler, A., Moroder, L., Rubin, D. M., Huber, R., Glickman, M. H., and Finley, D. A gated channel into the proteasome core particle. *Nat Struct Biol*, 7(11): 1062–7, 2000.

Groll, M., Ditzel, L., Lowe, J., Stock, D., Bochtler, M., Bartunik, H. D., and Huber, R. Structure of 20S proteasome from yeast at 2.4Å resolution. *Nature*, 386(6624):463–71, 1997.

Guo, F., Maurizi, M. R., Esser, L., and Xia, D. Crystal structure of ClpA, an Hsp100 chaperone and regulator of ClpAP protease. *J Biol Chem*, 277(48):46743–52, 2002.

Gur, E. and Sauer, R. Recognition of misfolded proteins by Lon, a AAA+ protease. *Genes Dev*, 22:2267–77, 2008.

Guterman, A. and Glickman, M. H. Complementary Roles for Rpn11 and Ubp6 in Deubiquitination and Proteolysis by the Proteasome. *J Biol Chem*, 279(3):1729–38, 2004.

Hamazaki, J., Iemura, S., Natsume, T., Yashiroda, H., Tanaka, K., and Murata, S. A novel proteasome interacting protein recruits the deubiquitinating enzyme UCH37 to 26S proteasomes. *Embo J*, 25(19):4524–36, 2006.

Hanna, J., Hathaway, N. A., Tone, Y., Crosas, B., Elsasser, S., Kirkpatrick, D., Leggett, D. S., Gygi, S. P., King, R. W., and Finley, D. Deubiquitinating Enzyme Ubp6 Functions Noncatalytically to Delay Proteasomal Degradation. *Cell*, 127(1):99–111, 2006.

Hanson, P. I. and Whiteheart, S. W. AAA+ proteins: have engine, will work. *Nat Rev Mol Cell Biol*, 6(7):519–29, 2005.

He, J., Kulkarni, K., da Fonseca, P., Krutauz, D., Glickman, M., Barford, D., and Morris, E. The Structure of the 26S Proteasome Subunit Rpn2 Reveals Its PC Repeat Domain as a Closed Toroid of Two Concentric α-Helical Rings. *Structure*, 20:513–521, 2012.

Hersch, G. L., Burton, R. E., Bolon, D. N., Baker, T. A., and Sauer, R. T. Asymmetric interactions of ATP with the AAA+ ClpX6 unfoldase: allosteric control of a protein machine. *Cell*, 121(7):1017–27, 2005.

Hinnerwisch, J., Fenton, W. A., Furtak, K. J., Farr, G. W., and Horwich, A. L. Loops in the central channel of ClpA chaperone mediate protein binding, unfolding, and translocation. *Cell*, 121(7):1029–41, 2005.

Hishida, T., Han, Y.-W., Fujimoto, S., Iwasaki, H., and Shinagawa, H. Direct evidence that a conserved arginine in RuvB AAA+ ATPase acts as an allosteric effector for the ATPase activity of the adjacent subunit in a hexamer. *Proc Natl Acad Sci U S A*, 101(26):9573–77, 2004.

Hochstrasser, M. Ubiquitin-dependent protein degradation. *Annu Rev Genet*, 30:405–39, 1996.

Horwich, A., Weber-Ban, E., and Finley, D. Chaperone rings in protein folding and degradation. *Proc Natl Acad Sci USA*, 96(20):839–48, 1999.

Husnjak, K., Elsasser, S., Zhang, N., Chen, X., Randles, L., Shi, Y., Hofmann, K., Walters, K., Finley, D., and Dikic, I. Proteasome subunit Rpn13 is a novel ubiquitin receptor. *Nature*, 453:481–88, 2008.

Inobe, T. and Matouschek, A. Protein targeting to ATP-dependent proteases. *Curr Opin Struct Biol*, 18:43–51, 2008.

Inobe, T., Fishbain, S., Prakash, S., and Matouschek, A. Defining the geometry of the two-component proteasome degron. *Nat Chem Biol*, 7(3):161–67, 2011.

Itsathitphaisarn, O., Wing, R. A., Eliason, W. K., Wang, J., and Steitz, T. A. The Hexameric Helicase DnaB Adopts a Nonplanar Conformation during Translocation. *Cell*, 151(2):267–77, 2012.

Iyer, L. M., Leipe, D. D., Koonin, E. V., and Aravind, L. Evolutionary history and higher order classification of AAA+ ATPases. *J Struct Biol*, 146(1-2):11–31, 2004.

Joshi, S. A., Hersch, G. L., Baker, T. A., and Sauer, R. T. Communication between ClpX and ClpP during substrate processing and degradation. *Nat Struct Mol Biol*, 11(5):404–11, 2004.

Jung, T., Catalgol, B., and Grune, T. The proteasomal system. *Molecular Aspects of Medicine*, 30(4):191–296, 2009.

Kajava, A. V. What Curves α-Solenoids?: Evidence for an α-helical toroid structure of Rpn1 and Rpn2 proteins of the 26S proteasome. *J Biol Chem*, 277(51):49791–98, 2002.

Kaneko, T., Hamazaki, J., Iemura, S., Sasaki, K., Furuyama, K., Natsume, T., Tanaka, K., and Murata, S. Assembly pathway of the Mammalian proteasome base subcomplex is mediated by multiple specific chaperones. *Cell*, 137(5):914–25, 2009.

Kenniston, J. A., Baker, T. A., Fernandez, J. M., and Sauer, R. T. Linkage between {ATP} Consumption and Mechanical Unfolding during the Protein Processing Reactions of an AAA+ Degradation Machine. *Cell*, 114(4):511–20, 2003.

Kenniston, J. A., Baker, T. A., and Sauer, R. T. Partitioning between unfolding and release of native domains during ClpXP degradation determines substrate selectivity and partial processing. *Proc Natl Acad Sci U S A*, 102(5):1390–95, 2005.

Kim, D. Y. and Kim, K. K. Crystal structure of ClpX molecular chaperone from Helicobacter pylori. *J Biol Chem*, 278(50):50664–70, 2003.

Kim, Y. C. and DeMartino, G. N. C termini of proteasomal ATPases play nonequivalent roles in cellular assembly of mammalian 26 S proteasome. *J Biol Chem*, 286(30):26652–66, 2011.

Kim, Y. C., Li, X., Thompson, D., and DeMartino, G. N. ATP-binding by proteasomal ATPases regulates cellular assembly and substrate-induced functions of the 26S proteasome. *J Biol Chem*, 2012.

Kohler, A., Cascio, P., Leggett, D. S., Woo, K. M., Goldberg, A. L., and Finley, D. The axial channel of the proteasome core particle is gated by the Rpt2 ATPase and controls both substrate entry and product release. *Mol Cell*, 7(6):1143–52, 2001.

Komander, D. The emerging complexity of protein ubiquitination. *Biochem Soc Trans*, 37 (1):937–53, 2009.

Komander, D. and Rape, M. The Ubiquitin Code. *Annu Rev Biochem*, 81(1):203–29, 2012.

Koodathingal, P., Jaffe, N. E., Kraut, D. A., Prakash, S., Fishbain, S., Herman, C., and Matouschek, A. ATP-dependent Proteases Differ Substantially in Their Ability to Unfold Globular Proteins. *J Biol Chem*, 284(28):18674–84, 2009.

Koppen, M. and Langer, T. Protein Degradation within Mitochondria: Versatile Activities of AAA Proteases and Other Peptidases. *Crit Rev Biochem Mol Biol*, 42:221–42, 2007.

Kraut, D. A. Slippery Substrates Impair ATP-dependent Protease Function by Slowing Unfolding. *J Biol Chem*, 288(48):34729–35, 2013.

Kraut, D. A., Prakash, S., and Matouschek, A. To degrade or release: ubiquitin-chain remodeling. *Trends in Cell Biology*, 17(9):419–21, 2007.

Kumar, B., Kim, Y. C., and DeMartino, G. N. The C terminus of Rpt3, an ATPase subunit of PA700 (19 S) regulatory complex, is essential for 26 S proteasome assembly but not for activation. *J Biol Chem*, 285(50):39523–35, 2010.

Lam, Y., Xu, W., DeMartino, G., and Cohen, R. Editing of ubiquitin conjugates by an isopeptidase in the 26S proteasome. *Nature*, 385:737–40, 1997.

Lander, G. C., Estrin, E., Matyskiela, M. E., Bashore, C., Nogales, E., and Martin, A. Complete subunit architecture of the proteasome regulatory particle. *Nature*, 482(7384): 186–91, 2012.

Langer, T. AAA proteases: cellular machines for degrading membrane proteins. *Trends Biochem Sci*, 25(5):247–51, 2000.

Lee, C., Schwartz, M., Prakash, S., Iwakura, M., and Matouschek, A. ATP-Dependent Proteases Degrade Their Substrates by Processively Unraveling Them from the Degradation Signal. *Mol Cell*, 7(3):627–37, 2001.

Lee, S., Augustin, S., Tatsuta, T., Gerdes, F., Langer, T., and Tsai, F. Electron Cryomicroscopy Structure of a Membrane-anchored Mitochondrial AAA Protease. *J Biol Chem*, 286:4404–11, 2011.

Lee, S., Moon, J. H., Yoon, S. K., and Yoon, J. B. Stable incorporation of ATPase subunits into 19 S regulatory particle of human proteasome requires nucleotide binding and C-terminal tails. *J Biol Chem*, 287(12):9269–79, 2012.

Leggett, D. S., Glickman, M. H., and Finley, D. Purification of proteasomes, proteasome subcomplexes, and proteasome-associated proteins from budding yeast. *Methods Mol Biol*, 301:57–70, 2005.

Li, X. and DeMartino, G. N. Variably modulated gating of the 26S proteasome by ATP and polyubiquitin. *Biochem J*, 421(3):397–404, 2009.

Liu, C. W., Li, X., Thompson, D., Wooding, K., Chang, T. L., Tang, Z., Yu, H., Thomas, P. J., and DeMartino, G. N. ATP binding and ATP hydrolysis play distinct roles in the function of 26S proteasome. *Mol Cell*, 24(1):39–50, 2006.

Lowe, J., Stock, D., Jap, B., Zwickl, P., Baumeister, W., and Huber, R. Crystal structure of the 20S proteasome from the archaeon T. acidophilum at 3.4Å resolution. *Science*, 268 (5210):533–39, 1995.

Maillard, R. A., Chistol, G., Sen, M., Righini, M., Tan, J., Kaiser, C. M., Hodges, C., Martin, A., and Bustamante, C. ClpX(P) generates mechanical force to unfold and translocate its protein substrates. *Cell*, 145(3):459–69, 2011.

Martin, A., Baker, T. A., and Sauer, R. T. Rebuilt AAA + motors reveal operating principles for ATP-fuelled machines. *Nature*, 437(7062):1115–20, 2005.

Martin, A., Baker, T. A., and Sauer, R. T. Distinct static and dynamic interactions control ATPase-peptidase communication in a AAA+ protease. *Mol Cell*, 27(1):41–52, 2007.

Martin, A., Baker, T. A., and Sauer, R. T. Pore loops of the AAA+ ClpX machine grip substrates to drive translocation and unfolding. *Nat Struct Mol Biol*, 15(11):1147–51, 2008a.

Martin, A., Baker, T. A., and Sauer, R. T. Diverse pore loops of the AAA+ ClpX machine mediate unassisted and adaptor-dependent recognition of ssrA-tagged substrates. *Mol Cell*, 29(4):441–50, 2008b.

Matyskiela, M. and Martin, A. Design Principles of a Universal Protein Degradation Machine. *J Mol Biol*, 425(2):199–213, 2013.

Matyskiela, M. E., Lander, G. C., and Martin, A. Conformational switching of the 26S proteasome enables substrate degradation. *Nat Struct Mol Biol*, 20(7):781–8, 2013.

Maupin-Furlow, J., Gil, M., Humbard, M., Kirkland, P., Li, W., Reuter, C., and Wright, A. Archaeal proteasomes and other regulatory proteases. *Curr. Opin. Microbiol.*, 8(6): 720–28, 2005.

Moldavski, O., Levin-Kravets, O., Ziv, T., Adam, Z., and Prag, G. The Hetero-Hexameric Nature of a Chloroplast AAA+ FtsH Protease Contributes to Its Thermodynamic Stability. *PLoS ONE*, 7(4):584–591, 2012.

Neuwald, A. F., Aravind, L., Spouge, J. L., and Koonin, E. V. AAA+: A class of chaperone-like ATPases associated with the assembly, operation, and disassembly of protein complexes. *Genome Res*, 9(1):27–43, 1999.

Nickell, S., Beck, F., Scheres, S., Korinek, A., Förster, F., Lasker, K., Mihalache, O., Sun, N., Nagy, I., Sali, A., Plitzko, J., Carazo, J., Mann, M., and Baumeister, W. Insights into the molecular architecture of the 26S proteasome. *Proc Natl Acad Sci USA*, 106:11943–47, 2009.

Nyquist, K. and Martin, A. Marching to the beat of the ring: polypeptide translocation by AAA+ proteases. *Trends in Biochemical Sciences*, 39:53–60, 2014.

Ogura, T., Whiteheart, S. W., and Wilkinson, A. J. Conserved arginine residues implicated in {ATP} hydrolysis, nucleotide-sensing, and inter-subunit interactions in {AAA} and AAA+ {ATPases}. *Journal of Structural Biology*, 146(1-2):106–12, 2004.

Ortega, J., Lee, H. S., Maurizi, M. R., and Steven, A. C. Alternating translocation of protein substrates from both ends of ClpXP protease. *The EMBO Journal*, 21(18):4938–49, 2002.

Park, E., Rho, Y. M., Koh, O. J., Ahn, S. W., Seong, I. S., Song, J. J., Bang, O., Seol, J. H., Wang, J., Eom, S. H., and Chung, C. H. Role of the GYVG pore motif of HslU ATPase in protein unfolding and translocation for degradation by HslV peptidase. *J Biol Chem*, 280(24):22892–8, 2005.

Park, S., Roelofs, J., Kim, W., Robert, J., Schmidt, M., Gygi, S. P., and Finley, D. Hexameric assembly of the proteasomal ATPases is templated through their C termini. *Nature*, 459 (7248):866–70, 2009.

Park, S., Li, X., Kim, H. M., Singh, C. R., Tian, G., Hoyt, M. A., Lovell, S., Battaile, K. P., Zolkiewski, M., Coffino, P., Roelofs, J., Cheng, Y., and Finley, D. Reconfiguration of the proteasome during chaperone-mediated assembly. *Nature*, 2013.

Pickart, C. M. Targeting of substrates to the 26S proteasome. *FASEB*, 11(13):1055–66, 1997.

Pickart, C. and Cohen, R. Proteasomes and their kin: proteases in the machine age. *Nat Rev Mol Cell Biol*, 5(3):177–87, 2004.

Prakash, S., Tian, L., Ratliff, K., Lehotzky, R., and Matouschek, A. An unstructured initiation site is required for efficient proteasome-mediated degradation. *Nat Struct Mol Biol*, 11:830–37, 2004.

Raasi, R. S.and Varadan, Fushman, D., and Pickart, C. Diverse polyubiquitin interaction properties of ubiquitin-associated domains. *Nat Struct Mol Biol*, 12:708–14, 2005.

Rabl, J., Smith, D. M., Yu, Y., Chang, S. C., Goldberg, A. L., and Cheng, Y. Mechanism of gate opening in the 20S proteasome by the proteasomal ATPases. *Mol Cell*, 30(3):360–8, 2008.

Riedinger, C., Boehringer, J., Trempe, J.-F., Lowe, E. D., Brown, N. R., Gehring, K., Noble, M. E. M., Gordon, C., and Endicott, J. A. Structure of Rpn10 and Its Interactions with Polyubiquitin Chains and the Proteasome Subunit Rpn12. *J Biol Chem*, 285(44):33992–34003, 2010.

Roelofs, J., Park, S., Haas, W., Tian, G., McAllister, F. E., Huo, Y., Lee, B. H., Zhang, F., Shi, Y., Gygi, S. P., and Finley, D. Chaperone-mediated pathway of proteasome regulatory particle assembly. *Nature*, 459(7248):861–5, 2009.

Román-Hernández, G., Hou, J., Grant, R., Sauer, R., and Baker, T. The ClpS adaptor mediates staged delivery of N-end rule substrates to the AAA+ ClpAP protease. *Mol Cell*, 43(2):217–28, 2011.

Rosenzweig, R., Bronner, V., Zhang, D., Fushman, D., and Glickman, M. H. Rpn1 and Rpn2 coordinate ubiquitin processing factors at proteasome. *J Biol Chem*, 287(18):14659–71, 2012.

Rubin, D. M., Glickman, M. H., Larsen, C. N., Dhruvakumar, S., and Finley, D. Active site mutants in the six regulatory particle ATPases reveal multiple roles for ATP in the proteasome. *Embo J*, 17(17):4909–19, 1998.

Saeki, Y., Toh, E. A., Kudo, T., Kawamura, H., and Tanaka, K. Multiple proteasome-interacting proteins assist the assembly of the yeast 19S regulatory particle. *Cell*, 137(5): 900–13, 2009.

Sakata, E., Bohn, S., Mihalache, O., Kiss, P., Beck, F., Nagy, I., Nickell, S., Tanaka, K., Saeki, Y., Forster, F., and Baumeister, W. Localization of the proteasomal ubiquitin receptors Rpn10 and Rpn13 by electron cryomicroscopy. *Proc Natl Acad Sci U S A*, 109 (5):1479–84, 2012.

Satoh, T., Saeki, Y., Hiromoto, T., Wang, Y.-H., Uekusa, Y., Yagi, H., Yoshihara, H., Yagi-Utsumi, M., Mizushima, T., Tanaka, K., and Kato, K. Structural Basis for Proteasome Formation Controlled by an Assembly Chaperone Nas2. *Structure*, 22:1–13, 2014.

Sauer, R. T. and Baker, T. A. AAA+ Proteases: ATP-Fueled Machines of Protein Destruction. *Annu Rev of Biochem*, 80(1):587–612, 2011.

Schlieker, C., Weibezahn, J., Patzelt, H., Tessarz, P., Strub, C., Zeth, K., Erbse, A., Schneider-Mergener, J., Chin, J. W., Schultz, P. G., Bukau, B., and Mogk, A. Substrate recognition by the AAA+ chaperone ClpB. *Nat Struct Mol Biol*, 11(7):607–15, 2004.

Schmidt, M., Lupas, N., and Finley, D. Structure and mechanism of ATP-dependent proteases. *Curr Opin Chem Biol.*, 3(5):584–91, 1999.

Schmidt, R., Zahn, R., Bukau, B., and Mogk, A. ClpS is the recognition component for *Escherichia coli* substrates of the N-end rule degradation pathway. *Mol Microbiol*, 72(2): 506–17, 2009.

Schreiner, P., Chen, X., Husnjak, K., Randles, L., Zhang, N., Elsasser, S., Finley, D., Dikic, I., Walters, K. J., and Groll, M. Ubiquitin docking at the proteasome through a novel pleckstrin-homology domain interaction. *Nature*, 453(7194):548–52, 2008.

Sen, M., Maillard, R., Nyquist, K., Rodriguez-Aliaga, P., Pressé, S., Martin, A., and Bustamante, C. The ClpXP Protease Unfolds Substrates Using a Constant Rate of Pulling but Different Gears. *Cell*, 155(3):636–46, 2013.

Seong, I. S., Kang, M. S., Choi, M. K., Lee, J. W., Koh, O. J., Wang, J., Eom, S. H., and Chung, C. H. The C-terminal tails of HslU ATPase act as a molecular switch for activation of HslV peptidase. *J Biol Chem*, 277(29):25976–82, 2002.

Singh, C. R., Lovell, S., Mehzabeen, N., Chowdhury, W. Q., Geanes, E. S., Battaile, K. P., and Roelofs, J. 1.15Å resolution structure of the proteasome-assembly chaperone Nas2 PDZ domain. *Acta Crystallographica Section F*, 70(4):418–23, Apr 2014.

Singleton, M. R., Sawaya, M. R., Ellenberger, T., and Wigley, D. B. Crystal structure of T7 gene 4 ring helicase indicates a mechanism for sequential hydrolysis of nucleotides. *Cell*, 101(6):589–600, 2000.

Sledz, P., Unverdorben, P., Beck, F., Pfeifer, G., Schweitzer, A., Forster, F., and Baumeister, W. Structure of the 26S proteasome with ATP-gammaS bound provides insights into the mechanism of nucleotide-dependent substrate translocation. *Proc Natl Acad Sci U S A*, 110(18):7264–9, 2013.

Smith, D. M., Kafri, G., Cheng, Y., Ng, D., Walz, T., and Goldberg, A. L. ATP binding to PAN or the 26S ATPases causes association with the 20S proteasome, gate opening, and translocation of unfolded proteins. *Mol Cell*, 20(5):687–98, 2005.

Smith, D. M., Chang, S. C., Park, S., Finley, D., Cheng, Y., and Goldberg, A. L. Docking of the proteasomal ATPases' carboxyl termini in the 20S proteasome's alpha ring opens the gate for substrate entry. *Mol Cell*, 27(5):731–44, 2007.

Smith, D. M., Fraga, H., Reis, C., Kafri, G., and Goldberg, A. L. ATP binds to proteasomal ATPases in pairs with distinct functional effects, implying an ordered reaction cycle. *Cell*,

144(4):526–38, 2011.

Song, H. K., Hartmann, C., Ramachandran, R., Bochtler, M., Behrendt, R., Moroder, L., and Huber, R. Mutational studies on HslU and its docking mode with HslV. *Proc Natl Acad Sci U S A*, 97(26):14103–8, 2000.

Stinson, B., Nager, A., Glynn, S., Schmitz, K., Baker, T., and Sauer, R. Nucleotide Binding and Conformational Switching in the Hexameric Ring of a AAA+ Machine. *Cell*, 153(3): 628–39, 2013.

Takagi, K., Kim, S., Yukii, H., Ueno, M., Morishita, R., Endo, Y., Kato, K., Tanaka, K., Saeki, Y., and Mizushima, T. Structural basis for specific recognition of Rpt1p, an ATPase subunit of 26 S proteasome, by proteasome-dedicated chaperone Hsm3p. *J Biol Chem*, 287(15):12172–82, 2012.

Thompson, D., Hakala, K., and DeMartino, G. N. Subcomplexes of PA700, the 19 S regulator of the 26 S proteasome, reveal relative roles of AAA subunits in 26 S proteasome assembly and activation and ATPase activity. *J Biol Chem*, 284(37):24891–903, 2009.

Thomsen, N. D. and Berger, J. M. Running in reverse: the structural basis for translocation polarity in hexameric helicases. *Cell*, 139(3):523–34, 2009.

Thrower, J. S., Hoffman, L., Rechsteiner, M., and Pickart, C. M. Recognition of the polyubiquitin proteolytic signal. *Embo J*, 19(1):94–102, 2000.

Tian, G., Park, S., Lee, M. J., Huck, B., McAllister, F., Hill, C. P., Gygi, S. P., and Finley, D. An asymmetric interface between the regulatory and core particles of the proteasome. *Nat Struct Mol Biol*, 18(11):1259–67, 2011.

Tian, L. and Matouschek, A. Where to start and when to stop. *Nat Struct Mol Biol*, 13(8): 668–70, 2006.

Tomko, J. R. J., Funakoshi, M., Schneider, K., Wang, J., and Hochstrasser, M. Heterohexameric ring arrangement of the eukaryotic proteasomal ATPases: implications for proteasome structure and assembly. *Mol Cell*, 38(3):393–403, 2010.

Tomko, R. and Hochstrasser, M. Order of the Proteasomal ATPases and Eukaryotic Proteasome Assembly. *Cell Biochem Biophys*, 60:13–20, 2011.

Tomko, R. and Hochstrasser, M. Molecular Architecture and Assembly of the Eukaryotic Proteasome. *Annu Rev Biochem*, 82:415–45, 2013.

Too, P., Erales, J., Simen, J. D., Marjanovic, A., and Coffino, P. Slippery Substrates Impair Function of a Bacterial Protease ATPase by Unbalancing Translocation versus Exit. *J Biol Chem*, 288(19):13243–57, 2013.

Verma, R., Aravind, L., Oania, R., McDonald, W. H., Yates, r. J. R., Koonin, E. V., and Deshaies, R. J. Role of Rpn11 metalloprotease in deubiquitination and degradation by the 26S proteasome. *Science*, 298(5593):611–5, 2002.

Verma, R., Oania, R., Graumann, J., and Deshaies, R. J. Multiubiquitin chain receptors define a layer of substrate selectivity in the ubiquitin-proteasome system. *Cell*, 118(1): 99–110, 2004.

Voges, D., Zwickl, P., and Baumeister, W. The 26S Proteasome: A Molecular Machine Designed for Controlled Proteolysis. *Annu Rev Biochem*, 68(1):1015–68, 1999.

Volker, C. and Lupas, A. Molecular evolution of proteasomes. *Curr Top Microbiol Immunol*, 268:1–22, 2002.

Wang, J., Song, J., Franklin, S., Kamtekar, S., Im, Y., Rho, S., Seong, I., Lee, C., Chung, C., and Eom, S. Crystal structures of the HslVU peptidase-ATPase complex reveal an ATP-dependent proteolysis mechanism. *Structure*, 9:177–84, 2001.

Weibezahn, J., Bukau, B., and Mogk, A. Unscrambling an egg: protein disaggregation by AAA+ proteins. *Microb Cell Fact*, 3(1):1, 2004.

Wendler, P., Ciniawsky, S., Kock, M., and Kube, S. Structure and function of the AAA+ nucleotide binding pocket. *Biochimica et Biophysica Acta (BBA) - Molecular Cell Research*, 1823(1):2–14, 2012.

Worden, E., Padovani, C., and Martin, A. Structure of the Rpn11-Rpn8 dimer reveals mechanisms of substrate deubiquitination during proteasomal degradation. *Nat Struct Mol Biol*, 21:220–27, 2014.

Yamada-Inagawa, T., Okuno, T., Karata, K., Yamanaka, K., and Ogura, T. Conserved pore residues in the AAA protease FtsH are important for proteolysis and its coupling to ATP hydrolysis. *J Biol Chem*, 278(50):50182–7, 2003.

Yao, T. and Cohen, R. E. A cryptic protease couples deubiquitination and degradation by the proteasome. *Nature*, 419(6905):403–7, 2002.

Yu, Y., Smith, D., Kim, H., Rodriguez, V., Goldberg, A., and Cheng, Y. Interactions of PAN's C-termini with archaeal 20S proteasome and implications for the eukaryotic proteasome-ATPase interactions. *EMBO J*, 29(3):692–702, 2010.

Zhang, F., Hu, M., Tian, G., Zhang, P., Finley, D., Jeffrey, P., and Shi, Y. Structural Insights into the Regulatory Particle of the Proteasome from Methanocaldococcus jannaschii. *Mol Cell*, 34(4):473–84, 2009.

Zhou, Y., Gottesman, S., Hoskins, J., Maurizi, M., and Wickner, S. The RssB response regulator directly targets sigma(S) for degradation by ClpXP. *Genes Dev*, 15(5):627–37, 2001.

APPENDIX A

October 2013 *NSMB* Journal Cover

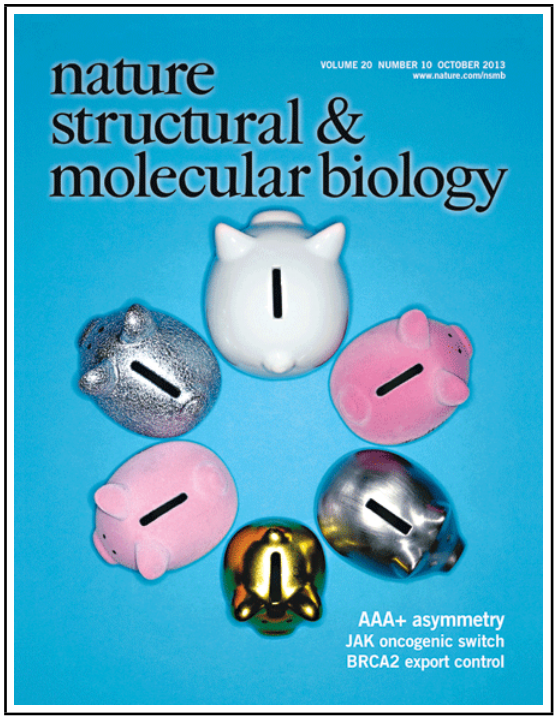

Figure A.1: Cover of October 2013 Issue of *Nature Structural & Molecular Biology*. The heterohexameric AAA+ complex of the eukaryotic 26S proteasome unfolds substrates prior to degradation. Martin and colleagues reconstitute proteasomes with recombinant subunits of the yeast unfoldase (Rpt1–6) to reveal distinct roles of each (Beckwith et al., 2013). © Andrew Paterson. pp 1164–1172.

APPENDIX B

Sequence alignment of proteasomal ATPases and ClpX

Protein sequences were obtained from the UniProt database using the following entry numbers: Rpt1 (A6ZZH6), Rpt2 (A6ZXV9), Rpt3 (A6ZYZ5), Rpt4 (A6ZP97), Rpt5 (A6ZNW5), Rpt6 (A6ZUU9) and ClpX (P0A6H1). Alignment of the sequences for the six distinct proteasomal AAA+ ATPase subunits (Rpt1-6) and the ATPase subunit of the bacterial AAA+ unfoldase, ClpX, were performed using the MAFFT (*M*ultiple *A*lignment using *F*ast *F*ourier *T*ransform) web server (https://www.ebi.ac.uk/Tools/msa/mafft). The protein comparison matrix used was BLOSUM62, with default parameter values for gap open (1.53) and gap extension penalties (0.123).


Rpt1 MPPKEDWEKYKA-PLEDDDKKPDDDKIVPLTEGDIQVLKSYGAAPYAAKLKQ------TE
Rpt2 M------GQ-GV-SSGQDKKKKKGSNQKPKYEPPVQ-------SKFGR--KKRKGGPATA
Rpt3 M------EELGI-VT---------PVEKAVEEKPAV-------KSYASLLAQLNGTVNNN
Rpt4 MSEEQDPLLAGLGETSGDNHTQQSHEQQPEQPQETE-------EHHEEEPSRV-----DP
Rpt5 MATLEELDAQTL---------PGDDEL-----------------------------DQ
Rpt6 M------TA-AV-TSSNIVLETHESGIKPYFEQKIQ-------E-------------TE
ClpX M---
Rpt1 NDLKDIEARIK------EKAGVKESDTGLAPSHLWDIM-----------------GDRQR
Rpt2 EKLPNIYPSTRCKLKLLRMERIKD-----HLLLEEEFVSNSEI-LKPFEKKQEEEKKQLE
Rpt3 SALSNVNSDIYFKLK--KLEKEYE-----LLTLQEDYIKDEQRHLKRELKRAQEEVKRIQ
Rpt4 EQEAHNKALNQFKRKLLEHRRYDD-----QLKQRRQNIRD----LEKLYDKTENDIKALQ
Rpt5 EILNLSTQELQTRAKLLDNEIR-------IFRSELQRLSHENNVMLEKIKDNKEKIKNNR
Rpt6 LKIRSKTENVR------RLEAQRN-----ALNDKVRFI-----------------KDELR
ClpX --TDKRKDGSGKLL
cis/trans proline
Rpt1 LGEEHPLQVARCTKIIKGNGESDETTTDNNNSGNSNSNSNQQSTDADEDDEDAKYVINLK
Rpt2 EIRGNPLSIGTLEEII---------------------------------DDDHAIVTSP
Rpt3 SV---PLVIGQFLEPI---------------------------------DQNTGIVSST
Rpt4 SI---GQLIGEVMKEL---------------------------------SEEKYIVKAS
Rpt5 QL---PYLVANVVEVMDMNEIEDKENSESTTQGGNVNLDNTA--------VGKAAVVKTS
Rpt6 LLQEPGSYVGEVIKIV---------------------------------SDKKVLVKVQ
ClpX YCSFCGKSQHEVRKLI---------------------------------AGPSVYICDE
Rpt1 QIAKFVVGLGERVSPTDIEEGMRVGVDRSKYNIELPLPPRIDPSVTMMTVEEKPDVTYSD
Rpt2 TMPDYYVSILSFVDKELLEPGCSVLLHHKTMSIVGVLQDDADPMVSVMKMDKSPTESYSD
Rpt3 TGMSYVVRILSTLDRELLKPSMSVALHRHSNALVDILPPDSDSSISVMGENEKPDVTYAD
Rpt4 SGPRYIVGVRNSVDRSKLKKGVRVTLDITTLTIMRILPRETDPLVYNMTSFEQGEITFDG
Rpt5 SRQTVFLPMVGLVDPDKLKPNDLVGVNKDSYLILDTLPSEFDSRVKAMEVDEKPTETYSD
Rpt6 PEGKYIVDVAKDINVKDLKASQRVCLRSDSYMLHKVLENKADPLVSLMMVEKVPDSTYDM
ClpX -----CVDLCNDIIREEIKE---------------VAPHRERSALPTPHEIRNHLDDY--
P-loop (Walker A)
Rpt1 VGGCKDQIEKLREVVELPLLS-PERFATLGIDPPK-GILLYGPPGTGKTLCARAVANRTD
Rpt2 IGGLESQIQEIKESVELPLTH-PELYEEMGIKPPK-GVILYGAPGTGKTLLAKAVANQTS
Rpt3 VGGLDMQKQEIREAVELPLVQ-ADLYEQIGIDPPR-GVLLYGPPGTGKTMLVKAVANSTK
Rpt4 IGGLTEQIRELREVIELPLKN-PEIFQRVGIKPPK-GVLLYGPPGTGKTLLAKAVAATIG
Rpt5 VGGLDKQIEELVEAIVLPMKR-ADKFKDMGIRAPK-GALMYGPPGTGKTLLARACAAQTN
Rpt6 VGGLTKQIKEIKEVIELPVKH-PELFESLGIAQPK-GVILYGPPGTGKTLLARAVAHHTD
ClpX VIGQEQAKKVLAVAVYNHYKRLRNGDTSNGVELGKSNILLIGPTGSGKTLLAETLARLLD

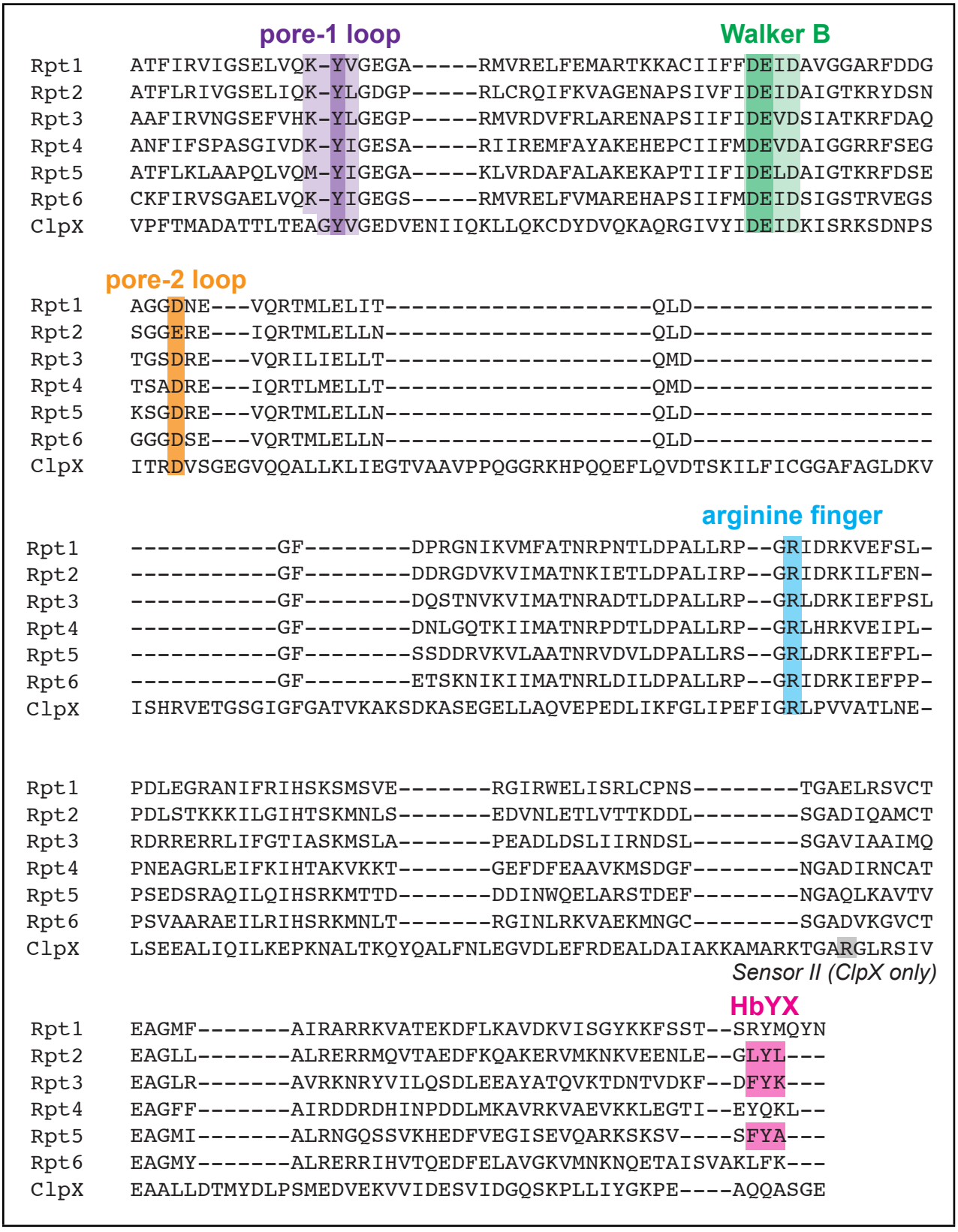
pore-1 loop
Walker B
Rpt1 ATFIRVIGSELVQK-YVGEGA-----RMVRELFEMARTKKACIIFFDEIDAVGGARFDDG
Rpt2 ATFLRIVGSELIQK-YLGDGP-----RLCRQIFKVAGENAPSIVFIDEIDAIGTKRYDSN
Rpt3 AAFIRVNGSEFVHK-YLGEGP-----RMVRDVFRLARENAPSIIFIDEVDSIATKRFDAQ
Rpt4 ANFIFSPASGIVDK-YIGESA-----RIIREMFAYAKEHEPCIIFMDEVDAIGGRRFSEG
Rpt5 ATFLKLAAPQLVQM-YIGEGA-----KLVRDAFALAKEKAPTIIFIDELDAIGTKRFDSE
Rpt6 CKFIRVSGAELVQK-YIGEGS-----RMVRELFVMAREHAPSIIFMDEIDSIGSTRVEGS
ClpX VPFTMADATTLTEAGYVGEDVENIIQKLLQKCDYDVQKAQRGIVYIDEIDKISRKSDNPS
pore-2 loop
Rpt1 AGGDNE---VQRTMLELIT----------QLD----------
Rpt2 SGGERE---IQRTMLELLN----------QLD----------
Rpt3 TGSDRE---VQRILIELLT----------QMD----------
Rpt4 TSADRE---IQRTLMELLT----------QMD----------
Rpt5 KSGDRE---VQRTMLELLN----------QLD----------
Rpt6 GGGDSE---VQRTMLELLN----------QLD----------
ClpX ITRDVSGEGVQQALLKLIEGTVAAVPPQGGRKHPQQEFLQVDTSKILFICGGAFAGLDKV
arginine finger
Rpt1 ----------GF--------DPRGNIKVMFATNRPNTLDPALLRP--GRIDRKVEFSL-
Rpt2 ----------GF--------DDRGDVKVIMATNKIETLDPALIRP--GRIDRKILFEN-
Rpt3 ----------GF--------DQSTNVKVIMATNRADTLDPALLRP--GRLDRKIEFPSL
Rpt4 ----------GF--------DNLGQTKIIMATNRPDTLDPALLRP--GRLHRKVEIPL-
Rpt5 ----------GF--------SSDDRVKVLAATNRVDVLDPALLRS--GRLDRKIEFPL-
Rpt6 ----------GF--------ETSKNIKIIMATNRLDILDPALLRP--GRIDRKIEFPP-
ClpX ISHRVETGSGIGFGATVKAKSDKASEGELLAQVEPEDLIKFGLIPEFIGRLPVVATLNE-
Rpt1 PDLEGRANIFRIHSKSMSVE-------RGIRWELISRLCPNS--------TGAELRSVCT
Rpt2 PDLSTKKKILGIHTSKMNLS-------EDVNLETLVTTKDDL--------SGADIQAMCT
Rpt3 RDRRERRLIFGTIASKMSLA-------PEADLDSLIIRNDSL--------SGAVIAAIMQ
Rpt4 PNEAGRLEIFKIHTAKVKKT-------GEFDFEAAVKMSDGF--------NGADIRNCAT
Rpt5 PSEDSRAQILQIHSRKMTTD-------DDINWQELARSTDEF--------NGAQLKAVTV
Rpt6 PSVAARAEILRIHSRKMNLT-------RGINLRKVAEKMNGC--------SGADVKGVCT
ClpX LSEEALIQILKEPKNALTKQYQALFNLEGVDLEFRDEALDAIAKKAMARKTGARGLRSIV
Sensor II (ClpX only)
HbYX
Rpt1 EAGMF-------AIRARRKVATEKDFLKAVDKVISGYKKFSST--SRYMQYN
Rpt2 EAGLL-------ALRERRMQVTAEDFKQAKERVMKNKVEENLE--GLYL---
Rpt3 EAGLR-------AVRKNRYVILQSDLEEAYATQVKTDNTVDKF--DFYK---
Rpt4 EAGFF-------AIRDDRDHINPDDLMKAVRKVAEVKKLEGTI--EYQKL--
Rpt5 EAGMI-------ALRNGQSSVKHEDFVEGISEVQARKSKSV----SFYA---
Rpt6 EAGMY-------ALRERRIHVTQEDFELAVGKVMNKNQETAISVAKLFK---
ClpX EAALLDTMYDLPSMEDVEKVVIDESVIDGQSKPLLIYGKPE----AQQASGE

APPENDIX C

Base Purification Protocol

OBJECTIVE: Purification of base subcomplex from E. coli

- Grow, induce and harvest liter-scale cultures
- Nickel affinity column
- Anti-FLAG affinity column
- Superose 6 gel filtration chromatography

Purification buffers
Make buffers without ATP/DTT, then add to the required amount of buffer prior to use

Nickel A
25 mM HEPES, pH 7.6
100 mM NaCl
100 mM KCl
10% glycerol
10 mM MgCl2
0.5 mM EDTA
20 mM imidazole
0.5 mM ATP

Nickel B
add 250 mM imidazole (solid) and re-adjust buffer to pH 7.6

Gel filtration
60 mM HEPES, pH 7.6
50 mM NaCl
50 mM KCl
10% glycerol
5 mM MgCl2
0.5 mM EDTA
0.5 mM ATP
1 mM DTT

Day 1

- Inoculate 50mL starter culture from cell stock
  - Amp^{res} : pETDUET (Rpn1/Rpn2/Rpn13)
  - Kan^{res}: pCOLA (Flag-Rpt1/Rpt2/His-Rpt3/Rpt5/Rpt6/Rpt4)
  - Chl^{res}: pACYC (chaperones Nas2/Nas6/Hsm3/Rpn14)
- Grow overnight at 30 °C

Day 2

- Wash culture with dYT and inoculate each 1 liter flask with approximately 5mL of saturated overnight culture
- Grow large cultures at 37 °C until OD_{600} = 0.4-0.5 (2-4 hours)
- Cool cultures to 18 °C and induce at OD_{600} = 0.6-0.8 with 1 mM IPTG overnight

Day 3

- Harvest liter cultures by centrifuging at 4000 rpm for 20-30 minutes
- Resuspend pelleted cells in 10 mL nickel A buffer per liter of culture
- Add lysozyme, benzonase and protease inhibitors (PMSF, leupeptin, aprotinin, pepstatin)
- Freeze at -80 °C

Day 3-4

- Freeze-thaw cell lysates 2-3 times total by thawing frozen lysate in cool or room temperature water and re-freezing at -80 °C for at least a few hours

Day 4

- Thaw frozen lysate
- Sonicate lysate in plastic container on ice: 90 % power for 15 seconds on, 1 minute 30 seconds off for total sonication time of 1 minute 30 seconds
- Centrifuge lysate at 15,000 rpm for 30 minutes at 4 °C
- Wash nickel resin (50 % slurry) twice with 25 ml nickel A buffer (use approximately 2 mL slurry per liter of culture)
- Incubate supernant with nickel resin for 30 minutes to 1 hour
  All buffers from here on contain 0.5 mM ATP
- Batch wash with nickel A buffer twice, then transfer resin to a column and wash until flow through no longer reacts with Bradford reagent
- Elute with nickel B buffer in 1 mL aliquots
- Run pooled nickel eluate over a column containing 3-5 mL anti-FLAG M2 resin, repeat 3-5 times
- Wash with 25-50mL of nickel A buffer until flow through is clean
- Elute from FLAG column with nickel A buffer containing 0.15 mg ml^{-1} 3X FLAG peptide in 0.5 mL fractions
- Pool FLAG eluate and add 5 mM DTT. Concentrate volume to less than 500 μL using a 30,0000- or 100,000-MWCO concentrator pre-equilibrated with nickel A buffer
- Filter concentrated eluate through a small spin filter before performing gel filtration chromatography
- Run Superose 6 sizing column with gel filtration buffer containing 1 mM DTT and 0.5 mM ATP
- Pool and concentrate fractions containing the base sub-complex, which elutes at a volume of approximately 12.5 mL from the Superose 6 column (see Figure 2.2a for representative size exclusion profile and Figure 2.2b for representative SDS-PAGE of purified base subcomplex). Aliquot, flash freeze and store at -80 °C.